HAWAI'I SPACE GRANT CONSORTIUM

UNDERGRADUATE FELLOWSHIP REPORTS

Fall 2006 – Spring 2007

NATIONAL SPACE GRANT COLLEGE AND FELLOWSHIP PROGRAM

NASA

HSGC Report Number 07-15

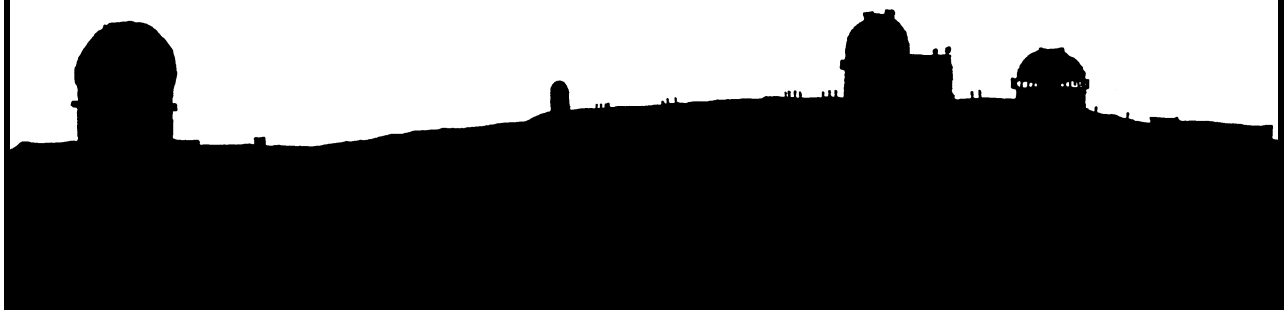

Compiled in 2007 by
HAWAIʻI SPACE GRANT CONSORTIUM

The Hawaiʻi Space Grant Consortium is one of the fifty-two National Space Grant Colleges supported by the National Aeronautics and Space Administration (NASA).

This report may be cited as

Hawaiʻi Space Grant Consortium (2007) *Undergraduate Fellowship Reports*. HSGC Report No. 07-15. Hawaiʻi Space Grant Consortium, Honolulu.

Individual articles may be cited as

Author, A.B. (2007) Title of article. *Undergraduate Fellowship Reports*, pp. xx-xx. Hawaiʻi Space Grant Consortium, Honolulu.

This report is distributed by:

Hawaiʻi Space Grant Consortium
Hawaiʻi Institute of Geophysics and Planetology
University of Hawaiʻi at Mānoa
1680 East West Road, POST 501
Honolulu, HI 96822

TABLE OF CONTENTS

L.E.O.N.I.D.A.S. TEAM REPORTS

Foreword

This volume contains twenty-five reports from Hawai‘i Space Grant Undergraduate Fellows at the University of Hawai‘i at Manoa and the University of Hawai‘i at Hilo. The students worked on their projects in the Summer/Fall 2006 and Spring 2007 semesters under the guidance of their faculty mentors. We congratulate all of the students for their outstanding reports and warmly thank their faculty mentors for generously supporting the Fellowship Program.

The Hawai‘i Space Grant Consortium is supported by NASA through its National Space Grant College and Fellowship Program with matching funds from the University of Hawai‘i. The goal of the program is to strengthen the national capabilities in space-related mathematics, science, and engineering and to prepare the next generation of space scientists. All of the students’ projects are related to the goals of NASA’s Strategic Plan.

For more information about the Fellowship Program, please visit our website: http://www.spacegrant.hawaii.edu/fellowships.html

Edward R.D. Scott
Associate Director, Fellowships

STUDY OF WATER CHANNELS AROUND OLYMPUS MONS: ANALYSIS OF THE SURROUNDING TOPOGRAPHY

Alexander M. Ambard
College of Arts and Sciences
University of Hawai‘i at Mānoa
Honolulu, HI 96822

ABSTRACT

Images obtained by the THEMIS instrument aboard the Mars Odyssey spacecraft reveal numerous channel systems near Olympus Mons volcano, Mars, which appear to have been cut into the surface by relatively recent water flows. Although the water has long since dried up, the channels formed can still be used to determine changes in ground slope which have occurred since their times of formation. To do this we compared flow directions with current maximum downhill gradients of underlying terrain and noted any inconsistencies between the two. The level of mismatch between indicators of slope indicates that either a large amount of ground deformation has recently occurred in this area, or that the flows were diverted by landforms (most likely glaciers or dunes) that are no longer present.

DISTRIBUTION AND MOPHOLOGY OF CHANNELS

Together with my mentor, I have identified three characteristics of channel systems around Olympus Mons. (1) A single channel to the west of the aureole (at 22.1°N, 208.7°E) that appears to have been a sink of water rather than a source; (2) a single channel system within a lobe of the western aureole deposit (at 25.6°N, 211.67°E); and (3) numerous channels to the SE of the basal escarpment of the volcano that originated from fractures in the young lava plains. Figure 1 shows an example of these channels. The fractures from which these channels originate can either be confined (near-circular) sources or linear fractures. An interesting second attribute of some of these channels is that they are not aligned with the current maximum topographic gradient, despite recent data from detailed crater counts [Basilevsky *et al*., 2006] that suggest that the lava flows within which the channels are carved may be very young (<25 – 40 Myr). This implies that the ground has either been recently tilted, or that topographic obstacles (such as glaciers) existed at the time that the channels formed. The identification and magnitude of this cause of this mis-match is the central theme of my Space Grant project.

In contrast to the single example of a channel that was discussed by Mouginis-Mark [1990], I have identified numerous long (>50 km long) channels complexes to the SE of the basal escarpment of Olympus Mons (Figure 1). Frequently, these channels are braided, with stream-lined islands along their length. Multiple levels within the channel floor can also be seen in some instances. Several of the source areas show signs of the accumulation of materials along the sides of the fractures so that the source areas have raised rims. The lack of lava flow lobes, or hills with summit pits, allows us to exclude a volcanic origin for these channels and source areas; our interpretation is that they are water-carved channels.

LOCATING WATER CHANNEL SYSTEMS USING THEMIS VIS IMAGES

Early in the project I downloaded from the THEMIS web site, catalogued, and mapped the location of all of the THEMIS images available from years 1-4 of the mission covering the area S.E. of Olympus Mons' basal escarpment (Fig. 2). This included a total of 384 images – many of which contain ambiguous channel structures that cannot be confirmed to have been formed by water.

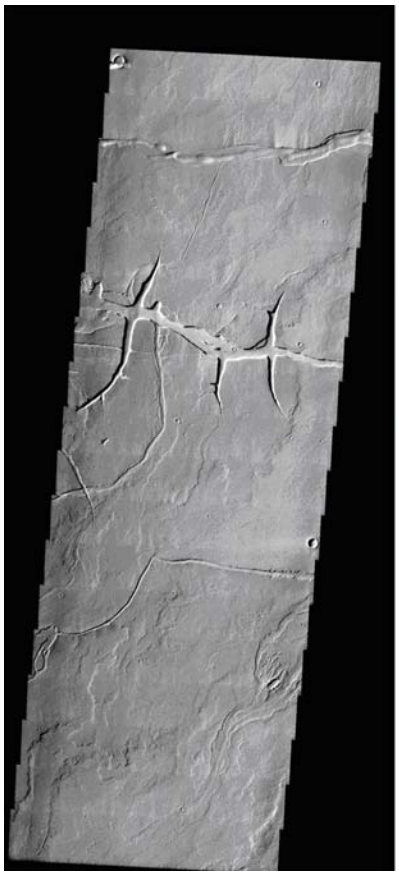

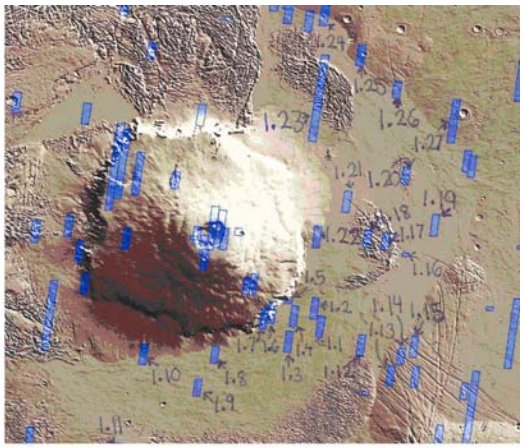

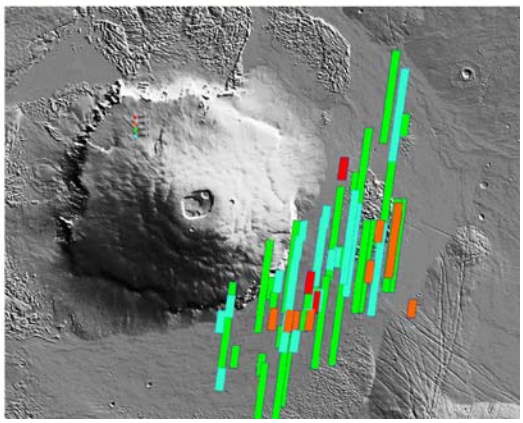

Figure 1 (left): THEMIS VIS image V04311005. This image is the best example of water channels that I have found so far. These channels probably were formed as water rushed out of large cracks in the ground formed under the weight of Olympus Mons. The location of this image is labeled as 1.1 in Figure 2.

Figure 2 (top right): Summary map for the locations of THEMIS images from year 1 of the mission. The purpose of generating these maps was so that I could easily locate the images I downloaded. Base image is a MOLA shaded-relief version of the topography of the landscape around Olympus Mons.

Figure 3 (bottom right): Summary map of images found to contain water channels from Years 1 to 4 of the mission. This map allows me to see the regional pattern of images I am studying. Year 1 images are in red, Year 2 in orange, Year 3 in green and Year 4 in blue.

To aid in the task of distinguishing water channels from lava channels we traveled to the Big Island for field work studying some of the lava channels associated with 1800 eruption of Hualalai volcano. With this background in the visual appearances of lava channels I could then identify the THEMIS images containing channels most likely caved by water (Fig. 3). Of these

images, the best examples were selected to be compared with the MOLA elevation data so that further analysis could be made (Fig. 1).

CHANNEL DIRECTIONS AND TOPOGRAPHIC SLOPE

With the help of Harold Garbeil, I was able to identify the channels which do not flow downhill. In order to do this, I used the program written by Harold called MOLApts, which overlays MOLA elevation data onto THEMIS images containing the best examples of water channels as well as a high level of MOLA coverage. In Figure 4, I show this overlay in the two different ways that I used to study the channel orientation with respect to topography. Figure 4a is a regional view to compare the flow direction to regional gradients. Figure 4b shows a local view, where I investigated the exact relationship between elevation contours and channel orientation. In Figure 4b, it is apparent that the channel floor is parallel to the 1,070 m contour; obviously, the channel should flow straight downhill, so something odd has been identified! Indeed, it had originally been proposed by Mouginis-Mark *et al*. (1982) that there had been some tilting of the lava flows around Olympus Mons in the recent past due to the load of the volcano; perhaps the water channels had been formed after this tilting took place?

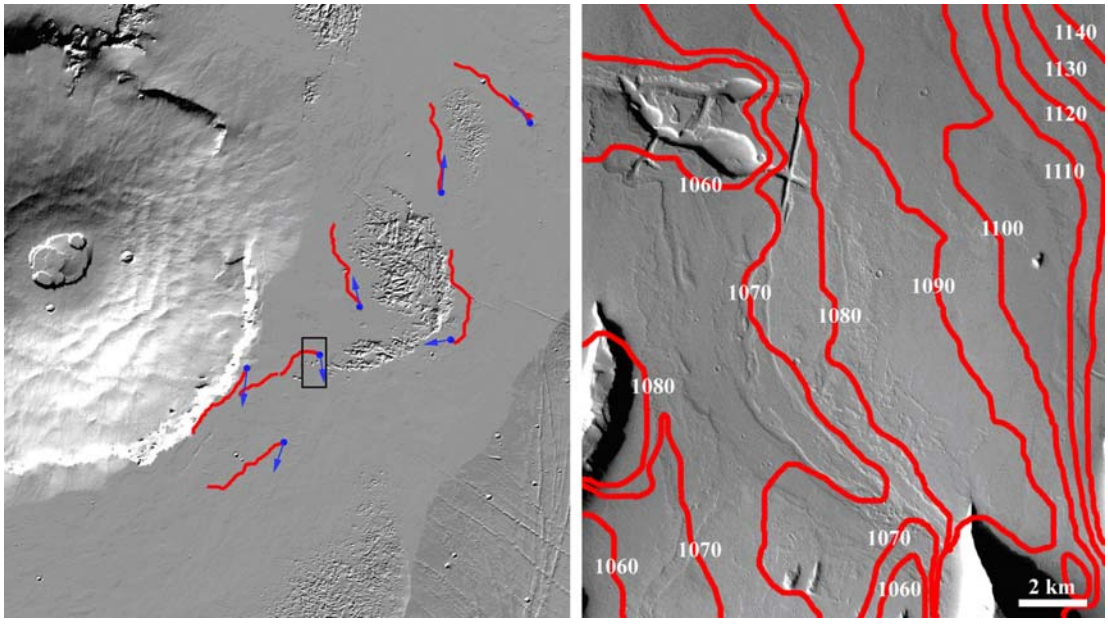

Figure 4: Left (a): Distribution of the seven large channel systems identified to the east of Olympus Mons. Blue arrows show observed flow-paths, and red lines indicate maximum down-slope gradient from the source. Note the mis-match in directions for four of these channels. Outline of Fig. 4b is also shown. Right (b): The source of the channel (located at 16.4°N, 232.6°E) is at the top left of the image, and the channel morphology indicates that the direction of water flow was towards the bottom right. Contours are in red are at 10-meter intervals relative to the MOLA datum. THEMIS image V17029009.

I also checked that the channels really do flow in directions other than straight down-hill. Figure 5a shows my efforts to use a grid of MOLA orbits that cover a channel. I used the program MOLApts to record individual elevations across this channel. In Figure 5b, I again used MOLApts, except this time I generated a profile from multiple MOLA orbits to show the direction of flow of the water within the channel. This work was quite time consuming as I had to work with all the individual MOLA orbits on each of the THEMIS images. Using this

technique, I was able to confirm the local slopes and flow directions (Fig. 5a) as well as the geometry of individual channels (Figs. 5b and 5c).

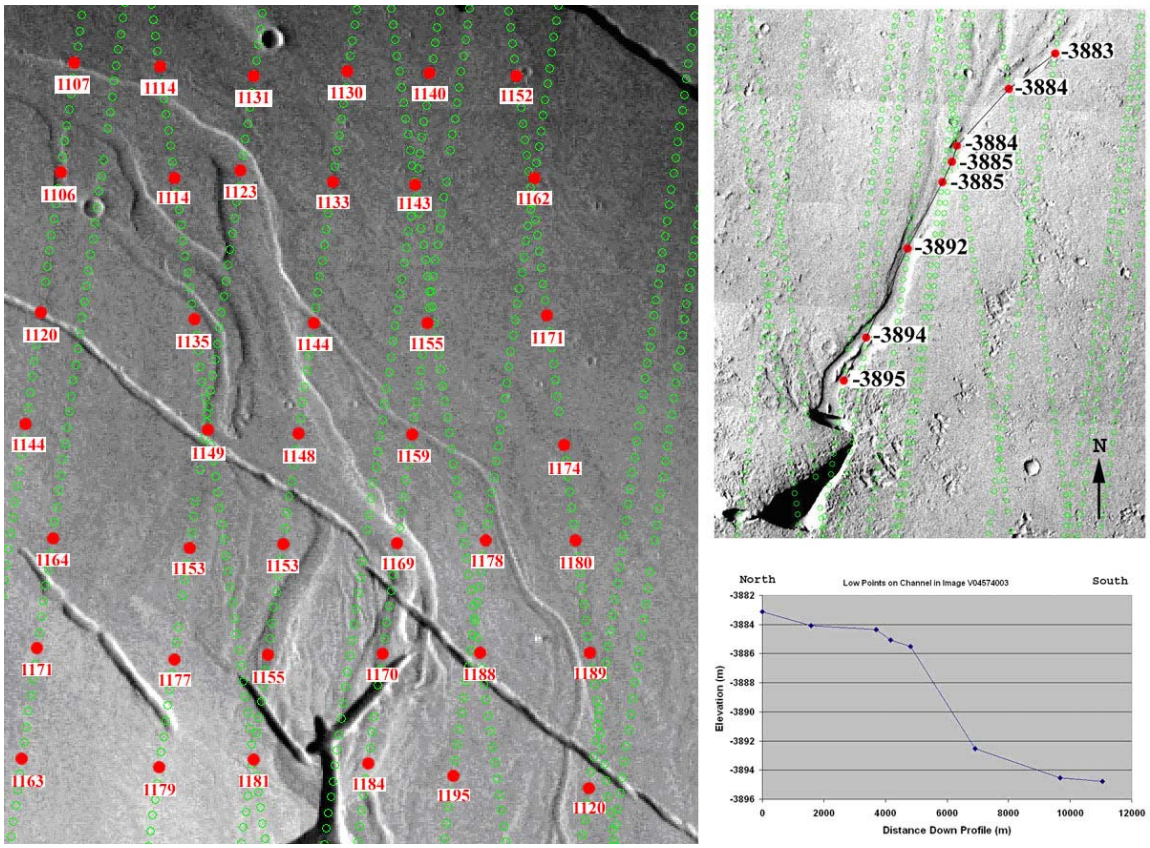

Figure 5. Left (a) MOLA elevation point overlay on THEMIS image V14558021. Image is located to the east of the Olympus Mons aureole, (at 16. 1°N, 233.3°E) displaying numerous water channels flowing from S to NW out of a large crack in the ground. Red dots mark the places where I have measured the elevation (in meters). Green open circles mark all the available MOLA shots. Top Right (b): Not all water flow came from the prominent fractures. To the west of the Olympus Mons aureole (at 22.1°N, 208.7°E), very close to the large fresh impact crater called Tooting, is a fracture (at lower left in this image) that has acted as the sink for surface water. Elevations are derived from raw MOLA shots taken from multiple orbits (shown as faint open green circles). Elevations are in meters relative to the MOLA Mars datum. Part of THEMIS image V04574003. Bottom right (c): Graph generated using the Excel program of the elevation points shown in Figure 5b. Data show that the water once flowed from NE of image down into a large crack to the SW. This is the only example of a water channel on Mars that I have found where the crack in the ground is the sink (rather than source) of the water.

DISCUSSION AND IDEAS FOR FUTURE RESEARCH

What could have caused the odd flow directions for the water channels? In Figure 6, I show a landscape just to the east of Olympus Mons where, instead of "normal-looking" lava flows, there is inverted topography and strange unusually smooth margins to the lava flows. These features could either have formed by a lava flow being erupted under a glacier or a sand dune. Glaciers have been proposed as a possible explanation for other landforms within the Tharsis region (Head *et al*., 2005), and so it is possible that bodies of ice and/or sediment-rich ice were recently found around the base of Olympus Mons volcano. Alternatively, Edgett (1997)

has suggested that there may once have been large volumes of volcanic ash (produced by explosive volcanism on Arsia Mons volcano) in this region. Detailed analysis of Arsia Mons by Mouginis-Mark (2002) also supports the idea that this volcano produced a lot of ash during an explosive phase of its recent history. In either case, the odd channel directions that I have identified would be consistent with the water flowing around obstacles that now no longer exist. Of course, if the water channels also carried sediment, this material would also have been deposited beneath this topography, leaving a similar-looking "mottled" terrain. Further work, including searching for the spatial distribution of this type of landscape is beyond the scope of this project, but offers an interesting new perspective on the origin of the Martian surface that could be productively studied using the high resolution images from the HiRISE experiment currently in orbit on the Mars Reconnaissance Orbiter. I raise the possibility of this type of research in the abstract that I will present at the 7th International Mars Conference (Ambard and Mouginis-Mark, 2007), and hope to produce a peer-reviewed publication on this topic in the coming months with the help of my mentor.

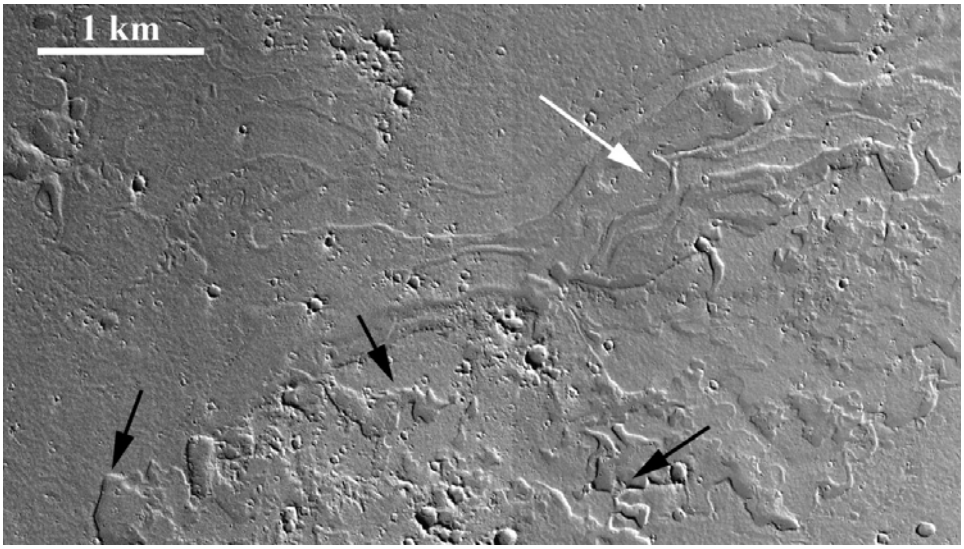

Figure 6: Example of landforms that suggest that unidentified additional topography once was on the surface of Mars just to the east of Olympus Mons at a time when the channels were formed. White arrow points to an odd, channel-like feature except that it has inverted topography. The braided outline of these positive-relief features hint at a depositional environment under unconsolidated material; either a glacier or a dune field would fit this requirement. Black arrows show places where the edges of what could be a lava flow are also odd; they seem to have been confined by an obstacle that has now been removed. Mosaic of MOC images S0500747, S0600674, and S0702594.

CONCLUSIONS

Water channels near Olympus Mons and their odd flow directions can be used to help us understand the changes that have occurred in the area within the past several million years. Channels no longer oriented in a downhill direction either flowed around glaciers or dunes that were later removed, or the channels have been influenced by ground deformation under the weight of the volcano that took place in the relatively recent history of Mars. The model of the water being obstructed by past landforms is consistent with the observed odd surface formations which were most likely formed under ice sheets or sand dunes. Further research should be done

in this subject (using the recently available very high-resolution HiRISE images) to help shed some light on Mars' somewhat mysterious past and apparent climate change.

ACKNOWLEDGENTS

I'd like to thank NASA and the Hawaii Space Grant College for giving me this opportunity to get involved in space research and to learn a whole new set of skills that will benefit me for the rest of my life. I'd also like to thank Dr. Ed Scott for encouraging me in my work and also for encouraging me to apply to other space-related programs. Thanks to Marcia for helping me keep the finances for this project sorted out and to Eric for letting me share his office space. Most of all I'd like to thank Pete Mouginis-Mark for serving as my mentor and for offering me this opportunity to begin with. I cannot easily put into words how much his guidance has helped me not only with this project but with planning the rest of my career. Thanks again for making this all possible.

REFERENCES

Ambard, A. and P. J. Mouginis-Mark (2007). Water channels near Olympus Mons, Mars. *7th International Conference on Mars*, Pasadena, CA July 2007. Abstract # 3043.

Basilevsky, A. T. et al. (2006). Geologically recent tectonic, volcanic and fluvial activity on the eastern flank of the Olympus Mons volcano, Mars, *Geophys. Res. Lttrs. 33*: L13201, doi: 10.1029/2006GL026396.

Edgett, K. S. (1997). Aeolian dunes as evidence for explosive volcanism in the Tharsis region of Mars. *Icarus 130*: 96 – 114.

Head, J. W. et al. (2005). Tropical to mid-latitude snow and ice accumulation, flow and glaciation on Mars, *Nature 434*: 346 – 351.

Mouginis-Mark, P.J. (1990). Recent melt water release in the Tharsis region of Mars. *Icarus 84*: 362 - 373.

Mouginis-Mark, P. J. (2002). Prodigious ash deposits near the summit of Arsia Mons volcano, Mars. *Geophysical Research Letters 29: doi 10*.1029/2002GL015296.

Mouginis-Mark, P. J., S. H. Zisk and G. S. Downs (1982). Ancient and modern slopes in the Tharsis region of Mars. *Nature 297*: 546-550.

PLANNING OF KEPLERIAN ORBITS: EXPLICIT ANALYTIC TRAJECTORIES

Vann Michael Bennett
Department of Mathematics
University of Hawai‘i at Mānoa
Honolulu, HI 96822

ABSTRACT

Periodic trajectories are a topic of interest in the planning of the transfer of a satellite from an initial orbit to an intermediate orbit and then back again to the initial orbit. Satellites must often transfer from one orbit to another, and in so doing, knowledge of the properties of periodic trajectories can ease the process. Our work has shed some light on some symmetrical properties of the controlled three-dimensional Kepler equations of motion as applied to periodic trajectories. Our work has also been to examine a method of explicitly calculating periodic trajectories given certain conditions that must be satisfied. This work on calculating periodic trajectories explicitly enables us to specify the size and the eccentricity of the initial and intermediate orbits and from this obtain a set of explicit functions that describe the controls needed to execute this transfer. This method will yield to us a set of equations with the symmetry properties mentioned above. Prior to this method, a set of control functions was first described and then it was determined where this set of control functions would navigate the satellite. From the described set of control functions was derived, based on the symmetry of the system, a complimentary set of control functions that would navigate the satellite from its intermediate orbit back to its initial orbit. The method of calculating periodic trajectories explicitly is much more powerful in that the size and shape (eccentricity) of the intermediate orbit are used to uniquely determine the set of control functions, rather than the set of control functions uniquely determining the intermediate orbit as was the case before the arrival of this new method. In this paper, we will describe the symmetrical properties inherent to the system. We will also describe certain implicit forms of the three-dimensional Kepler equations of motion that lend themselves to the derivation of explicit trajectories. In addition, we will include graphical simulations that describe both verbally and pictorially the use of the methods described above.

INTRODUCTION

On October 4, 1957, the U.S.S.R. launched Sputnik 1, and became the first nation to put an artificial satellite into orbit around the Earth. This is considered by many to be the height of the Cold War and the gun at the starting line of the Space Race. The U.S.A. answered shortly thereafter with Explorer 1, and for the next few years the two superpowers stayed neck and neck, with the U.S.S.R. a hair’s width in the lead. The American Alan Shepard was in fact the second human to enter space by a mere 23 days, having been beaten by the cosmonaut Yuri Gagarin, who crossed the threshold on April 12, 1961. However, the U.S.S.R. was overtaken on July 21, 1969 when Neil Armstrong stepped from Apollo 11 onto the surface of the Moon, marking a defining moment of the 20th Century as well as the culmination of the Space Race.

SYMMETRY OF THE PROBLEM

Newton's Law of Universal Gravitation in the case of a controlled satellite is as follows:

$$\ddot{r} = -kr/|r|^3 + \gamma,$$

where $\gamma = (\gamma_1, \gamma_2, \gamma_3)$ is the mathematical description of the thrust produced by the satellite throughout its flight. A change of coordinates from Cartesian to Gaussian gives the following equivalent equation:

$$\dot{\vec{x}} = \frac{d\vec{x}}{dt} = \vec{f}_0(\vec{x}) + \sum_{i=1}^{3} \gamma_i \vec{f}_i(\vec{x}),$$

where $\vec{x} = \begin{pmatrix} P \\ e_x \\ e_y \\ h_x \\ h_y \\ L \end{pmatrix}$, $\vec{f}_0 = \sqrt{\frac{\mu_0}{P}} \begin{pmatrix} 0 \\ 0 \\ 0 \\ 0 \\ 0 \\ W^2/P \end{pmatrix}$, $\vec{f}_1 = \sqrt{\frac{P}{\mu_0}} \begin{pmatrix} 0 \\ \sin L \\ -\cos L \\ 0 \\ 0 \\ 0 \end{pmatrix}$, $\vec{f}_2 = \sqrt{\frac{P}{\mu_0}} \begin{pmatrix} 2P/W \\ \cos L + (e_x + \cos L)/W \\ \sin L + (e_y + \sin L)/W \\ 0 \\ 0 \\ 0 \end{pmatrix}$,

and $\vec{f}_3 = \frac{1}{W}\sqrt{\frac{P}{\mu_0}} \begin{pmatrix} 0 \\ -Ze_y \\ Ze_x \\ \frac{C}{2}\cos L \\ \frac{C}{2}\sin L \\ Z \end{pmatrix}$ with $\begin{cases} W = 1 + e_x \cos L + e_y \sin L \\ Z = h_x \sin L - h_y \cos L \\ C = 1 + h_x^2 + h_y^2 \end{cases}$.

Consider the following transformations:

$R_1(x) = R_1(P, e_x, e_y, h_x, h_y, L) = (P, e_x, -e_y, h_x, -h_y, L)$,
$R_2(\gamma) = R_2(\gamma_1, \gamma_2, \gamma_3) = (\gamma_1, -\gamma_2, \gamma_3)$, $R(x, \gamma) = (R_1(x), R_2(\gamma))$, and
$F(x, \gamma) = f_0(x) + \sum_{i=1}^{3} f_i(x)\gamma_i$.

In the theory of dynamical systems, a reversing symmetry is a function T, such that $dT(x)/dt = -f(T(x))$ for some function f. Here, $\dot{x} = f(x)$ represents a dynamical system and $\dot{x} = f(x, \gamma)$ represents a controlled system.

Observe that $dR_1(x)/dt = -F(R_1(x), R_2(\gamma))$. Given the overwhelming similarity of this form with that of reversing symmetries in the theory of dynamical systems, *R* will be referred to now as a reversing symmetry in the *controlled case.* Observe that if $P, e_x, e_y, h_x, h_y, L, \gamma_1, \gamma_2$, and γ_3, where $e_y = h_y = 0$ at the junctions of t = 0 and t = T, satisfy the 3D-Controlled Kepler Equation on the time interval [-T,0], then the result of applying the reversing symmetry *R* is a trajectory continuous with the first and complementing the first into a periodic trajectory. A consequence of the equation

$$dR_1(x)/dt = -F(R_1(x), R_2(\gamma))$$

is that if $(x(t), \gamma(t))$ is a trajectory for a controlled system, then so is

$$(R_1(x(-t), R_2(\gamma(-t))).$$

Moreover, both trajectories are defined for periods of time of equal duration.

To understand the aspect of continuity in the above situation, consider the following sets of equations representing the first and second halves of the trajectory, respectively:

$$(P(t), e_x(t), e_y(t), h_x(t), h_y(t), L(t))$$

$$(P(T-t), e_x(T-t), -e_y(T-t), h_x(T-t), -h_y(T-t), L(T-t)).$$

Observe that if $e_y = h_y = 0$ at the junctions of t = 0 and t = T, then *P(t)* at the beginning of the first half is equal to *P(t)* at the end of the second half. This is in fact true for all of the variables describing the trajectory.

OBTAINING PERIODIC TRAJECTORIES

Imagine an arbitrary orbit along with an associated set of arbitrary control functions (denote this by $(P(t), e_x(t), e_y(t), h_x(t), h_y(t), L(t))$ and $\gamma = (\gamma_1, \gamma_2, \gamma_3)$, respectively). The discussion above concludes that this initial path can be extended into a periodic trajectory through the application of the transformations $R_1(x)$ and $R_2(\gamma)$ to the initial orbit and control functions. In essence, a particular ellipse (satellites without propulsion move on elliptical orbits) and a particular set of control functions are given, and from this another ellipse and another set of control functions (this set of control functions will lead the satellite to its initial elliptical orbit) are gotten. The following figures illustrate this concept. Observe the continuity between the beginning of one trajectory and the end of the other.

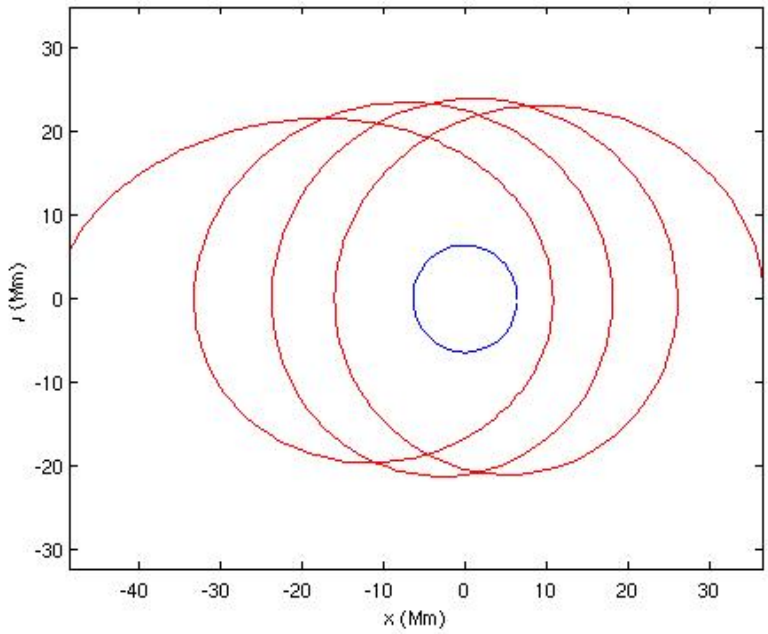

Figure 1: a graphical representation of a satellite on some arbitrary elliptical orbit put under the direction of an arbitrary set of control functions.

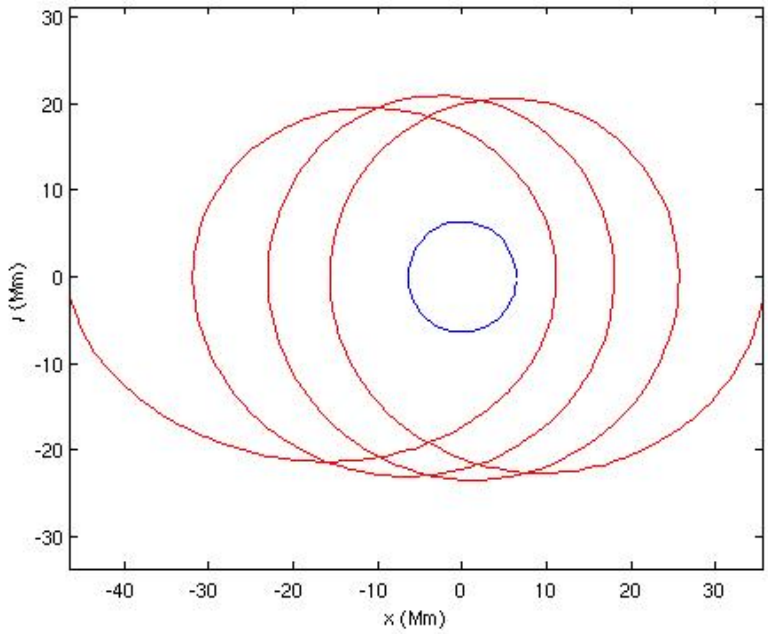

Figure 2: the trajectory depicted here is the result of applying the transformations $R_1(x)$ and $R_2(\gamma)$ with the orbital and control function parameters of the trajectory of Figure 1.

This method of obtaining periodic trajectories, however, leaves much to be desired. For one, the ellipse located at the end of the initial set of control functions operation is only determinable through computer simulation. It would be convenient to be able to specify the precise parameters of this ellipse. Also desirable is a control function given in an explicit analytic form. Explicit analytic equations are readily manipulated and lend themselves to computer calculations more so than their implicit counterparts.

CALCULATING EXPLICIT ANALYTIC TRAJECTORIES

Given two orbits, a method of calculating an explicit analytic trajectory transferring a satellite between the orbits and then back again has been developed. The mathematical justification of this method is fairly advanced, and hence will not be discussed in this paper. In essence though, this method involves the input of two sets of data that describe the two orbits and the output of one set of data that describes the control function necessary to complete the transfer. The following equations are at the core of this method:

$$\mathbf{e}' = P(z + \mathbf{e} \cdot \mathrm{Re}(z, \mathbf{e}^{iL})_C) \text{ and}$$

$$\gamma = k / |r|^2 T^{-1} R^{-1} e' \text{ where}$$

$$T = \begin{bmatrix} 1 & D/W \\ 0 & 2 \end{bmatrix} \text{ and } R = \begin{bmatrix} \sin L & -\cos L \\ \cos L & \sin L \end{bmatrix}. \text{ And it can be assured that the}$$

following condition on the control is met (this reflects the fact that possible thrusts are finite)

$$\|\gamma\|_\infty \le \Gamma .$$

This method was developed using optimal control theory.

Whereas in the first method an initial elliptical orbit and set of operating control functions are specified, only an initial orbit and intermediate orbit are specified in the second method. The ability to specify the elliptical orbit to which the satellite eventually travels is very valuable. Specifying the initial control function, however, is not particularly sought after as a goal.

The first method involves the input of an initial elliptical orbit and a set of operating control functions and the output of an intermediate orbit and a set of control functions that will bring the satellite back to its original elliptical orbit. The second method on the other hand involves the input of an initial and intermediate elliptical orbit and the output of the control functions necessary to complete the transfer. The differences are subtle but important.

ACKNOWLEDGEMENTS

The author would like to thank his mentor Dr. Monique Chyba along with Dr. Thomas Haberkorn, who was vital for the numerical integration with MATLAB. The author would also like to thank the Hawai‘i Space Grant Consortium for giving him this opportunity to experience the research process. Dr. Ed Scott, Marcia Rei Sistoso, and everyone else involved with the Hawai‘i Space Grant Consortium deserve special recognition for their efforts in facilitating the research experience for students participating in this program. Thank you very much.

REFERENCES

Hairer, E. (2004) *Solving Ordinary Differential Equations*, Springer Verlag, Berlin.

Lamb, J.; Roberts, J. (1997) Time-reversal symmetry in dynamical systems: a survey. *Physica D.*

Pollard, H. (1966) *Mathematical Introduction to Celestial Mechanics*, Prentice-Hall, Inc., New Jersey.

Sontag, E. (1998) *Mathematical Control Theory: Deterministic Finite-Dimensional Systems*, Springer Verlag, Sydney.

DISCRIMINATING FIREWEED IN HAWAII COUNTY PASTURES USING REMOTE SENSING

Kimberly Bieniasz
Department of Natural Resources & Environmental Management
University of Hawai‘i at Mānoa
Honolulu, HI 96822

ABSTRACT

Fireweed has been reported as a serious problem in pasture areas, causing yearly losses of $2 million in Australia. The weed reduces forage yield and is poisonous to livestock. The purpose of this study was to use an Analytical Spectral Device (ASD) FieldSpec Pro FR field spectrometer to determine the detectability of Fireweed and whether the use of satellites would be feasible in Hawaii County. Three sites were visited representative of typical Fireweed infestations including Parker's Ranch, Pu'u Wa'awa'a, and Mauna Kea. Sequential reflectance measurements from 100 - 0 percent flower cover were made to observe changes in Fireweed reflectance signatures with flower cover. In addition, transect measurements were conducted for other pasture vegetation types, providing a "background noise" level. These two data sets were analyzed together to find a detection limit for the flowers. The analysis have shown that yellow flowers can be used as an attribute for detecting Fireweed and that the detection limit was found to be ~15% flower cover (~80 yellow flowers and buds per 1.2 sq. ft. Using the ASD to gather information about Fireweed it became evident that the weather conditions in the study region were not best for optimal use of the instrument. However, so long as sky conditions remained consistently cloudy, useful preliminary data could still be gathered. Remote sensing is an applicable tool in detecting Fireweed though it may be best to observe ground vegetation from a helicopter or use instruments less sensitive to environmental elements than ASD.

1. INTRODUCTION

Senecio madagascariensis Poiret also known as Fireweed native to Madagascar and South Africa is a highly invasive weed in Hawaii. The weed is believed to have first appeared in Hawaii County pastures in the early 1980s. In Australia, scientists have reported that Fireweed has been a serious problem in the pastures of Queensland and New South Wales. It has caused yearly losses of about $2 million because the weed reduces forage yield and is also poisonous to livestock (Motooka et al., 2004). In the islands of Hawaii and Maui, the weed has already taken over large areas of pasture and range lands. In some areas about 60 percent of the vegetative cover has been discovered to be Fireweed (Thorne et al., 2005). An infestation has also been found in Kalihi Wai on the island of Kauai.

Pyrrolizidine alkaloids (PA) are the principle toxins in *Senecio* which are harmful and can be lethal to livestock depending on their amount of consumption. Out of 1,200 different species of the *Senecio* genus identified 25 species have been found to be toxic to animals (Thorne et al., 2005). Samples of the weed taken from Hawaii County and Maui were found to contain 10 different PA concentrations (Thorne et al., 2005). Similar to the problem in Australia, the toxic weed now poses an economic problem for the farmers and ranchers of Hawaii. The problem is amplified by the weed's prolific nature. *Senecio* produces numerous composite

flowers in which a single flower can produce up to 150 seeds that are wind dispersed and can remain viable for several years (Thorne et al., 2005). An entire plant can produce up to 30,000 seeds. The weed grows annually from seed but under certain conditions it may also reproduce vegetatively. In moist soils, roots and shoots can develop from the weed's stem nodes which become new, self-supporting plants (Thorne et al., 2005).

Due to Fireweed's fruitful and adaptable nature to different environments, the University of Hawaii's Department of Human Nutrition, Food and Animal Sciences, has developed an "Adaptive Management Approach" to control the weed. One of the critical actions identified in this approach is to investigate how far and where *Senecio* has spread in relation with environmental conditions, including elevations, weather conditions, and soil types. Remote sensing can offer a great potential in accomplishing this goal. Dr. Tomoaki Miura of the University of Hawaii's Department of Natural Resources and Environmental Management specializes in remote sensing of vegetation and soils, and GIS. By determining where *Senecio* has spread, sites most susceptible to future invasion can be identified and protected. However, a study was needed to determine whether remote sensing would be effective at differentiating Fireweed from other plant species. Thus, the objectives of this study were: 1) to assess the capabilities of remote sensing in detecting/differentiating Fireweed, and, if so, 2) to determine the detection limit of Fireweed with remote sensing methods.

2. BACKGROUND

Remote sensing is defined as "the acquisition of information about an object without touching it by means of some photographic or sensory instrument" (Jenson 2000). Different plant species often have different internal and external structures, which causes different plants to interact with electromagnetic energy from the sun differently. This individuality caused by a plants structure in turn reflects different proportions of energy in the solar reflective region of the electromagnetic (EM) spectrum (400 – 2500 nm), e.g., the blue, green, red and near-infrared wavelength regions. Plotting "reflectance" values at specific wavelengths, a "spectral signature" can be seen. Many plant species show different spectral signatures that are determined by a plant's color or pigment concentrations, health or water content, canopy structure, and biomass (Ustin, et al., 2004). For example, a green plant contains chlorophylls (photosynthetically-active pigments) that absorb much visible lights, resulting in a low visible reflectance (Curran, 1989). Likewise, greater biomass and water content would generally produce a greater near-infrared (NIR; ≈700-1400nm) and lower shortwave-infrared (SWIR; ≈1400-2400nm) reflectance, respectively (Ustin et al., 2004). All these characteristics inter-relate to each other making it difficult to comprehend their effects on reflectance (Asner, 1998). Fireweed is characterized by its yellow flowers and, thus, we hypothesized that yellow flowers and their abundance would be the "key" biophysical factor that makes Fireweed detectable by remote sensing.

To facilitate the assessment of vegetation with remote sensing, scientists have been using spectral vegetation indices (VIs). VIs maximizes sensitivity to plant biophysical parameters such as biomass or color by combining some particular wavelength regions, or bands, within the solar reflective region. VIs can partially normalize the internal and external effects which affect reflectance measures to make more consistent spatial and temporal comparisons (Jenson 2000). Maximizing sensitivity allows the index assessment to be available for a broad range of vegetation conditions while facilitating validation and calibration of the index (Jenson 2000). Internal effects include canopy background variations that are reflected in a spectral signature,

whereas external variations include the effects of the Sun and viewing angle, and variations affected by the atmosphere. The ratio vegetation index (RVI) and the normalized difference vegetation index (NDVI) are NIR to red reflectance ratios which respond to changes in the "greenness" of vegetation (Tucker, 1979). The NIR region ranges from about 700 - 1000 nm. The red reflectance region ranges from about 650 - 700 nm (Jenson 2000). Following these formulations, we also hypothesized that yellowness indices (YI's) could be formulated and used to effectively detect the yellow flowers of Fireweed.

3. MATERIALS AND METHODS

Three sites were selected in Hawaii County, representing typical Fireweed infestations, for this study. These included areas on Parker's Ranch, Pu'u Wa'awa'a, and Mauna Kea.

Reflectance measurements were made with an ASD field spectrometer between the hours of 9:00am and 5:00pm during consistent sky conditions. Sky conditions were evenly cloudy. Optimal measurement conditions require clear skies; however, clear sky conditions are rare in this region of Hawaii County and cloudy conditions dominate. If there had been clear skies the spectrometer could not have been used between 11:45am and 1:45pm. The sun angle between those times (near solar noon) would have caused a shadow on the ground vegetation being measured, disturbing their reflectance. Reflectance of the white reference plate was measured before and after each ground measure to reduce reflectance noise caused by the changing sky conditions. All points of measurement were delineated by a plastic hoop marking an area of 1.2 square feet. The ASD fiber optic cable was held right above the target and positioned relative to the center of vegetation height so that the exact area delineated by the hoop could be measured.

Two reflectance data sets were obtained in these sites. One data set was obtained along three 100 meter transects (two in Parker's Ranch and one in Pu'u Wa'awa'a) for estimating the "background noise" level, while the other data set was acquired in the Mauna Kea site for obtaining reflectance signatures of flowering Fireweed.

3-1. Background Noise

To assess the reflectance of Fireweed with other pasture vegetation, three 100 meter transects were drawn randomly within the pasture sites in Parker's Ranch and Pu'u Wa'awa'a. Within each transect 10 points were chosen at every 10 meters. At each point, reflectance was measured (plate, vegetation, plate). After taking each reflectance measurement, vegetation within the hoop was identified for species, and then harvested, and weighed.

3-2. Detecting Yellow Flowers

To assess the effect of yellow flowers on the spectral signature of Fireweed a test was conducted taking sequential reflectance measurements from 100 - 0 percent yellow flowers. The purpose of the test was to find a detection limit for the yellow flowers. First a thick patch of Fireweed in bloom was located within the Mauna Kea site to remove the effects of other vegetation on reflectance. A plastic hoop was placed to delineate an exact area for reflectance measurements and all of yellow flowers and yellow buds within the plastic hoop were counted (100 percent flowers or 349 flowers and buds). From that count, 10 percent (35 flowers and buds) of the flowers and buds were removed sequentially until no flowers or yellow buds were left. Starting at 100 percent flowers, reflectance was measured (plate, vegetation, plate). After 100 percent reflectance was measured, 10 percent of the flowers and yellow buds were removed

evenly across the point area and 90 percent flowers were measured. This procedure was continued until there were no flowers or yellow buds remaining in the point area and 0 percent flowers (i.e., no flowers at all) were measured in the end.

3-3. Yellowness Indices

The ratio vegetation index (RVI) and the normalized vegetation index (NDVI) involve a ratio of the NIR to the red reflectance regions:

$$RVI = \text{NIR/Red} \quad (1)$$

$$NDVI = (\text{NIR} - \text{Red})/(\text{NIR} + \text{Red}) \quad (2)$$

Yellowness indices (YI_1 and YI_2) were created by changing the NIR to red reflectance ratios to yellow reflectance (y) to blue reflectance (b) ratios. The yellow reflectance region from 578 - 592 nm and the blue reflectance region from 475 - 485 nm were used to form the YI's.

$$YI_1 = y / b \quad (3)$$

$$YI_2 = (y - b) / (y + b) \quad (4)$$

These two YIs were computed from the reflectance data sets described in the above two sections and used to test the hypotheses.

4. RESULTS

4-1. Typical Vegetation Spectra (Background Noise Level)

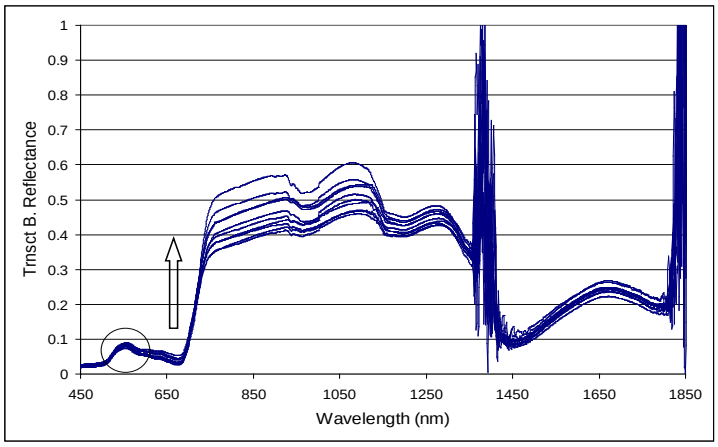

Figure 1. Typical spectra of green vegetation measured under evenly cloudy conditions collected from Transect B using an ASD FieldSpec Pro FR field spectrometer at Parkers Ranch.

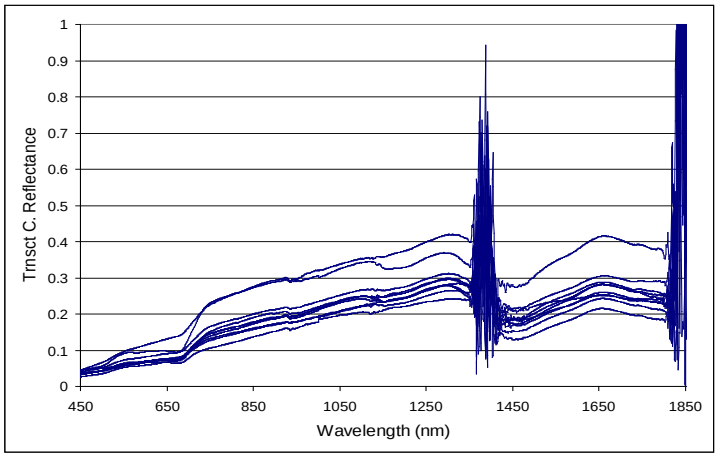

Figure 2. Typical spectra of dry, light brown/yellow vegetation measured under evenly cloudy conditions collected from Transect C using an ASD FieldSpec Pro FR field spectrometer at Pu'u Wa'awa'a.

In the field, several types of Fireweed infestations were observed. On Parkers Ranch Fireweed was observed in grazed and un-grazed pastures which primarily included Kikuyu Grass and a few other types of grasses. In the area Fireweed grew sporadically, often in small patches or as a single plant throughout the grass. A similar scenario was observed along the upper Pu'u Wa'awa'a area amid overgrown pasture land. In either setting, Fireweed did not establish in areas already well established by pasture grasses like Kikuyu. In the lower Pu'u Wa'awa'a area infested by Fountain Grass, another invasive plant in Hawaii County, Fireweed was less common or had already seeded or dried out.

The thickest and largest infestations of Fireweed were observed at Mauna Kea. Around the hunting grounds at Mauna Kea the area was not

well maintained and Fireweed grew profusely. This was especially true along the dirt road trails. Consistent throughout all scenarios, Fireweed grew amid most other vegetation which affected the reflectance of Fireweed observed measurements. Relative to Fireweed, pasture grass such as Kikuyu Grass and also Fountain Grass are considered background vegetation in the reflectance measurements. Figures 1 and 2 are examples of spectral signatures of the "background noise", or background vegetation typically observed. The transect figures provide an example of green (Figure 1) and yellow or dry (Figure 2) vegetation.

Figure 1 demonstrates the variability in reflectance across a 100 meter transect of un-grazed pasture grasses with little or no Fireweed. The peak around 550 nm (the circled region in the figure) is often referred to as the "green peak" which is followed by a sharp increase after 680 nm (marked by the arrow) referred to as the "red-NIR transitional" region. These are typical features observed in spectral reflectance of green vegetation. Note that the spectra of the green vegetation are consistent (overlapping) from about 450 - 700nm.

Figure 2 shows the variability in reflectance across a 100 meter transect over a Fountain Grass-dominated area with little Fireweed. Vegetation in the area were very dry and, unlike green vegetation in Figure 1, the spectra slope of dry vegetation was "dull" lacking prominent peaks in the visible color region at around 550 nm and an reflectance increase in the red-NIR transitional region was also modest. Note that the dry vegetation spectra in Figure 2 are quite variable and clearly defined.

4-2. Change in Reflectance with Yellow Flower Cover

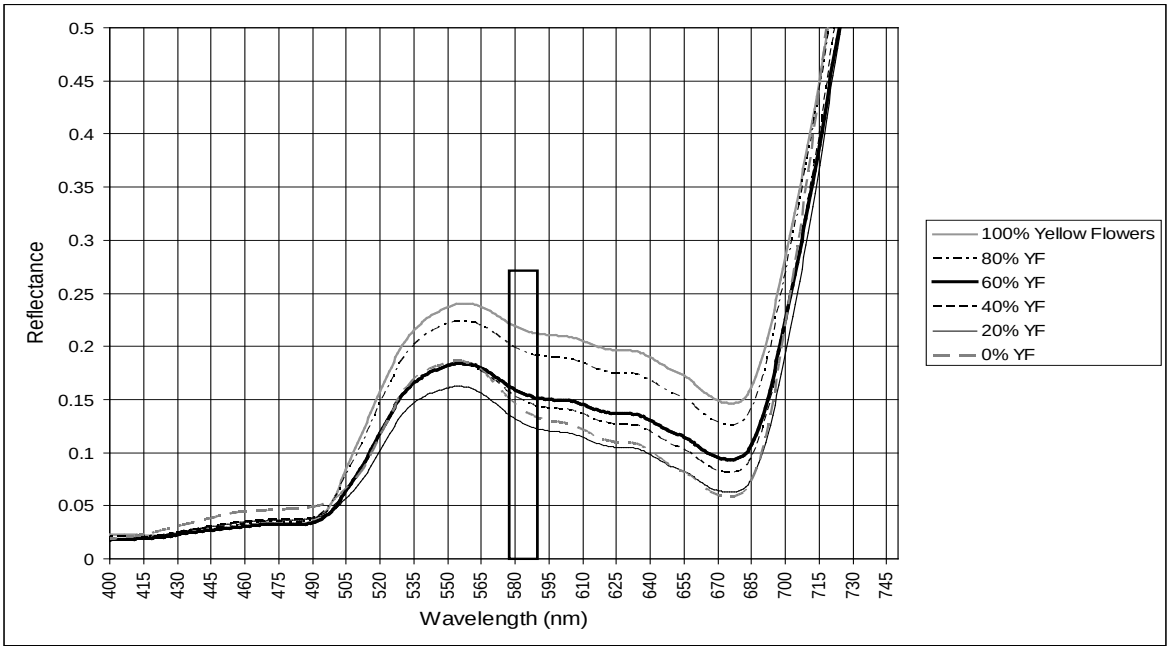

Figure 3. Assessment of the effect of yellow flowers on the spectral signature of Fireweed using an ASD FieldSpec Pro FR field spectrometer at Mauna Kea under even cloud cover.

In Figure 3, a visible-NIR portion of the spectral signatures taken for various yellow flower covers are plotted. The rectangle in the figure outlines the 578-592 nm wave band used to

create the yellowness indices. Within the rectangle and also for the wavelength region from 500 nm - 700 nm, the systematic decreases in reflectance are seen with decreasing flower cover.

In the experiment, about 349 yellow flowers and yellow buds were counted. About 35 yellow flowers and buds were removed after each percent cover was measured by the ASD. However, by the final round it seemed that more buds were opening up to become "yellow buds" while ASD measurements were being taken. After the 10 percent flower cover was measured, 54 yellow flowers and buds were removed in order to measure 0 percent flower cover. Of the 54 count, more yellow buds than flowers were removed.

From the results, reflectance decreased sequentially from 100 percent flower cover to 40 percent flower cover between 578-593 nm (Figure 3). The 0 percent flower cover seemed to reflect greater than 20 percent flower cover. Overall, the spectra became less distinctive after 60 percent flower cover. The spectra from 60 percent yellow flower cover to 20 percent cover overlapped, although the new yellow buds may have had some effect (Figure 3).

4-3. Yellowness Indices

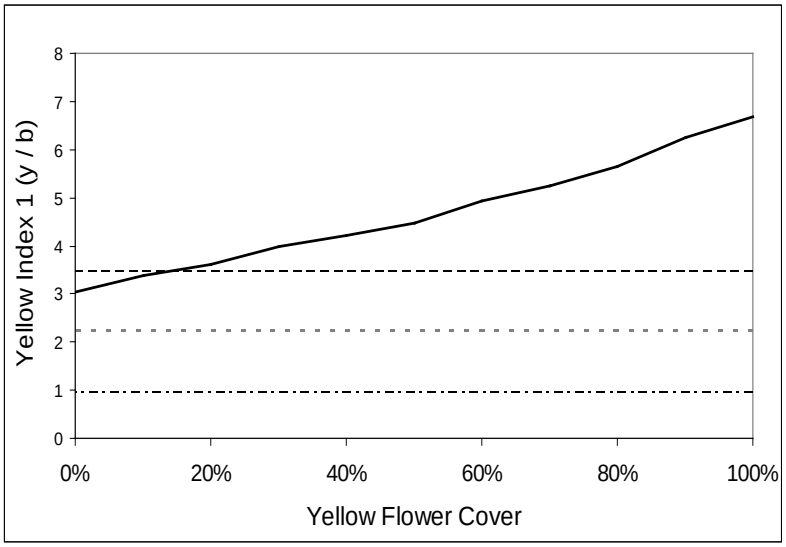

Figure 4. Yellowness Index 1 and decreasing reflectance of Fireweed plotted against percent of yellow flowers.

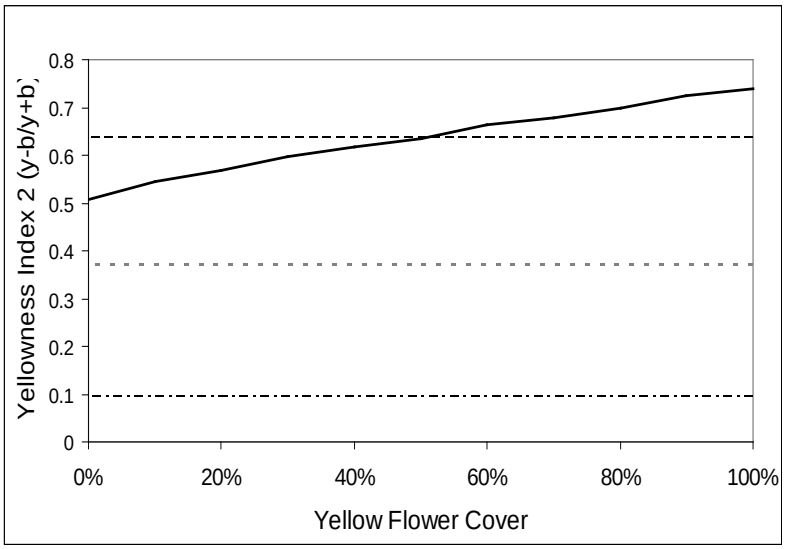

Figures 4 and 5 plot the YI's against yellow flower cover percent. The center horizontal lines in Figures 4 and 5 are the mean values of YI_1 (2.23017) and YI_2 (0.369594). The top/bottom horizontal lines in Figure 4 are the mean value of YI_1 plus/minus three standard deviations (3.489152/0.971188). The top/bottom horizontal lines in Figure 5 are the mean value of YI_2 plus/minus three standard deviations (0.639493/0.099695). The range of YI values, or the background level, was computed from reflectance spectra measured along the three transects.

Figure 4 shows that, with YI_1, the yellow flowers of Fireweed are detectable at about $\geq$15 percent yellow flower cover. This seems to correlate best to the 578 - 593 nm band (Figure 3) where the 0 percent flower cover seemed to reflect greater than the 20 percent flower cover. That was unlike the consecutive descending reflectance observed from 100 - 40 percent flower cover within the band width.

Figure 5. Yellowness Index 2 and decreasing reflectance of Fireweed plotted against percent of yellow flowers.

With YI_2 (Figure 5), the yellow flowers of Fireweed are detectable at about ≥51 percent yellow flower cover. This seems to correlate best to the general spectras in Figure 3 where the 60-20 percent flower cover spectras overlap and are the least defined.

5. DISCUSSION

Flowering Fireweed, in full bloom, was the easiest to detect. From field observations it was evident that the weed goes through various growth stages (Pre- flowering, flowering, seeding (dry), etc.) which change biomass and colors associated with the weed (green, yellow, brown). This issue will make detecting Fireweed difficult, especially as individual weeds go through their various stages at different times. When some of the weeds begin flowering, some may not, and some may already be seeding or dried out.

The yellow flowers of Fireweed are just one of many characteristics of the weed which may affect its spectral signature. However the ratio of yellow flowers to the rest of the plants biomass may not always be great enough to affect its reflectance significantly. The different structure and biomass of Fireweed could create the greater difference in the weeds reflectance signature compared to other green pasture vegetation. Fireweed is a branched herb that develops dark green leaves in an alternating pattern along the stem. This is unlike typical grasses characterized by dense patches of long, slender leaves. Also, Fireweed is known to reduce the overall forage production of a pasture area by 30-40 percent when the vegetative cover of Fireweed reaches 60 percent (Thorne et al., 2005). Reduced biomass in *Senecio* dominated areas may produce higher visible, lower NIR, and higher SWIR reflectance than in other pasture grass areas.

In using the ASD to gather information about Fireweed it became evident how the weather conditions in Hawaii County were not best for optimal use of the instrument. Although the visible region of the spectra about 400- 750 nm was applicable (Figure 3), the overall spectral signature (450-1850 nm) of Fireweed from the Yellow Flower experiment was too noisy for general comparison due to inadequate environmental issues. However, we also found that so long as sky conditions remained consistently cloudy, useful data could still be gathered.

In detecting Fireweed, background noise/ vegetation will be another issue that must be dealt with. This will make detecting the weed in smaller, less dense patches much more difficult. However, from field observations the flowering weed was quite obvious with its yellow flowers amongst other green vegetation. Over smaller regions of the island, it may be best to observe fields from above using a helicopter to detect where Fireweed is growing. From the ground view (side view), the flowers are less obvious. The plants are about a foot high on average in the pasture regions and the yellow flowers only show on the uppermost portion of the plant.

6. CONCLUSION

From the study, it is felt that remote sensing is an applicable tool in detecting Fireweed from other pasture vegetation, primarily grasses, because the weed has a very different structure and its yellow flowers are visibly detectable. Using ASD the flowers are detectable at, at least ≥15 flower cover. Nevertheless, weather conditions in Hawaii were not best for optimal use of the instrument and the issue may be the same for satellites. Cloud cover would prohibit satellites from receiving a clear picture of the ground vegetation making it difficult to observe and locate where Fireweed has spread to throughout the island. In future studies concerning the detection of

Fireweed, it may be best to use photographic methods from a helicopter that are less sensitive to environmental elements than ASD.

ACKNOWLEDGEMENTS

The author would like to thank NASA, the Hawaii Space Grant Consortium, and Dr. Luke Flynn for granting the opportunity to study under an outstanding mentor Dr. Tomoaki Miura of the University of Hawaii Department of Natural Resources and Environmental Management*. A special thanks to Dr. Jonathan Deenik* and Dr. Mark Thorne and Matt Stevenson of the Cooperative Extension Service (UH) office in Waimea, Hawaii for their hard work and creative input out in the field. This was an interesting, entertaining, and enjoyable experience. Thank you all!

REFERENCES

Adams, M. L., Philpot, W. D., Norvell, W. A. (1999) *Yellowness index: an application of spectral second derivatives to estimate chlorosis of leaves in stressed vegetation*. Vol. 20. Issue 18, 3663 – 3675.

Asner, G. P. (1998) Biophysical and biochemical sources of variability in canopy reflectance. *Remote Sensing of Environment* 64(3):234-253.

Curran, P. J. (1989) Remote sensing of foliar chemistry. *Remote Sensing of Environment* 30(3):271-278.

Jenson, J. R. (2000) *Remote sensing of the environment: An earth resource perspective*. New Jersey: Prentice Hall.

Motooka, P., Nagai, G., Onuma, K., DuPonte, M. Kawabata, A., Fukumoto, G., and Powley, J. (2004) *Control of madagascar ragwort (aka madagascar fireweed, senecio madagascariensis).* University of Hawaii at Manoa, College of Tropical Agriculture and Human Resources publication WC-2.

Thorne, M., Powley J. and Fukumoto, G. (2005) *Fireweed control: An adaptive management approach*. Cooperative Extension Service: University of Hawaii.

Tucker, C. J. (1979) Red and photographic infrared linear combinations for monitoring vegetation. *Remote Sensing of Environment* 8(2):127-150.

Ustin, S. L., Jacquemoud, S., Zarco-Tejada, P. J., and Asner, G. P. (2004) Remote sensing of the environment: State of the science and new directions. In S. L. Ustin (Ed.), *Remote Sensing for Natural Resource Management and Environmental Monitoring. Manual of Remote Sensing (3rd Ed.) Vol. 4.* John Wiley & Sons, Inc., Hoboken, New Jersey, pp.679-729.

BRINGING MARS SCIENCE TO HAWAI'I'S STUDENTS: MAKING SCIENCE CULTURALLY RELEVANT TO NATIVE HAWAIIAN AND PACIFIC ISLANDERS

Michelle Lee Bradley
Department of Interdisciplinary Studies
University of Hawai'i at Mānoa
Honolulu, HI 96822

ABSTRACT

The goal of this yearlong work was to develop standards-based, hands-on 6th-8th grade Mars science curriculum that is culturally relevant to Hawaii. The work was done as part of "Bringing Mars Science to Hawaii's Students: An exercise in cultural adaptation, inclusivity and partnership", which is a study being done by Dr. Barbara Bruno through NASA's Education and Public Outreach program. I began my fellowship study by familiarizing myself with existing high-quality Mars science curriculum and I then adapted those lessons to make it more relevant to Hawai'i's students (especially native Hawaiian and Pacific Islander students). By the end of the first semester as a fellow I developed an 8-lesson unit that linked Mars science and the Polynesian culture of exploration and Hawaiian sustainability. I was also able to pilot a few of the lessons at cooperating public schools to gain insight and feedback from the students and their in-service teachers. During the second semester of my fellowship I was able to pilot my entire 8-lesson unit, which was highly beneficial to the overall quality of the final lessons. During the second semester of work I was also able to test and finalize a board game that Dr. Bruno and I created. The eighth lesson of the unit is a board game called "Hawai'i to Mars: A Voyage of Discovery," which is an informal assessment tool for the teacher. The board game culminates all of the knowledge gained from the previous 7 lessons. This project is relevant to NASA's Strategic Goal 6 on K-12 education in science, technology, education and mathematics

INTRODUCTION

I concentrated my efforts on adapting existing Mars science curriculum to (1) make both the content and teaching methodologies culturally relevant to Hawaiian and Pacific Islanders and (2) align them with Hawaii Science Content and Performance Standards (HCPS III) and national standards for inquiry. Although this new curricula will benefit all of Hawai'i's students, I was interested in helping Native Hawaiians and Pacific Islanders, who have among the poorest educational performance and are the least represented group among college graduates when compared to other ethnic and racial groups in Hawaii. In order to gain insight into Hawai'i's classrooms, I developed partnerships with Primary and Secondary school teachers at different public schools around the islands. The reason that I created these partnerships with in-service teachers was to be able to pilot my lessons to their class of students and in turn allow the teachers to critique and offer suggestions as to what worked and did not work in the lessons. The partner teachers were selected because they taught classes with a high number of Hawaiian and Pacific Islander students. The finalized 8-lesson unit is available to teachers as a resource online.

METHODS

The methods used to develop the curriculum and assess the students understanding of the materials covered were two separate endeavors. In order to obtain a real sense of how the students were retaining the information from the entire unit, a Pre-test and a Post-test was administered. The Pre and Post-tests were identical, having the exact same questions on both tests. The Pre-test was given before the start of the first lesson and the Post-test was given after the final 8th lesson of the unit was completed. In this way I could ascertain what was working in the 8-lesson unit and what the students were having a hard time understanding. The assessment of the students was integral in preparing quality lessons for publication and use by in-service teachers.

The second important facet to the methods I employed to create quality curriculum was critiquing and input from the in-service teachers. Their knowledge of the class dynamic and their experience as a working teacher was an important step in developing the 8-lesson unit. Upon completion of a day of teaching a lesson to 2-4 classes I would discuss the lesson with the teacher and ask them for suggestions on how to improve the lecture, the handouts, the visual aides or the laboratory experiment. In this way the students and the teachers that I worked with over the past year were very important to the success of the final 8-lesson unit.

RESULTS

The entire 8-lesson unit "Bringing Mars Science to Hawai'i's Students: Making Science Culturally Relevant to Hawaiian and Pacific Islander Students" can be found at the website: Mikala.Bradley.googlepages.com. The eight lessons are summarized below:

1. **Hawaiians as Space Explorers**
   Students are asked to consider "Why people move?" and draw parallels between their personal experiences moving, Polynesian voyaging to Hawai'i, and modern day space exploration. Students then examine NASA data to determine which planet would be a good choice for human exploration and settlement. Typically, they choose Mars for its Earth-like temperature and rocky surface.

2. **Life on Earth and Mars- The Role of Water**
   Here we examine the essential requirements of life, including the role of water. First the students learn about how the Polynesian explorers brought water on their long ocean journeys and also how Polynesian sailors might have hypothesized about water existing on the far away islands that they were sailing towards (Hawai'i). Next the students look at NASA images of Mars to try to hypothesize, like the Polynesians, if there might be evidence of water on the far away planet. "Kitchen Science" laboratory experiments are conducted to see if students can use water to recreate features seen in the images (e.g., pouring water onto a 'Martian surface' to create channels). Typically they can recreate what they see in the NASA images of Mars, suggesting water existed-and may still exist-on Mars, which supports their choice of Mars as a reasonable planetary home.

3. **The Hawaiian Ahupua'a and Sustainable Development of Mars**
   Students are asked to plan the first human settlement of Mars. Who would they take? What would they bring? How would they set up a sustainable living system on their new planetary home? To help answer these questions, they turn to Hawaiian history. When the Polynesians traveled to Hawai'i in voyaging canoes, they similarly had to make difficult decisions (e.g., what to bring in highly limited space, what would be needed to live sustainably in their new island home). Students review the Ahupua'a system (traditional Hawaiian system of land-division which maximized self-sufficiency and sustainability) as a possible model, and evaluate its relevance to modern (and future) society. The students are then given a short list of issues that the Polynesians and the modern Mars explorers may have to deal with (e.g., transportation, energy use, food production, housing, etc.) In small groups the students use poster boards to draw their ideas of how the Polynesians dealt with one of the issues and on the reverse side how modern explorers may deal with the same issue.

4. **Volcanoes vs. Impact Craters**
   The students begin by looking at one of Hawai'i's volcanoes in a satellite image and briefly learn about the Hawaiian mythology that the volcanoes embody. Students revisit the NASA images of Earth and Mars that they previously examined in Lesson 2. The class then hypothesizes about the processes for the features that they do not believe were formed by water in the Mars images. In particular, students hypothesize possible origins of circular features (e.g., volcanic or impact craters). Then, the students conduct hands-on experiments intended to simulate the impact process. By comparing their resulting craters to those in the images, they can test their hypothesis the same way that NASA scientist use models when investigating features seen in satellite images.

5. **How do we get there?**
   The class begins with an overview of how Polynesians might have gotten to Hawai'i. The students learn that Polynesians used their knowledge of astronomy, climatology, ethology and other sciences to successfully explore the Pacific Ocean. Next the students learn how modern day explorers might navigate to another planet using some of the knowledge that the Polynesians employed as well as contemporary knowledge of energy transfer, rocket technology, and computers. Students learn basic (Newtonian) physics through hands-on activities and demonstrations using Cat-A-Pult rocket launchers. Students also learn that landing on Mars requires hitting a moving target (since Mars is in motion around the Sun) and conduct a hands-on activity to simulate this.

6. **Introduction to Biospheres**
   and
7. **Making an in-class Biosphere**
   These two lessons focus on Biospheres. In Lesson 6, students tackle the issue of surviving in the Martian thin, oxygen-poor atmosphere. The class revisits the Hawaiian land management idea of the Ahupua'a and discusses the hydrologic cycle, nitrogen cycle, and nutrient use of the land for sustainable living. Next, the students learn the how's and why's of building a biosphere to support human life on Mars. Lesson 7 involves creating a biosphere using basic materials (e.g., glass jar soil, native plants).

Once created students seal the biospheres and predict how long each organism will survive (it is common for plants to live for years).

8. **Hawai'i to Mars: A Voyage of Discovery (Board game)**
   The final lesson and culminating activity of this unit is a board game entitled "Hawai'i to Mars: A Voyage of Discovery" (Appendix 1). This activity is designed as a fun, engaging way of assessing student's knowledge of Hawaiian culture and Mars science.

Appendix 1: "Hawai'i to Mars: A Voyage of Discovery" board game

DISCUSSION

Linking cultural values and science is a way for students to feel a connection with a seemingly abstract subject. Creating hands-on curriculum that brings together a culture and science makes the subject matter relevant and important to the students. When I was teaching the lessons, I found that the students who normally do not raise their hand and participate (according to their regular teacher) were enthusiastically interacting with my lecture. Linking the science of today and the science of the past was an important step in getting the students to identify with the idea that science matters. Polynesian voyagers and Hawaiian culture used science everyday to be successful civilizations. Astronomy, climatology, oceanography, ethology, and hydrology were just a few of the sciences that were employed by the ancient Pacific Islanders. Making the link between modern day exploration (Mars) and ancient Polynesian exploration is an easy way to make the sciences relevant and important to Hawai'i's students.

CONCLUSION

The use of NASA data and existing high quality curriculum was an important factor with regards to the success of the unit. Developing culturally relevant lessons and making the entire unit available online as a resource for educators was another goal of my fellowship that was obtained. Inspiring Hawaiian and Pacific Islander students to study science was a key goal in my Space Grant fellowship and I believe that the goals were accomplished in this 8-lesson unit.

FUTURE WORK

Since I have been a Space Grant fellow I have enjoyed working with many talented scientists and educators. In the future I plan to continue to present my 8-lesson unit at teacher's workshops and educational conferences. I will be presenting the 8-lesson unit at a teacher's workshop at Windward Community College on June 12th 2007. I am also organizing a teacher's workshop (to be held in October 2007) to continue to disseminate the curriculum that I have developed during my fellowship.

ACKNOWLEDGEMENTS

I would like to say Mahalo Nui Loa to all of the teachers that have been an important part of this Mars science-Hawaiian culture unit. They are: BarbaraJean Kahawai'i from Laie Elementary, Scott Oberg from Makaha Elementary, Mahina hou Gandharva from Moloka'i Middle and High, and Kristen Phillips from Highlands Middle. Without these educators allowing me to pilot my lessons to their students and giving their time to guide me in writing the lessons I would not have been nearly as successful. I would like to thank Tracy Tayama for sharing her great knowledge of Adobe Photoshop which was integral in creating the "Hawai'i to Mars: A Voyage a Discovery" board game. I would like to thank the University of Hawai'i at Manoa Space Grant office, in particular Marcia Rei Sistoso and Edward Scott, for all of their organization, hard work and dedication to the trainees and fellows. I would also like to thank my mentor, Dr. Barbara Bruno. Dr. Bruno has the amazing ability to challenge and encourage people to work together and strive for the highest goals. And last I would like to thank NASA for knowing the importance of education to our national scientific community and giving people like me the opportunity to make a difference to our young future scientists.

REFERENCES

Lesson 1

- Ancient Times in the Islands
  http://www.hawaiischoolreports.com/history/ancient.htm
- Hawaiians as Navigators and Seamen by Samuel Wilder King
  http://pvs.kcc.hawaii.edu/hawaiians.html
- Greenpeace: Climate

- Greenpeace: Pollution
  http://www.greenpeace.org/international/campaigns/toxics
- Greenpeace: War and Weapons

http://www.greenpeace.org/international/campaigns/peace
- U.S. Census: Population
  http://www.census.gov/popest/archives/1990s/popclockest.txt
- ONE: Poverty
  http://www.one.org/
- ONE: Disease
  http://www.one.org/gvideo/view/34
- Map of the Solar System
  http://www.gcse.com

Lesson 2
- NASA Educators Resource Guide: Mars and Earth Science Learning Activities for Afterschool Participants ages 5-12/ Activity #5
  http://mars.jpl.nasa.gov/classroom/resources.html
- Hawaiian Ahupua'a
  http://www.pixi.com/~isd/ahupuaa.html
  http://www.k12.hi.us/~ahupuaa/
- Ancient times in Hawai'i
  http://hawaiischoolreports.com/history/ancient.htm
- Artistic rendering of a Hawaiian ahupua'a
  http://www.asahi-net.or.jpg
- The Hawaiian Canoe by Tommy Holmes, Polynesian Voyaging Society website
  http://pvs.kcc.hawaii.edu/holmesprovisions.html
- Island Wake
  http://cat.inist.fr/?aModele=afficheN&cpsidt=15362804
- Images of sandy beach, Ka'a'awa Beach Park, O'ahu, by Dr. Barbara Bruno 2006

Lesson 3
- Greenpeace: Climate

- Greenpeace: Pollution
  http://www.greenpeace.org/international/campaigns/toxics
- Greenpeace: War and Weapons
  http://www.greenpeace.org/international/campaigns/peace
- U.S. Census: Population
  http://www.census.gov/popest/archives/1990s/popclockest.txt
- ONE: Poverty
  http://www.one.org/
- ONE: Disease
  http://www.one.org/gvideo/view/34
- The Ahupua'a Land divisions of O'ahu
  http://www.pixi.com/~isd/map.html
- Hawaiian Ahupua'a
  http://www.pixi.com/~isd/ahupuaa.html
  http://www.k12.hi.us/~ahupuaa/

- The Hawaiian Ahupua'a system and population
  http://hawaiischoolreports.com/history/ancient.htm
- Nitrogen Cycle
  http://www.physicalgeography.net/fundamentals/9s.html
- Hawaiian vocabulary
  Pukui Mary Kawena and Elbert Samuel H. (1979) *Hawaiian Dictionary.* Honolulu: University Press of Hawai'i.

Lesson 4

- NASA Educators Resource Guide: Mars and Earth Science Learning Activities for Afterschool Participants ages 5-12/ Images
  http://mars.jpl.nasa.gov/classroom/resources.html
- Compact Reconnaissance Imaging Spectrometer for Mars Curriculum Guide
  http://crism.jhuapl.edu/

Lesson 6 and 7

Websites

- Building Terrarium
  http://edis.ifas.ufl.edu/BODY_MG356
- Arizona Living Biosphere
  http://www.biospheres.com/experimentchrono1.html
- Nitrogen Cycle in Terrariums
  http://www.boomspeed.com/shadowedfate/imgs/biology.htm
- Biosphere 2 Center website:
  http://www.desertusa.com/mag99/apr/stories/bios2.html
- Living in the Biosphere: Production, Pattern, Population, and Diversity By Dwight Brown
  http://www.colorado.edu/geography/virtdept/module/biosphere/toc.html

Books

- Elbert, V. & G.A. (1973). *Fun With Terrarium Gardening*. New York: Crown Publishing.
- Kramer, J. (1969). *Gardens Under Glass*. New York: Simon and Schuster.
- Kramer, J. (1974). *The Complete Book of Terrarium Gardening*. New York: Charles Scribner's Sons.
- Parker, Alice. (1977). *Terrariums*. New York: Franklin Watts.
- Wong, H.H. & Vessel, M. F. (1969). *Our Terrariums*. Addison-Wesley.

ALGORITHM TO CORRECT FOR ATMOSPHERIC DIFFERENTIAL REFRACTION ON OSIRIS DATA CUBES

Denny C. Dement III
Department of Physics and Astronomy
University of Hawai‘i at Hilo
Hilo, HI 96720

ABSTRACT

Near the diffraction limit of the 10-meter Keck II telescope, a state-of-the-art integral field imaging spectrograph called OSIRIS works with adaptive optics in near-infrared wavelengths. OSIRIS data cubes are tainted by the effect of atmospheric differential refraction (ADR). ADR is observed as a shift in pixels over wavelength, where each pixel represents a spectrum. In order to compensate for this using software, previous work used computer models in Interactive Data Language (IDL) to compare ADR correction equation shift predictions with actual shifts. However, only the distance, not direction of the shifts was compared. A recent experiment conducted by OSIRIS PI, James Larkin, Ph.D. was made to test if there were other factors involved in the shift. The IR-transmissive dichroic on the AO bench was discovered to cause light dispersion as well. Using a quadratic fit equation from this study, a function was written in IDL to blend both the ADR and AO bench predictions. Furthermore, using the parallactic and position angle, a direction function was incorporated as well. In the end, a more complete algorithm was produced. This will help create a future data reduction pipeline module to significantly improve the quality of spectra.

INTRODUCTION

Infrared spectrographs are an invaluable tool to astronomers who study the role of interstellar molecules in the universe. W.M. Keck Observatory, a leader in innovation, has added a new integral field spectrograph, OSIRIS (OH Suppressing Infra-Red Imaging Spectrograph) in February 2005. At present OSIRIS is being utilized in symbiosis with adaptive optics (AO) at the 10-meter class Keck II telescope on Mauna Kea, Hawaii. OSIRIS may act as an imager or spectrograph and has an average resolution of 3800 at 0.02, 0.035, and 0.50 plate scales. In broadband mode (Z, J, H and K), between 1 and 2.4 microns tiny lenses allow 64 X 64 (1019) spectra to be taken at once. These spectra are then processed electronically through the data reduction pipeline that creates 3-D OSIRIS data cubes (Figure 1). However, scientists who use OSIRIS recognize a problem with the quality of spectra in these cubes. Atmospheric differential

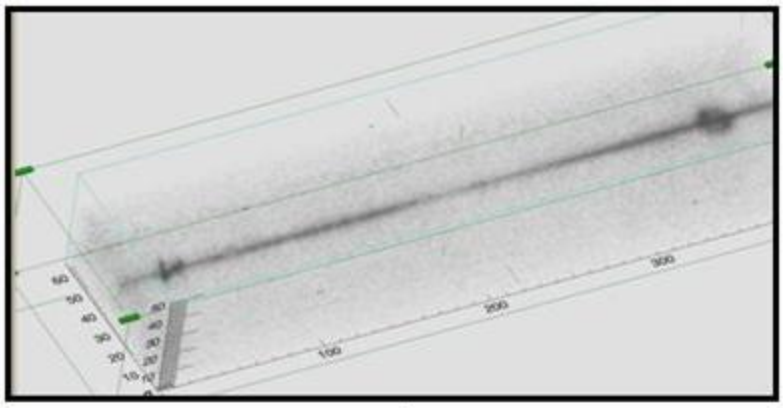

Figure 1: IDL image of a 3-D OSIRIS data cube

refraction (ADR) causes a pixel shift over wavelength, where each pixel represents an individual spectrum. That means by following any pixel through the cube, part of its associated spectrum bleeds over to one or more neighbor pixels. ADR is a phenomenon where the atmosphere acts like a prism and disperses light into its spectral components.

This project is a foundation for creating a new data reduction module to correct for ADR shifts through software written in Interactive Data Language (IDL). In order to correct the shifts, each slice of the cube must be repositioned so that the shift in essence gets straightened out. It would seem that straightening out a point source through the cube would be the simplest solution, but not every target is a point source. What is wanted is a general algorithm that will predict how ADR will shift every pixel before the light reaches OSIRIS.

HISTORY

This project is derived from an analysis done in the summer of 2007. Mathematical models were created in IDL based on ADR correction equations from previous studies by Henry Roe (2002), Alex Fillipenko (1982), and Edson Peck & Kaye Reeder (1972). Basically each of these models calculated indices of refraction for two wavelengths, found the difference and multiplied it by the tangent of the zenith angle to find the desired dispersion in arc seconds. By continually doing this procedure between the first and every other wavelength in the array, the result would be the desired ADR shift over the OSIRIS data cube. The models would plot these predicted shifts with measured ones. In order to measure the shift, a Gaussian fit routine from OSIRIS specific software; Quick Look 2 (UCLA) calculates a centroid for any slice in the ADR cube. By running this routine for every slice in the cube, two long arrays of horizontal and vertical shifts are gained. Next, these arrays are combined into one by using the distance equation, and then converted from pixels to arc seconds (20 milli-arc second per pixel. Although similar, each ADR correction equation was unique. The closest prediction of the measured shift was made by the Peck & Reeder model. The final results are seen in three broad bands in Figure 2. However close, the model still had some flaws. The problem of finding the direction of the shift was never challenged and the greatest separation (7.38 milli-arc seconds) is good, but at almost half a pixel off, not great.

NIR Window microns	Pixel Spectra Array	Start Cent. (X,Y)	End Cent. (X,Y)	M Shift arcsec	C Shift arcsec	Diff. milli-arcsec
Zbb (1.04-1.18)	64x19 x1218	(5.48, 5.17)	(8.14, 2.60)	.0740	.0800	6.00
Jbb (1.20-1.44)	64x19 x1587	(4.37, 5.51)	(6.75, 3.07)	.0679	.0753	7.38
Hbb (1.47-1.80)	64x19 x1620	(4.48, 4.01)	(6.31, 2.39)	.0488	.0523	3.47

Figure 2: Results from Peck and Reeder (1972) model

Within a month following this analysis, the principal investigator for OSIRIS, Professor James Larkin, Ph.D. (UCLA) conducted an experiment using white light fiber though the AO bench and OSIRIS. By taking broad band images of the fiber and using the Gaussian routine mentioned earlier, significant dispersion parallel to the AO bench was discovered. The culprit was found to be the IR transmissive dichroic in the adaptive optics. Larkin was able to calculate

the direction of the newfound shift to be -48.3 degrees relative to the optical bench and to fit the data, a 2nd order polynomial to the square of the total motion was used to create equation (1).

$$\text{Total Motion (mas) relative to 1000 nm} = -20.40 + \sqrt{-16204 + 19.66\lambda - 0.00304\lambda^2} \quad (1)$$

CODE

A student version of IDL was used in the project. Editing, reading and writing IDL code was done to incorporate the direction problem and the new dispersion shift discovered by the Larkin experiment. Two new models were created to separate the horizontal (x) and vertical (y) shifts, thus making it easier to test the code. The measured shift was easily adaptable to both versions because the Gaussian fit routine returns both X and Y.

In the beginning, the direction of the X-shift was first calculated from the OSIRIS data cubes provided by W.M. Keck Observatory. New code was written to find the average of the first and last twenty entries of the array, and then use trigonometry to find the angle. To find the direction angle of the ADR shift without the data cube, information on the position and parallactic angle from the observing night is required. Roe explains the former as measured from the positive Y-direction on the detector array clockwise to the vector pointing north on the sky and the latter as measured from the vector pointing north on the sky counterclockwise to the vector pointing to zenith (Figure 3).

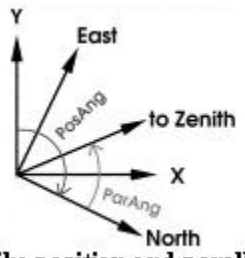

Figure 3: The position and parallactic angle

```
for i =0, num_slice-1 do begin

    lambda1[i] = lambda1[i]*1000  ;conversion to nanometers

    ;*****************************Quadradic Equation*********************************

    bench[i] =(-20.40+ sqrt(-16204+(19.66*lambda1[i])-(.00304*(lambda1[i]^2))))  ;

    lambda1[i] = lambda1[i]/1000  ;reconversion to microns

    x_bench[i] = (bench[i] * cos(-.84299)) ;USES -48.3 deg *(pi/180) =.84299
    y_bench[i] = (bench[i] * sin(-.84299)) ;USES -48.3 deg *(pi/180) =.84299

    ;                          *note: -48.3 deg is the observed angle of deviation
    ;                                 from the AO Bench
endfor
```

Figure 4: IDL code that uses results from the Larkin experiment to compensate for the IR-tranmissive dichroic contribution to the dispersion through an OSIRIS data cube.

The angle of the ADR shift is just the position subtracted from the parallactic.

Continuing with the X-shift, the next code was written to compensate for the dispersion caused by the IR-transmissive dichroic on the AO bench. Two parameters from the Larkin experiment were used. They are the angle of dispersion (-48.3 degrees) and equation (1). Equation (1) works with wavelengths in nanometers and the result is in milli-arc seconds. This fit well in the routine and finalized excerpt of the code is seen in Figure 4. Even with these

additional routines for the X-shift model, the measured was not even close the predicted using the Peck and Reeder function.

An investigation into the past analysis was made. The other two previously tested equations, Roe (2002) and Alex Fillipenko (1982) was retested. Before running through the functions, a simplification was made in finding the dispersion after calculating the associated indices of refraction of two wavelengths. Previous to this change all models followed equation 2 from Roe. The index of refraction correction for the smallest wavelength would replace the visible component in the equation (n_{vis}) while the index is filled with the result for every sequential wavelength until the end of the cube. To translate this equation into IDL was not trivial. Larkin also did a study on the effect of ADR and had a very simple equation that does the same work to find the differential atmospheric refraction (equation 3). This equation only subtracts the indices before multiplying by the tangent of the zenith angle (α).

$$R_{\text{vis}} - R_{\text{ir}} = 206{,}265 \left(\frac{n_{\text{vis}}^2 - 1}{2n_{\text{vis}}^2} - \frac{n_{\text{ir}}^2 - 1}{2n_{\text{ir}}^2} \right) \tan z_t \text{ arcsec.} \qquad (2)$$

$$\delta\alpha = \Delta\alpha_2 - \Delta\alpha_1 = (n_2 - n_1) \times \tan(\alpha) \qquad (3)$$

The Fillipenko model combined with this new simplification for the ADR correction gave the best fit to the data. The code for the Fillipenko model is seen in Figure 5. Ambient temperature and pressure is used in the equation. The small amount of precipitation on Mauna Kea made correcting for water vapor unnecessary.

```
function refract2, lam, f_h2o = f_h2o

;from Filippenko(1982), PASP

if not keyword_set(f_h2o) then f_h2o = 0.0

x1 = double(64.328 + 29498.1/(146 - (1/lam)^2) + 255.4/(41-(1/lam)^2))
                ; Mauna Kea correction
                    ; based on P = 456mm, T = 2degC, cohen & cromer, PASP
T = 2.0
P = 456.0


pt_corr  =  (P * (1.0+(1.049-0.0157 * T)*1.0e-6* P)) / (720.883*(1+0.003661 * T))

f_corr = f_h2o*(0.0624-0.000680 / lam^2)/ (1.0+0.003661 * T)

n = double(((x1-f_corr)/1.0e6)*pt_corr + 1.0)
return, n
end
```

Figure 5: The ADR correction equations from Fillipenko (1982)

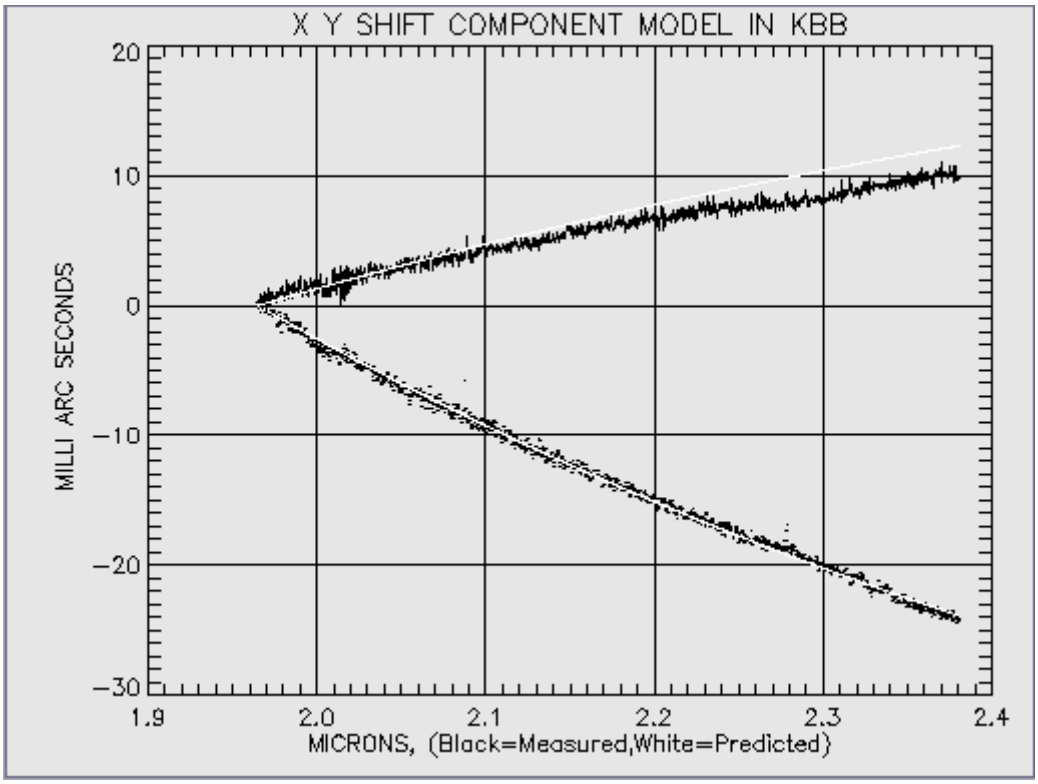

Fig 6: The final result of the new algorithm

RESULT & CONCLUSION

The model was tested with Jbb and Kbb broad band OSIRIS data cubes. The largest gap was less than three milli-arc seconds. The IDL plot in Figure 6 shows the correlation between measured and predicted and Y shifts. The aberrations found in the measured data come from noise. A condition has been set in the algorithm to take the previous data if the difference exceeds more that one pixel. In order to get all the functions to plot together it was tough to zero in all the data. Because the significance of the AO bench contribution is so high the data is always pulled toward the direction, thus we happen to get positive X values and negative Y values. The next step is to use this algorithm to correct a cube. This can be done by re-sampling the data cube and somehow shifting each slice to conform to the prediction of the dispersion as described in this new algorithm. Last, all that is needed is a new module to be added to the data reduction pipeline to produce higher quality spectra. Astronomers can then use this to more accurately describe the universe that surrounds us.

ACKNOWLEDGEMENTS

The author wishes to thank his family for their ongoing support of my scientific endeavors. Randy Campbell, my mentor, has been very supportive and patient while working with me. Thanks for taking time out of your schedule to help me with this project. NASA Space Grant staff deserves credit for answering all of my questions and following up on all that I forgot. A special thanks to the Center for Adaptive Optics and National Science Foundation for

help with my previous internship that led to this project. Thank you to Jim Lyke, David Le Mignant, Al Conrad, Sarah Anderson, and W.M. Keck Observatory staff for providing me with great suggestions on how to approach difficult problems.

REFERENCES

Fillipenko, Alexei V. (1982) The Importance of Atmospheric Differential Refraction in Spectrophotometry. Publications of the Astronomical Society of the Pacific, **715-721**.

Larkin, James "OSIRIS Manuel" www. Keck.hawaii.edu. 17 November 2006 < http://www2.keck.hawaii.edu/inst/osiris/>

Peck, Edson R. and Kaye Reeder (1972) Dispersion of Air. Journal of the Optical Society of America Vol. 2 No.8: **958-962**.

Roe, Henry (2002) Implications of Atmospheric Differential Refraction for Adaptive Optics Observations. Publications of the Astronomical Society of the Pacific, 114: **450-461**.

CUBESAT-TO-GROUND COMMUNICATION AND MOBILE MODULAR GROUND-STATION DEVELOPMENT

Dylan Ichikawa
Department of Electrical Engineering
University of Hawai‘i at Mānoa
Honolulu, HI 96822

ABSTRACT

A mobile modular ground station is described for direct communication and tracking of CubeSats from various locations. The ground station operates in the UHF range and employs a circularly polarized Yagi-Uda antenna. A two-piece wooden antenna base with a telescoping mast was constructed for mounting the antenna. For an orbit height of 600 km, satellite transmit power of 27.0 dBm, satellite antenna gain of 5 dB, and ground station antenna gain of 19.1 dBic, the calculated signal power at the ground station is -89.9 dBm and the calculated signal power at the transceiver is -70.9 dBm. The mobile modular ground station successfully tracked three CubeSats named CubeSat XI-IV, Cute-1, and Quakesat.

INTRODUCTION

Nanosatellites are a class of small satellites that have a mass between 1-10 kg [1]. Within this class is the so-called CubeSat that is a 10-cm cube with a mass of up to 1 kg [2]. Most of these satellites can fit in the palm of your hand and perform sensing missions or technology demonstrations. Typically, CubeSats are launched as secondary payloads into a circular sun-synchronous low-earth orbit at 500-600 km [2]. Eventually the satellite de-orbits due to Earth’s gravity and burns up in the atmosphere. Compared to conventional large satellites, CubeSats are easily deployable and can potentially be used for natural disaster evaluation and for battle line assessment. The development time for a CubeSat is roughly one year with constant improvements in each generation. Distributed networks of CubeSats are also promising alternatives to conventional large single satellites.

The ground station is of primary importance for mission success as it is the first and final piece in the communication link. Its main purpose is to track and receive data from CubeSats for data analysis. Since all communication with CubeSats is done wirelessly, the ground station serves as the access point on Earth. A simple example is the cellular phone. As long as you are in the range of a base station, you can make and receive calls. Going out of that range means that you have no reception and are cutoff from communication. Therefore, without a ground station, the CubeSat is useless.

A basic ground station consists of hardware and software to transmit and receive data reliably. The components include transmit and receive antennas, a computer programmed with orbital-prediction software compatible with the hardware for auto- tracking, and a transceiver to transmit and receive data. The antenna’s input return loss should be measured with a network analyzer to ensure that the maximum amount of the transmitted power transfers to the antenna. Conventional ground stations are stationary and therefore can only be used in a single location. This makes the station useless if it is needed at another location. Mobility of a ground station is important because it allows for use in remote locations. With a mobile ground station, the

ground station operator is able to access the satellite at different points on earth to analyze the data that is received.

GROUND STATION DESIGN

The design of the ground station is based on the Friis Transmission formula, the physical constraints that the University of Hawaii's location, and the design of the University of Hawaii's first CubeSat, named Mea Huaka'i or Voyager.

By using the Friis Transmission Formula, a simplified model of the CubeSat-to- ground station communication link can be calculated.

$$P_r\ [dBm] = P_t\ [dBm] + G_t\ [dB] + G_r\ [dB] - 20*\log_{10}(4\pi R / \lambda) \qquad (1)$$

The transmit power (P_t) of the ground station and satellite, the receive power (P_r) at the ground station and satellite, and the gain of the ground station and satellite antenna (G_t,G_r) can be determined for a certain frequency of operation and distance (R) of the communication channel. The frequency of operation determines the wavelength (λ).

Mea Huaka'i was designed to work at a frequency of 436 MHz, with a transmit power of 27.0 dBm, a quarter-wavelength whip monopole antenna gain of 5 dB [3], and have a circular sun-synchronous orbit at an altitude of 600 km. The maximum distance that can be experienced in a single pass is 2,830.9 km, at the horizon, and the minimum distance is 600 km, at a location directly above the ground station. The free space loss, which is the last term in (1), is -154.3 dB at 2,830.9 km and -140.8 dB at 600 km. The ground station antenna was chosen to be a commercial-off-the-shelf M2 436CP42 U/G which is a circularly-polarized Yagi-Uda antenna with a gain of 19.1 dBic. Therefore, the maximum power received at the ground station location is -89.9 dBm and the minimum power received at the ground station is -103.4 dBm. The Friis Transmission Formula is a simplified model that does not include the effective noise temperature, pointing losses, and coaxial cable losses. The coaxial cable chosen for the ground station was Belden 8214 RG-8 with a loss of 1 dB per 25 feet. Therefore a SP-7000 Super Amp GaAsFET Series 432/435 MHz mast-mounted low-noise amplifier (LNA) was included immediately after the Yagi-Uda antenna for a minimum signal to noise ratio of 9 dB and a signal amplification of 20 dB. The antenna's input return loss was measured with a Hewlett Packard network analyzer at a center frequency of 435 MHz to ensure a low input return loss.

The University of Hawaii at Manoa has several physical obstructions that can hinder wireless communication. They include wide-tall buildings made from concrete, glass, and other types of materials, and Manoa Valley to the north, which consists of high mountains and thick cloud cover. This eliminates the options of placing a permanent ground station at ground level because the window for communication would be too small. Therefore, a higher elevation for a ground station was needed. A permanent on- campus ground station placed on the top of Holmes Hall was initially proposed, but the rules and regulations prevented the construction of student-designed structures on top of buildings. This eliminated the possibility of a permanent ground station at a suitable height. Therefore, a mobile modular ground station was designed to achieve the option of possibly using a higher location for tracking.

The mobile modular ground station hardware consists of a collapsible quad-pod which is connected to a foldable square base, as shown in Figure 1 and 2, respectively.

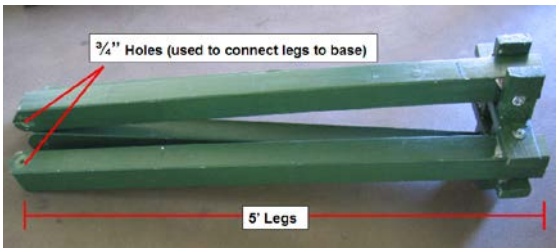

Figure 1: Quad-pod of antenna base

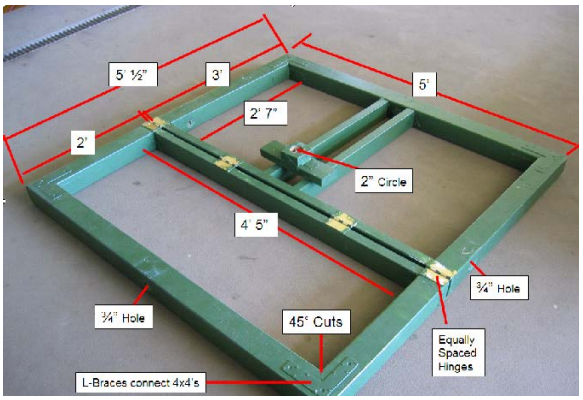

Figure 2: Square bottom of antenna base

The quad-pod and square base were chosen to be constructed out of wood because it is heavy enough to support the rotator, fiber glass boom, and antennas in light winds, but not so heavy that it would be too hard to move. The telescoping mast is provided to obtain unobstructed rotation of the antenna-boom assembly. The fully assembled mobile modular base is shown in Figure 3.

Figure 3: Fully assembled ground station set up

The mobile modular ground station software consists of a laptop computer that is programmed with NOVA for Windows (NOVA), a Yaesu G-5500 elevation-azimuth dual rotator controller, and a Yaesu GS-232A computer interface. The main reason why NOVA is chosen as the primary software is because it is compatible with the computer interface and rotator controller and provides auto tracking. This program allows us to automatically track CubeSats and predict the time, elevation and azimuth level for satellite passes. This program uses Keplerian elements to make all of the calculations. The total system block diagram is shown in Figure 4.

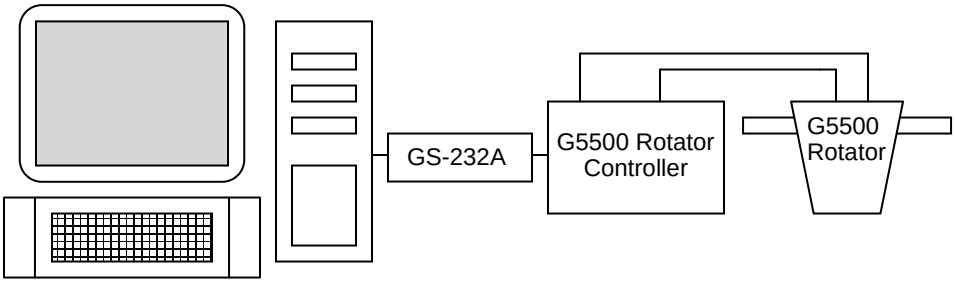

Figure 4: System block diagram

FABRICATION AND ASSEMBLY

The mobile modular base was constructed using wood from a local hardware store. The quad-pod was made from 4x4 beams and the square bottom was made from 2x4 beams. With the help of Kaneohe City Mill and other CubeSat students we measured and cut the wood to meet the specified design. Each section was connected using straight and L-brackets, nails, and wood glue. The folded portion of the wood base was connected with copper door hinges. The extendable mast was constructed using two fence posts, one with a larger diameter than the other and both having the same length. Three holes were drilled through the larger diameter post. The first hole was drilled 5.5 inches above the bottom and two are drilled 4.25 and 7.5 inches from the top of the post. Two holes are drilled at the bottom of the inner post. These two holes were drilled inline with the two in the outer post. To connect the quad-pod to the square base post holders, 6-inch long, 0.5-inch diameter bolts and nuts were used. The telescoping mast is than inserted in the connected base, as shown in Figure 6. On top of the mast a Yaesu G-5500 rotator is connected and finally two fiber glass booms are attached to the rotator at the two opposite ends the VHF and UHF Yagi-Uda antennas are placed. A Yaesu FT-847 dual VHF/UHF input/output transceiver is connected to the 435 MHz antenna by using type-N connectors and 25 feet of RG-8 coaxial cables.

Figure 5: Complete raised VHF/UHF mobile-modular ground station

EXPERIMENTAL RESULTS

The UHF Yagi-Uda antenna's input return loss was measured using a network analyzer at two different antenna lengths to ensure that it had a lowest nominal value. The antenna's input return loss was first measured for its entire length of 21 elements. The value was measured to be -17 dB after tuning and the measured input return loss for 13 elements of the antenna was -21 dB after tuning.

The mobile-modular ground station was tested on four separate occasions. During the final three occasions four signals were received from three different CubeSats; they where Cute-1, CubeSat X-IV, and QuakeSat. The operating frequencies of these CubeSats were 436.837.500 MHz and 436.675 MHz.

ANALYSIS AND DISCUSSION

A mobile-modular ground station was designed and built. The ground station was designed to provide reliable communications with CubeSats, while being mobile. The ground station was tested for its operation in the UHF range and the results were good. As mentioned in

the preceding section, an antenna length of 21 elements has a higher input return loss than an antenna length of 13 elements. Although the shorter antenna has a lower input loss, the gain of the antenna decreased because the number of elements of the antenna decreased [4]. I decided to use the shorter portion of the Yagi-Uda antenna because the gain of the antenna does not decrease linearly with the number of elements and the gain curve flattens out as the number of elements exceeds 10 elements [4]. Therefore, I was able to decrease the input return loss by over two times while maintaining a high gain of the antenna. As stated the ground station was able to receive signals from three different satellites during four different attempts. The first attempt failed because we did not account for Doppler shift, which is a change in the observed frequency of a wave occurring when the source and observer are in motion relative to each other, as seen in Figure 6, with the frequency increasing when the source and observer approach each other and decreasing when they move apart. In the final three tries we accounted for the Doppler shift and were successful in tracking Cute-1, CubeSat XI-IV, and QuakeSat.

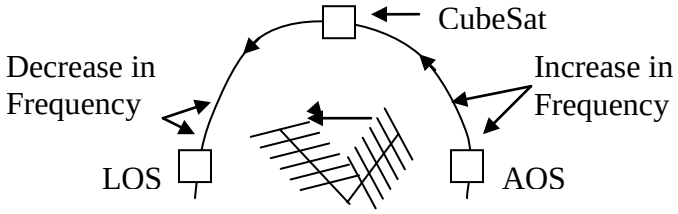

Figure 6: Diagram of Doppler shift

CONCLUSION

A mobile modular ground station was designed and built for CubeSat tracking and communication. Through measured data it can be seen that the input return loss is lower with an antenna length of 13 elements of the Yagi-Uda antenna. Therefore, this portion of the antenna is used instead of the entire section. The modularity of the ground station allowed the CubeSat team to test the ground station at different locations and allowed us to track at locations that would not have been available to us if we were to have a permanent ground station. We were able to successfully track three CubeSats.

Future improvements for this project would be to upgrade the tracking software to one that automatically account for the Doppler shift. Also, the VHF antenna could be measured and calibrated for a low input return loss and could be tested similarly to the UHF antenna. Once these improvements are done the mobile ground station would be able to join the CubeSat community set forth by Cal Poly San Luis Obispo.

ACKNOWLEDGMENTS

The author would like to thank the Hawai'i Space Grant Consortium and NASA for giving him and other individuals the opportunity to do research in their field of interest. Thank you to Kaneohe City Mill for helping cut the lumber to the specifications that we wanted when no other hardware store would do it for us. The author would also like to thank Dr. Wayne Shiroma for serving as his mentor during the research process and his graduate student Justin Akagi for lending much needed guidance over the past semester. Thank you to the University of

Hawaii's CubeSat team. Finally, a special thank you goes out to his mom, Noraine, dad, Wayne, and sisters, Dara and Nerissa, for being good role models and supporting him. He would like to thank all his friends for reminding him that there is still a world outside of school. Thank you to all!

REFERENCES

[1] Small Satellites Home Page. Surrey Space Center. Est. 1995. University of Surrey, U.K. January 2, 2007. <http://centaur.sstl.co.uk/SSHP/sshp_classify.html>.

[2] CubeSat Home Page. California Polytechnic State University, San Luis Obispo, CA. January 2, 2007. <http://cubesat.atl.calpoly.edu/>.

[3] Staff of Lab-Volt (Quebec) Ltd. Antennas: Antenna Fundamentals Exercise 2-1 Monopole Antennas. Canada: 1996.

[4] Staff of Lab-Volt (Quebec) Ltd. Antennas: Antenna Fundamentals Exercise 2-4 Parasitic Array (Yagi-Uda) Antennas. Canada: 1996.

[5] NASA Ames Research Center Amateur Radio Club Home Page. Ames Amateur Radio Club. December 14, 2006. Moffett Field, CA. January 8, 2007. <http://hamradio.arc.nasa.gov/coaxcableloss.html>.

ADVANCEMENT OF THE LEONIDAS MISSION CONCEPT STUDY TEAM

Zachary Lee-Ho
Department of Mechanical Engineering
University of Hawai‘i at Mānoa
Honolulu, HI 96822

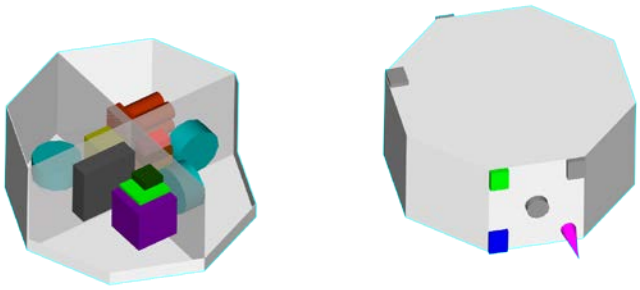

ABSTRACT

Throughout the summer, I continued my role as a member of the LMCST by finishing the mission concept report, preparing a proposal for the Nanosat Competition, mentoring two students from the Summer Bridge Program and assisting Professor Lloyd French with other prospective missions. By continuing to work with Professor Lloyd French I hope to advance the LMCST in preparation to achieve our ultimate goal of building and launching our satellite.

INTRODUCTION

With the conclusion of last semester, many tasks remain unfinished and more work continues to accumulate. Since I was the only member of the LEONIDAS Mission Concept Study Team (LMCST) who was available this summer, I assisted Professor Lloyd French to devise a plan to prepare our team for future endeavors. During this past spring semester, the LMCST began preparing a satellite concept report showing our design for a 30 kg low Earth orbit satellite. We researched various components and payloads to meet our spacecraft specifications and accomplished the desired mission. We also developed a concept drawing and drafted basic system operations of our satellite. A lot of research was accomplished to prepare the satellite concept report, but the final draft was not completed to include in the Undergraduate Fellowship Final Report booklet, that was scheduled to be published this summer by the Hawaii Space Grant Consortium.

In addition, this summer marked the start of the Summer Bridge Program, funded by the Native Hawaiian Science & Engineering Mentoring Program (NHSEMP). The NHSEMP assists students by providing support, guidance, tutor, mentorship and, in some cases, financial aid to ensure successful completion of a degree in their respective field. The Summer Bridge Program assists incoming freshmen, transitioning from high school to college, who are pursuing an engineering degree at the University of Hawaii at Manoa. It also gives them insight into the fields associated with their degree. Joshua Kaakua, the director of NHSEMP asked me to mentor two of his students from the Summer Bridge Program and to introduce them to the mission design process.

CONTINUING LEONIDAS MISSION CONCEPT STUDY TEAM PROGRESS

My first task while working for Professor Lloyd French was to finish the satellite concept report. Several parts were needed to meet the Space Grant Consortium format. I wrote the missing pieces that included abstract, objectives, goals, conclusion and the background from information attained through my interview with Dr. Luke Flynn. Ms. Gindi French helped me with alterations and to ensure that the report flows properly. By working with David Hampton, Engineering specialist, I made slight modifications to the concept design drawing to meet the specifications given by Professor Lloyd French.

My next task was to begin a proposal for the Nanosat Competition sponsored by the Air Force Research Laboratory (AFRL). Prior to the August announcement for this year's Nanosat Competition I searched for the competition guidelines of 2004 Nanosat Competition to get a head start in preparing the LMCST proposal. Via the internet, I found the Nanosat Competition guidelines and the AFRL procedures for proposal submittal.

Next, I comprised an outline for LMCST proposal, to assist the team's writing of the proposal. I performed a cost analysis of the satellite bus by contacting the various manufactures for the chosen subsystem components of the concept satellite. Contacting the various manufacturers and by the using quotes similar to products of our concept design, I computed that the cost of the components themselves will run approximately half a million dollars. My interaction with the manufacturers also allowed me to attain a better understanding of each component's capabilities and to distinguish whether they are still applicable to our design.

For the cost analysis of the structure I worked with David Hampton, the lead design for Space Grant. We discussed possible ways to construct the structure using customizable brackets and faces. By incorporating already manufactured parts. Afterwards, I met with Professor Lloyd French, and we decided that it would be best to use customizable parts thus ensuring structural integrity. The cost analysis will be completed upon Matthew Patterson's return. Matthew and I will work to develop possible designs for the unique angles needed on the satellite's structure's brackets, faces, and shear panels for. Other significant issues addressed are the absence of a propulsion system and determining the capabilities of our ground station.

Through the research of the Summer Bridge Program students, I drafted a paper comparing cold gas and sublimation propulsion systems, and created a theoretical link budget using a link-budget calculator found through the Internet. However, the ground station in Hawaii is not currently equipped to use S-band frequency but Dr. Torben Nielsen, an expert in ground systems, says it has been done before. Figure 1 illustrates the link budget calculator that was founded by Jennie Castillo. Some values for the ground station capabilities had to be approximated because of it not being presently equipped to handle S-band.

Frequency GHz	2.2
Transmit antenna diameter m	.663
Transmit antenna aperture efficiency e.g. 0.65	.85
Transmit antenna transmit gain dBi	22.973
Transmit antenna, power at the feed W	5
Transmit EIRP dBW	29.963
Range km	350
Path (spreading) loss dB	150.17
Power flux density at receive end dBW/m^2	-91.19
Bandwidth Hz	22000000
Receive antenna diameter m	5
Receive antenna aperture efficiency e.g. 0.65	.8
Receive system noise temperature (antenna+LNA) K	100
Signal power at output of receive antenna dBm	-48.98822
Receiver sensitivity (see manufacturer spec e.g -80 dBm)	-85
Receive margin dB (0-5dB=marginal, 10-15dB=good)	36.011777
Receive antenna gain dBi	40.25931
Receive G/T dB/K	20.259318
Link C/N dB	55.218

Figure 1: Link-budget calculator

MENTORING OF SUMMER BRIDGE STUDENTS

In addition to my work on the LMCST proposal, I mentored two students from the Summer Bridge program, Jennie Castillo and Kaipo Kent. Jennie and Kaipo are incoming electrical engineering freshmen hoping to learn about the mission design process and obtain insight into the space technology field. During their first week, I gave a brief overview of the satellite's various components and LMCST's objectives and goals. Each subsequent week thereafter, they were given a research assignment, approved by Professor Lloyd French, to help them understand the basic mission concepts, build their researching skills, assess their work ethic and attain valuable research to prepare a proposal. At the end of each week they presented their research by either submitting a one to two page document or by oral presentation. During the third week I assigned each student a separate subsystem to research. Their research of the assigned subsystem provided the necessary information to complete the LMCST spacecraft design. Their research also served as the topic of the presentation given to parents and members of the Summer Bridge Program. Both students completed the Summer Bridge Program successfully and hope to pursue a more active role within the LMCST.

Figure 2: Graduation of the Summer Bridge Program
From right to left Kaihoolulu Rickard, Jennie Castillo, Kaipo Kent, and Zachary Lee-ho

FUTURE ENDEAVORS

My summer final task is to assist Professor Lloyd French with other prospective missions. We are working to expand the opportunities for LMCST and the Hawaii Space Grant Consortium by attempting to secure a mission partnering with Jet Propulsion Laboratory (JPL) and Ames Research Center (ARC). Initially, JPL was interested in partnering with the University of Hawaii to perform an asteroid mission using our microsatellite bus. If the mission was successful it would mean additional funds for developing LMCST satellite and opportunities for future collaborations with JPL. I assisted Professor Lloyd French by providing needed system information, collaborating with student scientist and participating in teleconferences with JPL and ARC. However, JPL and Ames focus shifted from an asteroid mission to a lunar mission. The new goals for the lunar mission proved to be to demanding for the LMCST satellite bus. We were unable to participate in the anticipated JPL and Ames mission, but Professor Lloyd French remains a closely affiliated with both organizations to ensure that the University of Hawaii remains our leading option for future mission collaborations.

CONCLUSION

Through my summer work with Professor Lloyd French I have learned a great deal more about system architecture and component capabilities. The students I mentored have an increased understanding of the space technology field and show enthusiasm for continuing their research with LMCST. This summer's research activities assisted in improving the LMCST satellite design.

ACKNOWLEDGEMENTS

I will like to first thank the Hawaii Space Grant Consortium (HSGC), Dr. Luke Flynn and Dr. Ed Scott for the opportunity to continue my work on LMCST during the summer and for allowing me to be affiliated with the SGC Program. A big thank you goes out to Professor Lloyd French who has been an inspirational person, motivating me and ensuring I stay focus to achieve my ultimate goal. My gratitude also goes out to Ms. Gindi French, Dr. Torben Nielsen and Mr. David Hampton for providing added guidance and help to me through my work. Thank you to Ms. Marcia Sistoso for her patience, assistance and her aid in ensuring I meet my deadlines. I want to finally say thank you to Jennie Castillo and Kaipo Kent for their help with research this summer and allowing me to instill in them some of the knowledge I received from the instrumental people that I stated above.

REFERENCE

Cardin J. M. and Acosta J. (2000) "Design and Test of an Economical Cold Gas Propulsion System", 14th Annual/USU Conference on Small Satellites

Coimbra C. (2005?) "Micro-Thruster Propulsion System Description"

Radio link budget calculator – line of sight link. (July 2006)
Available [Online]: http://www.satsig.net/link-budget.htm

ANALYSIS OF *HALOCARIDINA RUBRA* IN AN ENDOGENOUSLY CONTROLLED CLOSED ECOSYSTEM

Luke J. Linhoff
Department of Marine Science
University of Hawai‘i at Hilo
Hilo, HI 96720

ABSTRACT

The biota from Hawaiian anchialine ponds (isolated saline pools) has have been known to survive for long periods of time in sealed containers. The keystone species *Halocaridina rubra* was used in a laboratory model which examined how density of shrimp effects a closed ecosystem. Multiple, small systems were used to simulate closed anchialine environments with the response variable of in order to study survival of the small endemic shrimp *H. rubra*. *H. rubra* were stocked at different densities with 3 replicates for each treatment of 4, 8, 11, 13, and 16 individuals per 1-liter container which was sealed. Optimum density was found to be 3.2 shrimp per liter of semi-sealed environment with evidence of a negative, cumulative boom and bust cycle only of 8 shrimp per liter causing an ecological crash. The biology of *H. rubra* was also examined by a salinity tolerance LC50 study which the shrimp to have a 5-40 ppt salinity tolerance. Subsequent starvation trails showing range showed *H. rubra* to survive 42 days without food. Natural anchialine habitats were explored by visiting several pond complexes to understand how the natural system works to aid in creating better closed ecosystems. A list of environmental parameters and biota from field observations useful for the creation of closed ecosystem was created.

INTRODUCTION

The islands of Hawaii contain unique environments and ecosystems. Particularly, the big island of Hawaii because of its unusual abundance of anchialine ponds. Anchialine ponds are isolated saline pools generally restricted to the porous substrates such as lava flows. The ponds are unusual because they have a subsurface connection with the water table and are tidally influenced and have no surface connection to the ocean. Some Anchialine ponds can be found with very little nutrients going in or out of the system due to extremely sparse rainfall combined with their extreme isolation from nearby vegetation. These ponds have developed an ecosystem with extremely high rates of nutrient recycling making them ideal for closed ecosystem research. A closed ecosystem, also known as a microcosm, is a small sealed container with biota which survives for an extended period of time through recycling nutrients between organisms. This biota has been used in several studies of closed ecosystems in a two-year microgravity environment including over 2 years on the International Space Station.

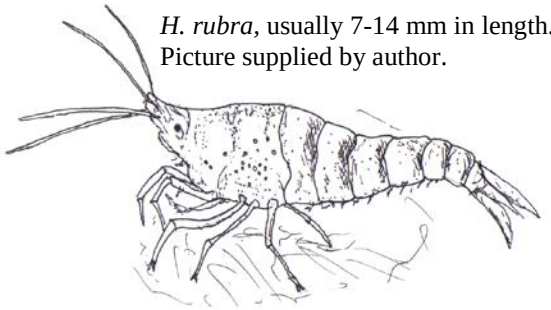

H. rubra, usually 7-14 mm in length. Picture supplied by author.

Halocaridina rubra (Figure 1), is an extremely important inhabitant of anchialine ponds. It is endemic and found only on the main Hawaiian island chain. *H. rubra*is is a small (7-14mm), red omnivorous shrimp that can be found in pristine ponds with densities approaching over 100 per square foot. They have extremely flexible nutritional requirements and lifespan of at least 10 years. *H. rubra* shrimp often spend much of their time in the underground hypogeal environment of porous rock around and underneath anchialine ponds. *H. rubra* comes to the surface of the anchialine ponds to obtain food and retreat underground for safety and to breed (Maciolek, 1983).

In order to better understand the anchialine biota for closed ecosystems it was necessary to explore three areas of study. First, a laboratory model examined how density of shrimp affects the closed ecosystem. Secondly, the biology of *H. rubra* was explored though salinity tolerance and starvation trails. Third, the natural anchialine habitat was explored by visiting several pond complexes. Numerous readings were taken in the field such as maximum density of shrimp, survey of various biota, and water quality measurements. This data helped to understand how the natural system works in order to aid in creating more complex closed ecosystems.

METHODS OF DENSITY IN 1-LITER LAB MICROCOSMS

Laboratory microcosms consist of 1 L. glass Erlenmeyer flasks were sealed to contain the following: 900 mL of sea water (35 ppt salinity), 125 g “seeded” gravel, 1 inch square porous sponges used as substrate for development of algae and phytoplankton, a varying quantity of the shrimp *Halocaridina rubra*, and 2 g of photosynthetic *Melosira* sp. algae. The differing numbers of shrimp are 4, 8, 11, 13, 16 individuals with 3 replicates of each density. Each flask was given a number and letter for identification. The first number corresponds to number of initial shrimp and letter (A, B, or C) the specific replicate. A maturation period of 7 days was applied before the shrimp were added to the flasks. The microcosms were subjected to a natural light cycle of 12 hours of light, and 12 hours of darkness. Lighting was from a 30” 64 watt Orbit artificial marine aquarium light consisting of 1 dual actinic [420 nm + 460 nm] and 1 dual daylight [6,700K + 10,000] bulbs. Once the experiment began, after the shrimp were added, nothing was removed or added to the flasks. The only time they were unsealed was for taking water quality measurements with a YSI probe. Measurements of salinity, temperature, dissolved oxygen, percent oxygen saturation specific conductivity and number of living shrimp was taken every other day and recorded on a data sheet.

METHODS OF SHRIMP LC50 STUDY

The LC stands for "Lethal Concentration". Lethal LC values usually refer to the concentration of a chemical in air or water. The concentration of the chemical in air/water that kills 50% of the test animals in a given time is the LC50 value. To accomplish this study, 50 mL plastic sample vials were filled with water at 8 different salinity concentrations of 0, 5, 10, 35, 40, 45, 50, and 55 ppt. Three replicates for each and 1 shrimp were placed in each vial and deaths were recorded every 60 minutes for 72 hours after loading. Surviving shrimp were left without food to see how long they can survive without food in a subsequent starvation trial. These and all were

METHODS OF FIELD SURVYING

Sampling was conducted at 27 ponds in the Makalawena and Awakee coastal area. Also, brief surveys and collections were done at Hilton Waikoloa anchialine pond complex, Lua O Palahemo, and Leleiwi. This data was then compared to the survey performed in May 1988. At each pond several different types of data was taken. First, the presence/absence of *Halocaridina rubra* was noted at each pond site. This was conducted by running visual transects with snorkel gear if the pool was large enough to dive in. Ponds that were too small to dive in, thorough observations were made by walking in and around the pool to search for the shrimp. If the shrimp density was considerably high, maximum density of the shrimp was found by taking 5 random photo quadrates with an underwater digital camera. Readings of temperature and salinity were taken within the top 10 cm of the water column. Measurements were taken using a portable refractometer and a Hanna Instruments portable pH, EC, TTD, and C^{o} water tester.

RESULTS AND DISCUSSION OF DENSITY IN 1 LITER LAB MICROCOSMS

After laboratory experimentation, optimum or stable density for the H. rubra in a semi-closed microcosm appears to be 3.2 individuals per liter of environment. Success of each system seems somewhat dependent on the initial number of shrimp in the system. The average number of living shrimp after 56 days was as follows, 2.33 for replicates with 4 initial shrimp, 0.0 for 8 initial shrimp, 4 for 11 initial shrimp, 2.66 for 13 initial shrimp, and 5.66 for 16 initial shrimp F. Of the 5 different densities initially added, they can be split into 3 groups for discussion. The first group, 1, is flasks with 4, 11, and 13 initial shrimp. These dropped down to 2-4 shrimp within 32 days and seem to have stabilized at 2-4 per flask and then they seemed to level off. Next, the flasks that contained 8 shrimp exhibited an ecological unbalancing with the resulting death of nearly all shrimp within 24 days. The In all densities except for those with 4 initial shrimp, there was a loss of 6 shrimp on average within 8 days. After 8 days the death rate slowed in all densities.3rd group is flasks that which contained 16 shrimp initially. These lost an amount of shrimp similar to the other flasks then the death rate slowed and is declining towards the more assumed more stable number of 2-4 shrimp.

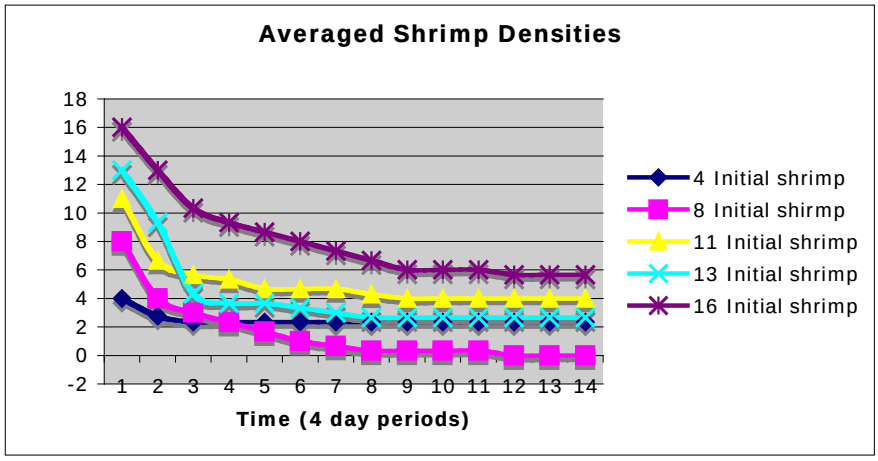

All replicates with 8 initial shrimp experienced rapid death of all shrimp while densities both higher and lower stayed relatively stable was unusual. However, Straphanopoulos and Liepmann also mention this phenomenon though provided no explanation. I believe this may be explained by an unstable boom and bust cycle or a series of cyclic growth and decline between the shrimp and algae, the shrimp's main food. The microcosms had a minimum of seeded

substrate containing aerobic bacteria therefore the primary producer of CO^2 was most likely the shrimp. While the higher densities of shrimp offer a greater CO^2 output from respiration and the breakdown of their waste for a faster production of algae, though the grazing pressure is also much higher. At a lower density of shrimp there would be a much smaller grazing pressure on the algae combined with less CO^2 production and less algae growth. Both higher and lower densities experienced a boom and bust cycles that eventually stabilized into a constant of a nearly equal rate of grazing versus algae growth. At a density of 8 shrimp, all replicates first experienced a typical cycle however it slowly and cumulatively deteriorated until the ecological system crashed. This may have been due to the grazing rate being very slightly higher then the growth rate of algae as it oscillated back and forth. Once this negative feedback cycle was started, it continued even as shrimp died off. The continuation, even with less shrimp, was probably caused by lower production rates of CO_2 and the grazing rate still exceeding the rate of algae growth. As algae levels got smaller, a dip in O_2 was noticed once all shrimp had died, a sharp spike in O_2 followed by a reversal, ending in very high levels of CO_2 as the ecological systems crashed.

RESULTS OF LC50 STUDY AND STARVATION TRIAL

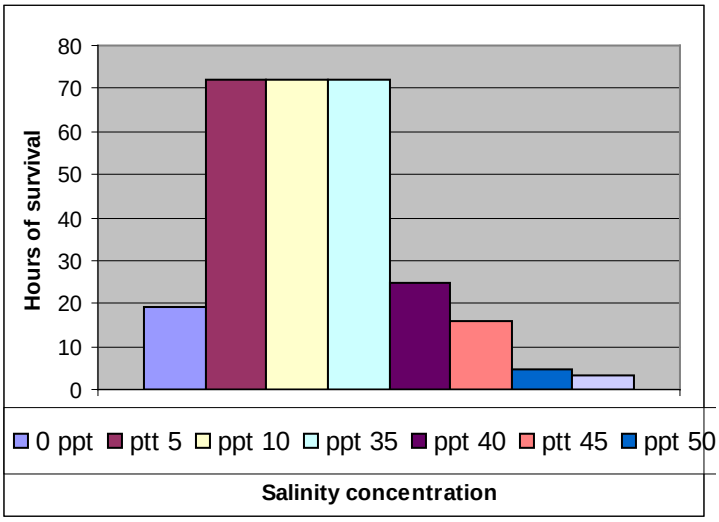

The lowest salinity concentration the shrimp, *H. rubra,* could survive in was 5 ppt and a maximum of 35 ppt salinity for the duration of 72 hours (Figure 2). The shrimp that survived in the 5, 10, and 35ppt replicates were then kept without food to see how long they will survive. These shrimp being put through subsequent starvation survived for a maximum of 42 days proving their extremely flexible nutritional requirements.

RESULTS FROM FIELD SURVAYING

Surveying several field sites gave a much better idea of the complexity of an anchialine habitat. Some ponds at Awakee may be half a mile from the ocean and any vegetation in a rugged `a`a lava flow; yet will be teaming with shrimp and only 10 cm deep. These are both important species in the anchialine environment, which may be useful for creating larger more complex environments. Ideally it would be good to get large amounts of environmental biota collected from natural ponds for anchialine microcosm research. Also, using data from the actual anchialine pond collections are made from may increase success. By modeling water quality parameters, and collecting biota straight from a pond gave a noticeably smaller initial die off of biota. If natural collection is not available, Table 1 gives recommended environmental parameters found in the natural environment that should be mimicked in order to accurately

recreate an anchialine system. Table 2 gives recommendations for biota that was commonly found in natural, oligotrophic anchialine ponds and can be used in closed ecosystem creation.

Table 1

Chemical parameter	Recommendation
Water Salinity	20-35ppt
Water pH	pH 8.2 ± 1.5
Temperature	20-28 ^{0}C
Lighting	Light levels are particularly harsh in the western part of the Hawaii island. Also, the shallow water in the pools filters little light so a broad light range (6,700-10,000K) is needed to mimic natural sunlight.

Table 2

Biota	Recommendation	Notes
Shrimp	*Halocaridina rubra*	Microcosms should be loaded with an initial density of 3.2 shrimp per liter of environment plus an additional 20 percent of the total number to account for initial die offs.
Algae	*Milosara spp.*	Best if collected directly from natural environment.
Encrusting Cyanobacteria	Species unknown	Environmentally collected, orange/yellow/brown in color.
Snails	*Assiminea nitida* *Thiara granifera*	Small, herbivorous snails common throughout anchialine ponds good for larger microcosms.
Maturation period	Shrimp should be added 2 weeks after all other biota added to allow the bacteria and algae to establish and mature.	Little or no maturation time may cause systems to ecologically crash within 1 week.

CONCLUSION

The density of the H. rubra appears to fluctuate toward equilibrium for optimum stability in these small closed ecosystems and not spatially for individual shrimp. The density levels would most certainly change with different biota such as faster growing algae, longer periods of sunlight or greater amount of substrate. The phenomenal length of time that these microcosms may persist is astounding and may be attributed to *H. rubra* acting as a buffer organism. The shrimp may act as a "buffer" in a closed system to keep other species from over-growing enough to cause a major shift in nutrients and species succession to crash the system. *H. rubra* probably acts as an endogenous control to regulate the levels in the rest of the system. The shrimp's long life span, extremely flexible diet of both macro and micro biota, it not gaining in mass to a sizable amount and not breeding without suitable habitat makes them an extremely effective control mechanism. It acts almost as a simple, autonomous machine to keep all levels of the food chain in check. In designing other closed ecosystems, a buffer organism similar to *H. rubra*

with these traits would be highly desirable. *H. rubra* is a chemically tolerant organism with extremely sparse nutritional requirements make it idle for the fluctuating conditions found in a microcosm. Also, when designing a closed ecosystem it is important to take into consideration oscillations and negative feedback like that which occurred at a medium density such as 8 shrimp per liter. Many small anchialine microcosms sold commercially or homemade often only last 2-3 years. This slow deterioration is probably due to a very slow version of what happened to all replicates containing 8 initial shrimp. It has been proven that a microcosm may last 25 years or more and long-term success is very possible.

The microcosms based off existing anchialine ponds provide a cheap, small scale and very robust system for research. During the course of fieldwork, it was very difficult to find pristine anchialine ponds with high levels of shrimp. The majority of anchialine habitat has already been destroyed and much of what is left may soon be developed. Some ponds such as Lua O Palahemo, a rare deep lava tube pond sampled, contains a shrimp species found only in that pond and no were else on earth. Yet has no protection from collection or dumping of refuse into the pond exists and even less for most other anchialine ecosystems. Conservation measures are greatly needed for the fragile anchialine habitat.

ACKNOWLEDGMENTS

Without the never-ending unyielding support and guidance of my mentor Dr. Jason Turner of the Marine Science Department at University of Hawaii, Hilo this project would never become a reality. Thanks also to Dr. Patrick Hart whose advice and help with data analysis and statistical tests made everything make sense. Thanks to Kevin Donmoyer for his hours compiling data on the computer and Chris, Margret, Sara, and Lisa for covering the water quality tests when I was busy. Finally, thanks to the Hawaii Space Grant Consortium and the NASA Space Grant Undergraduate Fellowship Program for funding this amazing opportunity.

CITATIONS

Maciolek, J.A. (1983**)** Distribution and Biology of Insular Hypogeal Shrimp. Bull. Mar. Sci. 33:60-616.

Maciolek, J.A . (1987) Evaluation of Anchialine Pools in the Awakee, Kohahaiki, and Makalawena Land Divisions, North Kona, Hawaii. Prepared for County of Hawaii, No. 87-132 30. June.

Straphanopoulos and Liepmann. (1985) Development and Global Sensitivity, Analysis of a Closed Ecosystem Ecological Modeling, CA, April 15.

AN INVESTIGATION OF PROGENITOR-INJECTED RADIONUCLIDES DURING SOLAR SYSTEM FORMATION

Daniel R. Rogers
Department of Physics and Astronomy
University of Hawai‘i at Mānoa
Honolulu, HI 96822

ABSTRACT

This project explored how the initial conditions of young star clusters can later affect the distribution and compositions of its individual stars. Emphasis was placed on solar mass stars, as a long-term goal is to describe the conditions that allow for the formation of a solar system with properties similar to our own- and to determine how probable it is that this can happen. One such property is its chemical composition. This prompted a study of progenitor-injected isotopes by a supernova event during the sun's formation. It was made possible by the online NBODY4 simulation test bed. The simulator was used to estimate the contribution of injected ^{60}Fe in comparable solar systems by multiple progenitor stars. The results indicate that, under *very* particular conditions, a single supernova event could have supplied the amount of ^{60}Fe estimated to have been present in our solar system during its formation. There are still many facets of this process, however, that need to be investigated to fully confirm this theory.

INTRODUCTION

A star cluster is a collection of stars in which there is a constant cycle of birth, death, and rebirth. Stars are primarily composed of simple elements such as hydrogen and helium. However, the extreme temperatures and pressures deep within the interior of a mature star can initiate the production of heavier elements. Considerable amounts of such elements can be produced during this process, especially in very massive stars. The death of a star of this magnitude is marked by gravitational collapse followed by an abrupt outward explosion (known as a supernova event) from which these heavier elements are discharged into space.

Now consider if part of this expelled cloud of isotopes were to fall into the gravitational field of a neighboring star that is in the early stages of its formation. At this point the young star is surrounded by what is known as a protoplanetary disk, which is the dense disk of gas and dust from which planets and asteroids form. If the ejecta from the supernova event collided and blended with this disk, it would contribute to its chemical composition and perhaps even accelerate its collapse into planetary objects [(6)].

This is the prediction of one of the leading theories that attempts to explain the presence of heavier elements in our own solar system, and others. This is obviously impossible to prove by experiment, but fortunately there are ways to justify this process by studying observable properties of the solar system.

One such property is the concentration of the stable isotope ^{60}Ni, which has been detected and measured in meteorites that have remained essentially untouched since the collapse of our sun's protoplanetary disk. Studies have proven that a correlation exists between ^{60}Ni and stable isotopes of iron in these meteorites, specifically ^{56}Fe [(5)]. Basic chemistry predicts that the unstable isotope ^{60}Fe will decay into ^{60}Ni with a half-life of only 1.5 million years, and thus it is

theorized that it was initially ^{60}Fe that was present in the meteorites [6]. Coincidentally, it is known that ^{60}Fe is one of the isotopes that massive stars form in their cores in the process described above. In fact it is possible determine the exact amount of ^{60}Fe a star will produce based only on its mass [3]. Therefore, ^{60}Ni might serve as an indicator as to how much supernova ejecta our solar system collected during its formation.

There are many factors that might have affected our sun's absorption of such ejecta. This includes the size of the star cluster in which it formed, and the ratio of the total potential and kinetic energies in that star cluster (known as the virial ratio). As these properties change, the average distances between solar mass stars and likely supernova do as well. This is significant since stars that are further from supernova events will receive less ejecta. As mentioned earlier, a long-term goal of this project is to determine the probability that a solar system like our own will form. This implies that if comparable amounts of ^{60}Fe ejecta can be received by solar mass stars through this process across an assortment of star cluster radii and virial ratios, then it is likely that supernova events were a significant part of our sun's formation. This also means that there may be similar solar systems elsewhere in the galaxy.

THEORY

The amount of ejecta that a solar nebula can receive is inversely proportional to its square distance from a supernova explosion [6].

$$(\text{mass } ^{60}\text{Fe injected}) = \frac{(\text{total mass } ^{60}\text{Fe ejected})}{(4(\text{pi})r^2)} (\text{pi})(\text{radius of protoplanetary disk})^2$$

The assumption here is that the total amount of ejecta from the supernova is spread out over a uniform sphere, from which the amount collected by a young star depends on the radius of its protoplanetary disk. Since it is impossible to know exactly how much ^{60}Fe was initially present in our solar system, we use an estimated ratio between ^{60}Fe and ^{56}Fe based on meteoritic evidence [5].

$$\frac{(^{60}\text{Fe})}{(^{56}\text{Fe})} = \frac{(\text{mass } ^{60}\text{Fe injected})}{(\text{mass of protoplanetary disk})(\%\text{ mass of } ^{56}\text{Fe in the disk})}$$

By combining these two equations, it is possible to calculate the minimum radius of a solar nebula for it to have received an appropriate amount of the isotopes.

$$(\text{radius of protoplanetary disk}) = \sqrt{\frac{\frac{(^{60}\text{Fe})}{(^{56}\text{Fe})} (\text{mass of protoplanetary disk})(\%\text{ mass of } ^{56}\text{Fe in the disk})(4r^2)}{(\text{total mass } ^{60}\text{Fe ejected})}}$$

This calculation can be made using estimated values for each of the variables.

$$(\text{mass of protoplanetary disk}) = \sim 0.01 \text{ solar masses around a solar mass sized star}$$

This value is a mass estimation for the protoplanetary disk around a solar mass star [1]. It is actually thought to be somewhere between 0.01 and 0.10 solar masses, but a lower estimation was chosen to increase the precision of the results.

$$(\%\ \text{mass of}\ {}^{56}\text{Fe in the disk}) = (\%\ \text{mass of total Fe in disk})(\text{fraction of}\ {}^{56}\text{Fe in total Fe})$$

$$= (\sim 0.014\%)(0.9157) = 0.01282\ \%$$

The iron in our solar system is thought to comprise roughly 0.014% of the mass of the entire system. An estimated 91.57% of this iron consists of the isotope ^{56}Fe. This predicts the total amount of ^{56}Fe in the solar system to contribute to 0.01282% of its mass [4].

$$(\text{total mass}\ {}^{60}\text{Fe ejected}) = \sim 0.0002512\ \text{solar masses (from a 60 solar mass progenitor)}$$

$$= \sim 0.00006309\ \text{solar masses (from a 45 solar mass progenitor)}$$

As mentioned before, the amount of ^{60}Fe produced in the interior of a star throughout its lifetime can be determined from its mass. The above estimates were taken from research by Marco Limongi and Alessandro Chieffi in 2006 [3]. The highest estimate was used for this study.

$$\frac{(^{60}\text{Fe})}{(^{56}\text{Fe})} = \sim 10^{-7}$$

This ratio has been determined from the studies of meteorites discussed above. The actual approximations range from 10^{-6} to 10^{-7}, but again a smaller value was used to increase the precision of the results [5]. This ratio is one of the most critical estimated variables in these calculations. Its actual number is still being investigated.

Calculating a minimum radius for the protoplanetary disk of a solar mass star using known properties of our solar system suggests how probable it is that a supernova event played a role in its formation. Protoplanetary disks rarely exceed a few hundred astronomical units (AU) and have never been known to stretch beyond 1000. The farthest we have observed a body orbiting our sun is roughly 47 AU, indicating that it may have been reduced to a few tens of AU before planet formation. Thus, if these calculations yield reasonable values over a wide range of initial cluster radii and virial ratios, then they will provide support for the progenitor star theory.

METHOD

The dynamics of star clusters are complex and it can take millions of years to see any observable differences, both of which render direct observation of these systems impossible. The online NBODY4 simulation test bed, however, has helped to make this study possible. It uses the GRAPE-6a supercomputer located at Cambridge to allow for the study of star systems on such grand scales. Physical variables and numerical parameters are easily assigned using a straightforward input interface.

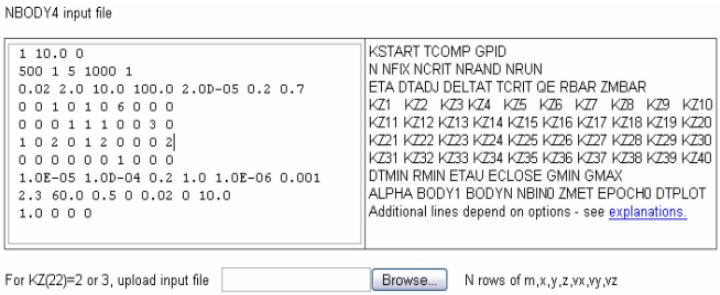

(Figure 1) This is the input interface described in the text. To use the simulator, visit the website http://nbodylab.interconnect.com.

As seen in Figure 1, it is possible to manipulate many properties of the simulation. The most notable of which are the number of stars in the cluster (N), the initial radius (RBAR, in parsecs), the virial ratio (Q), the simulation time period (TCRIT), and the average, maximum, and minimum masses (ZMBAR, BODY1, and BODYN respectively, all in solar

masses). The simulator creates randomized clusters that behave accurately with respect to these numbers. It then outputs a spreadsheet with the initial and final masses, positions, and velocities of every star in the system. This spreadsheet is printed in an eight column format; mass, x-axis, y-axis, and z-axis position components, x-axis, y-axis, and z-axis velocity components, and an assigned star number. This text is output to a file that can be downloaded and easily read by a number of computer programs; IDL (Interactive Data Language) was used for this study. Alternatively, it is possible to *create* a file with the same eight column format to use as the initial cluster distribution in a simulation. This allows for star systems with specifically selected properties to be run through the simulator for any desired amount of time.

PROCESS

The first step of this project was to determine the distribution of a star cluster that might be considered representative (a good example of an "average" cluster). Initially, it was decided that a 500 star cluster ranging from 0.5 to 60.0 solar masses (with an average of 0.72 solar masses) would be sufficient.

It must be noted that there is a relatively small window of time during the formation of a solar system in which supernova ejecta is optimally received. This window is on the scale of a couple million years for a solar mass star. This is the reason that the maximum mass value was set at 60 solar masses; stars of this size have short lifetimes of about 3.89 million years, which improves the probability of it becoming a supernova during the necessary time period [6].

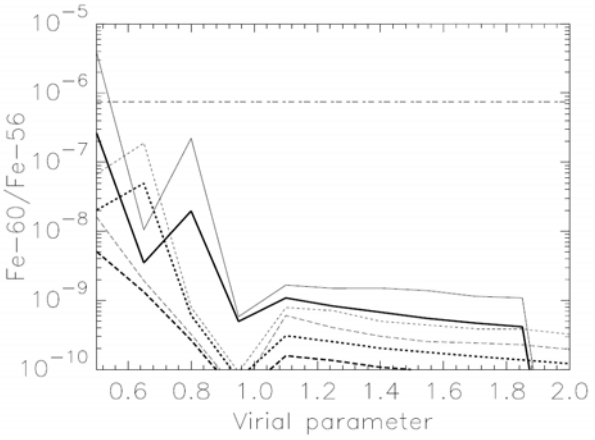

(Figure 2) The results from several N=500 simulations. None of the combinations reach the desired threshold.

These parameters were then tested with varied initial radii (ranging from 0.2 to 2.0 parsecs, in increments of 0.2) and virial ratios (ranging from 0.5 to 2.0, in increments of 0.15). Figure 2 is a visual of our results. Each line is a probability curve representing a specific radius. The dark line is a cluster with an initial radius of 0.2 parsecs; the dotted line, 0.6 parsecs; the dashed line, 1.0 parsec. The horizontal line is the threshold for the 60Fe/56Fe ratio predicted to have been present in the early solar system. Even with an array of virial ratio and initial radius combinations, it became clear that this particular model did not account for the needed amounts of isotopes. It was then decided that more realistic conditions were required. A cluster of 8500 stars ranging from 0.1 to 60.0 solar masses (with an average mass of 0.72 solar masses) was chosen in hopes that it might yield more accurate, and promising, results. The minimum mass was lowered because the NBODY4 simulator seems to prefer that stars below 0.5 solar masses, generally considered to be negligible, are present.

A second supernova event was included to see if it could significantly add to the total of ^{60}Fe injected. Understanding the role of multiple supernovae is a crucial part of the progenitor star theory. Based on the initial mass function, the second most massive star in a cluster of this size would be approximately 45 solar masses and have a lifetime of about 4.6 million years.

With a new cluster size having been determined, the NBODY4 program was allowed to run for 3.8 million (real-time) years. The output from this simulation was used in an IDL

program written to find all of the stars between 0.9 and 1.1 solar masses, and calculate their distances in parsecs from the largest star in the cluster (again, set to be 60 solar masses). It then used this distance to calculate and output $1/(4\pi r^2)$ for each of the solar mass stars.

The output file from the 3.8 million year simulation was then used as the input file for another simulation. The numbers in the NBODY4 interface were changed to account for stars ejected from the system in the first simulation and the maximum mass was set to 45 solar masses. This was run for 0.8 million years to bring the total amount of simulation time to 4.6 million years, the expected lifetime of a star of this size. Again, the output was run through the IDL program.

This process was repeated for four sets of initial radii and virial parameters. Two of these sets held the radius (R) constant at 1.0 parsec and varied the virial ratio (Q) between 0.5 and 2.0. The other sets held Q constant at 1.0 and varied R between 0.2 and 2.0 parsecs.

After $1/(4\pi r^2)$ was calculated by IDL, it was necessary to convert the units from $1/(\text{parsecs}^2)$ to $1/(\text{astronomical units}^2)$ so that the calculated radius of each solar nebula would be in astronomical units ($1\ \text{parsec}^2 \sim 4.25\text{e}10\ \text{AU}^2$). The maximum, minimum, 50%, and 90% percentile values of $1/(4\pi r^2)$ were then used to do the calculations outlined in the theory section.

RESULTS

(Figure 3) These graphs show the relative amounts of ^{60}Fe contributed by the 60 solar mass progenitors (the black bars) and the 45 solar mass progenitors (the white bars) in each of the four cases. Each bar represents one solar mass star. The values on the y-axis designate (in solar masses) the amount of ^{60}Fe available to each star per square astronomical unit (AU), based on their distances from the supernovae. The *exact* amount of ejecta these stars might have received is dependent on the area of their protoplanetary disks.

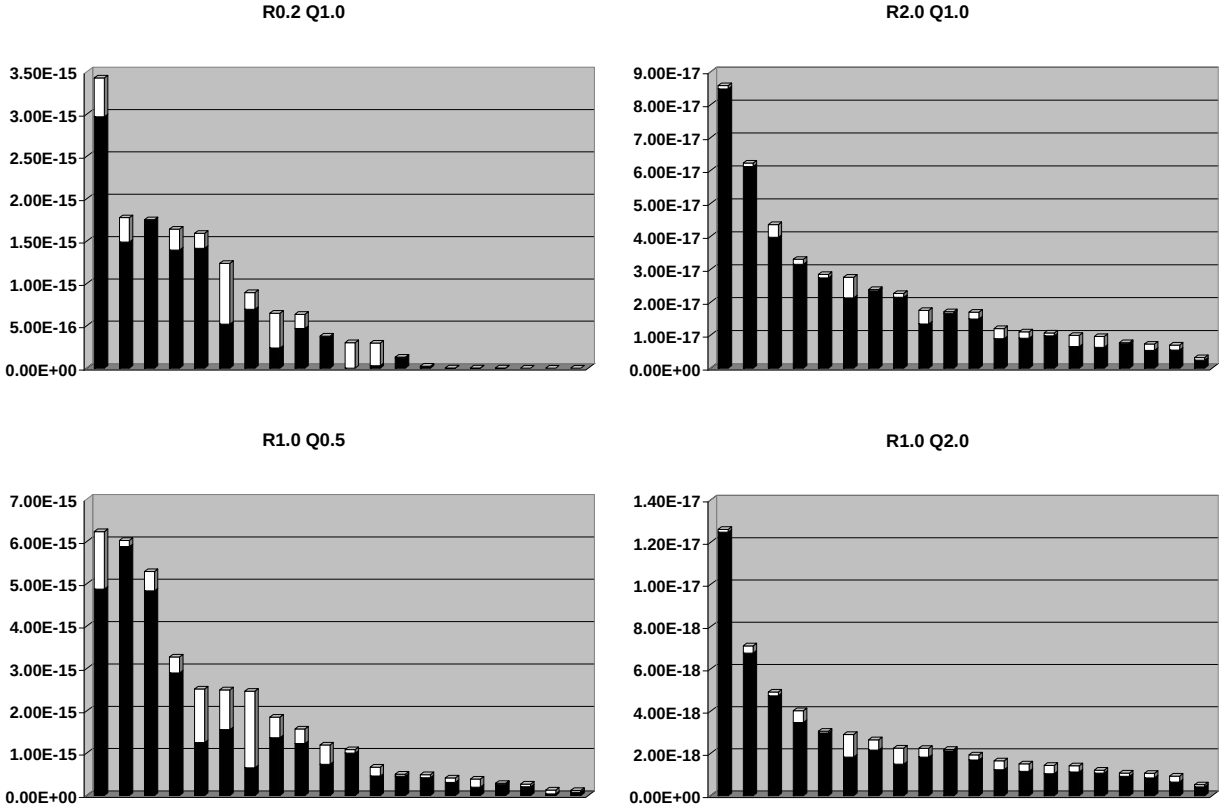

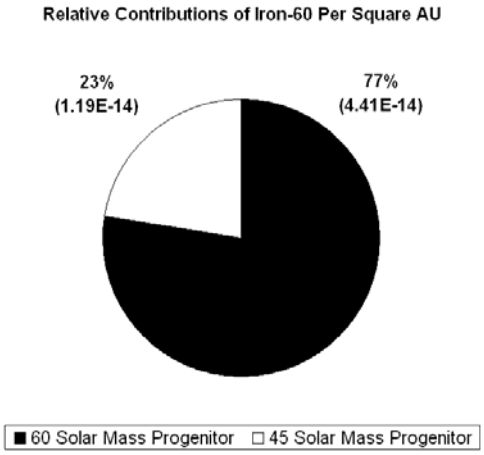

(Figure 4) This displays the sum of all the ^{60}Fe available to each star per square AU of area, from all four cases. The values are given in solar masses per square AU.

The visuals in Figure 3 show, for each of the four cases, how much ^{60}Fe per square AU the twenty closest stars could have received from the supernovae. The exact amount of ^{60}Fe that would have been collected, however, is dependent on the area of each protoplanetary disk. It is apparent from Figure 4 that the 60 solar mass progenitors are dominant in contribution, at a total of 77%. The 45 solar mass progenitors supplied about 23% of the overall abundance. Stars in the clusters with relatively higher values of *R* and *Q* were able to absorb total amounts of ^{60}Fe of up to 10^{-17} solar masses per square AU of area. The two clusters with relatively lower values of *R* and *Q* saw total contributions on the order of 10^{-15} solar masses per square AU; these saw comparably more involvement from the 45 solar mass progenitors than the other two sets.

Table A presents the required radius of a solar mass star's protoplanetary disk to have collected enough ejecta to produce ^{60}Fe/^{56}Fe=10^{-7}. The minimum and maximum distances represent the closest and farthest stars from the first supernova event, respectively. Half of all the solar mass stars in a system fall within the median distance of the supernova, giving a good indication of the distribution in each data set.

(Table A) The data here is the required radius in terms of astronomical units.

	Star At Minimum Distance	Star At Median Distance	Star At 90% Distance	Star At Maximum Distance
R0.2 Q1.0 (case 1)	3.71	5.24	18.43	318.92
R1.0 Q0.5 (case 2)	2.64	2.91	7.89	45.31
R2.0 Q1.0 (case 3)	21.94	35.98	66.97	161.43
R1.0 Q2.0 (case 4)	57.19	92.87	165.45	384.48

There are two major conclusions that can be drawn from these results. The first is that the amount of ^{60}Fe contributed by a second progenitor is not nearly as much as the first. Although it supplies almost a fourth of the total from all four cases, only four out of these eighty stars saw more contribution by the second supernova event than the first. Had this fraction been closer to one half, the second progenitor would have been considered in later calculations. It is also more probable that a star of 60 solar masses will contribute during the appropriate time period. We can then make the assumption that (in this particular study) a second progenitor is negligible in comparison to the first due to its relatively low contribution and the fact that the 4.6 million year lifetime of a 45 solar mass star pushes the limit of the opportune absorption time frame.

As expected, stars in simulations run with lower values of *R* and *Q* received more ejecta than in those with relatively higher values. This is because they represent more tightly bound clusters, implying that the solar mass stars will be closer on average to the supernova events. This also means that the required radius of each protoplanetary disk is smaller (Table A). Remember that the farthest object observed to be revolving around our own sun does so at about 47 AU. The solar mass stars *closest* to the supernova events in cases 3 and 4 require that the radius of their protoplanetary disks be about 23 and 57 AU, respectively. Half of the solar mass

stars in these cases require a radius larger than 36 and 93 AU. It is *possible* that they could have received the necessary amount of ^{60}Fe, but not nearly as likely as in cases 1 and 2. In these cases, 90% of all the solar mass stars in each system need a radius no larger than 18 and 8 AU. This is *well* within the scale of our own solar system, and presents the exciting possibility that a single progenitor star could indeed have provided the nourishment it needed to become what it is now. This also suggests the possibility that similar solar systems could have formed within our sun's star cluster, if said cluster has a relatively small radius and low virial ratio.

CONCLUSION

This study has determined that the contribution of ^{60}Fe by a second progenitor star is negligible, and that the amount provided by one could have been enough for our solar system under certain conditions. There are limitations on the realism of these results, however. Many assumptions were made about the nature of the early solar system, as estimated values were used for critical variables while making these calculations (based on legitimate studies, of course). There are also the inherent problems of using a computer to simulate the behavior of nature. The simulation test bed used here, for instance, does not take into account mass loss due to gas ejection- an important part of any stellar process. Even without these particular drawbacks, there is still one *very* important assumption that has been made; that all of the protoplanetary disks are face-on relative to the supernova event (to maximize the flux of the ejecta through the disk). Very little ejecta would be received by a disk if it were facing a progenitor edge-on. These shortcomings are not grounds for abandoning this study, however. In fact it gives astronomers even more reason to continue researching, as this is still a likely explanation for the chemical abundances seen in our solar system. Conclusions are sure to get increasingly closer to the truth as mathematical techniques and computer programs improve in accuracy over the years to come.

ACKNOWLEDGMENTS

I would like to thank both NASA and the Hawai`i Space Grant Consortium for providing this wonderful opportunity. My first research experience has been very fulfilling. This is due, of course, to my exceptionally encouraging mentor, Dr. Eric Gaidos. He has taken me under his wing for over a year and a half, and I can't thank him enough for introducing me to the world of cutting-edge science.

REFERENCES

(1) Lada C. and Lada E. (2003) Embedded Clusters in Molecular Clouds. *Annu. Rev. Astron. Astrophys:* ***41***, 57-115.

(2) Leshin L. A., Ouellette N., Desch S. J., and Hester J. J. (2005) A Nearby Supernova Injected Short-lived Radionuclides into our Protoplanetary Disk. *Chondrites and the Protoplanetary Disk: ASP Conference Series:* ***341***.

(3) Limongi M. and Chieffi A. (2006) The Nucleosynthesis of ^{26}Al and ^{60}Fe in Solar Metallicity Stars Extending in Mass from 11 to 120 Solar Masses. *The Astrophysical Journal:* ***647***, 483-500.

(4) Palme H. and Jones A. (2003) Solar System Abundances of the Elements. *Treatise on Geochemistry:* ***1***, 41-61.

(5) Tachibana S., Huss G. R., Kita N. T., Shimoda H., and Morishita Y. (2005) The Abundances of Iron-60 in Pyroxene Chondrules from Unequilibrated Ordinary Chondrites. *Lunar and Planetary Science:* ***XXXVI***, 1529-1530.

(6) Tobin J. J., Looney L. W., and Fields B. D. (2006) *Radioactive Probes of the Supernova-Contaminated Solar Nebula: Evidence that the Dun was Born in a Cluster*. Faculty Publication, Univ. of Illinois at Urbana-Champaign.

BIO-INSPIRED DESIGN OF THERMAL SYSTEMS FOR SMALL SATELLITES

Kristian Sexton
Department of Mechanical Engineering
University of Hawai‘i at Mānoa
Honolulu, HI 96822

ABSTRACT

This work explores the optimization of fin geometry for tubular space radiators. The significance of this work to both NASA and the UH Cube Sat program is discussed in the introduction that follows. The methodology used consists of a unique approach utilizing the Lindenmayer or L-system as well as the turtle interpretation to generate geometric structures. These structures will then be evaluated using finite element analysis and a genetic algorithm will be used to allow them to evolve to an optimum geometry. The approach is discussed in further detail in the methods section of this report. The project is still in progress and the accomplishments thus far are presented in the results section.

INTRODUCTION

There is currently a great deal of interest in small satellites. This interest stems in part from lower costs, shorter time of elaboration and potential to include sophisticated payloads. Small satellites allow for a greater number of entrants into a realm that is otherwise cost prohibitive for most.

The reduced mass and available volume creates definite challenges for the thermal control of small satellites. Currently thermal control is a limiting factor in the extent and sophistication of the payload systems that these satellites can handle. Any technological advancement in the ability to remove heat from the satellite would allow for greater complexity in the electronics equipment carried. This would allow expansion of the capabilities and potential uses for these satellites. The lower cost and greater ease in launching these systems makes any improvements in their versatility and capabilities significant to the space industry with obvious benefits for both NASA and smaller organizations such as universities that have, or wish to develop satellite programs.

Heat transfer within the satellites is primarily via conduction through structural elements and special conductive lines. Heat is dissipated to the environment via radiation alone. One way to improve heat transfer from the satellite to the environment is to improve the geometrical configuration of the heat dissipating fin structure. The present work will focus on the optimum geometric fin structure for a tubular space radiator. This area has been explored by others including Krikkis and Razelos who optimized the geometry for both rectangular and triangular fins. However, the present work is unique in that no part of the geometry will be apriori. The structure of the fin system will be allowed to evolve in the same manner as biological systems found on earth. We will use the result of Krikkis and Razelos as the benchmark with which to compare out results.

METHODS

The initial model consists of a simple three-dimensional tree like fin structure. The base of the fin is set to a constant temperature, T_b, while the rest of the boundaries conditions allow heat to radiate from the fin to outer space. The defining equation for these boundary conditions stems from the Stefan Boltzman Law.

$$q = \sigma\varepsilon(T^4 - T_E^4) \qquad (1)$$

where q is the heat flux, σ, is the Stefan-Boltzmann constant (5.67 x 10^{-8} W/m^2K^4), ε is the emissivity, T is the surface temperature of the fin, and T_E is the temperature of space. Radiation between the structures within the fin and other fins will be ignored for the initial analysis, but will be added at a later time to allow for more realistic results.

Heat transfer through the fin will be accomplished through conduction and as such will be modeled using Fourier's Law of Heat Conduction. For an isotropic medium Fourier's Law in terms of Cartesian coordinates in three dimensions is

$$q_x = -k\frac{\partial T}{\partial x}; \quad q_y = -k\frac{\partial T}{\partial y}; \quad q_z = -k\frac{\partial T}{\partial z} \qquad (2)$$

where q_x, q_y and q_z are the components of heat flux in the x, y, and z directions respectively, k is the thermal conductivity and $\frac{\partial T}{\partial x}$, $\frac{\partial T}{\partial y}$ and $\frac{\partial T}{\partial z}$ are the changes in temperature in the x, y and z directions respectively.

The heat flux out of the surface of the fin can be calculated by integrating the heat loss along the length of the fin.

$$Q = \int_0^L P\varepsilon\sigma(T^4 - T_E^4) \qquad (3)$$

where L is the length of the fin and P is length of the perimeter of the fin.

We have input this simple model into the finite element analysis toolbox Comsol Multiphysics and have been successful in attaining a numerical solution. Figure 1, below, shows the temperature distribution for a copper fin with its base temperature at 500 K, an emissivity of 0.8 and the temperature of the surrounding environment at 0 K. The program also allows us to integrate over the boundaries of the fin and thus obtain the net heat flux out of the fin. The internal properties of the fin can be easily changed which will allow us to explore the geometries developed with different fin materials.

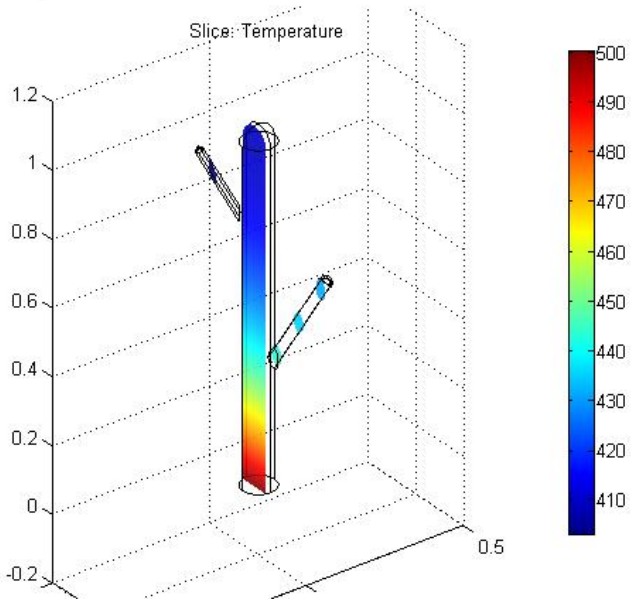

Figure 1. Temperature distribution for 3-D fin structure. Solution generated using finite element toolbox COMSOL

The main distinction between our approach to the given problem and those used in the past lies in the fact that we will not make any assumptions regarding the geometry. At the heart of this approach is the L-system. L-systems were originally conceived by Aristid Lindenmayer as a way to model the development of branched topology in plants. They are parallel rewriting systems that can be used to generate words. These words can then be translated to generate graphs using what is known as the turtle interpretation. L-systems consist of an alphabet $\sum$, an axiom ω, and a finite set of production rules *P*. The application of the L-system and its turtle interpretation will be described using examples closely related to our particular application.

The alphabet used in our application consists of the letters A to I, and the symbols [,], +, -, ^, ., #, !, *, /. To demonstrate the L-system we will reduce the alphabet to the letters A through D and use the following production rules: $A \to BC$, $B \to CDA$ and $D \to A$. Letters and symbols for which no production rules exist simply remain unchanged so in our example: $C \to C$. The axiom is the point where we start and we will select $\omega_0 = A$. We can then apply the production rules as many times as we wish to obtain more complicated words. The results for up to four applications of the production rules are shown below.

$\omega_1 = BC$
$\omega_2 = CDAC$
$\omega_3 = CABCC$
$\omega_4 = CBCCDACC$

It is easy to see that the words created can quickly become more complex. As a result the graphs that are generated using the turtle interpretation can also become complicated quickly.

The turtle can be thought of as a logo style turtle that moves as directed by the letters and symbols of the generated words. In our application the letters A to I move the turtle forward one step, the symbols + and – turn the turtle left or right by a specified angle, the symbols ^ and . turn the turtle up or down by a specified angle, the symbols # and ! change the branch width by a fixed amount, and the symbols * and / change the step length by a fixed amount. The symbols [and] begin and end branches respectively. An example of a graph generated in COMSOL with MATLAB using this system is shown in Figure 2.

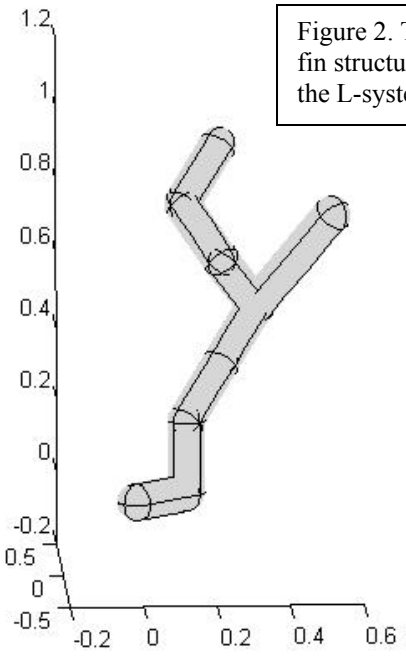

Figure 2. Three Dimensional fin structure generated using the L-system

Figure 2 was generated by the word [C^^A.BB[++C+D--A]+**B]. In this example, the step length is initially set at 0.2, the change in step length applied by the symbols * and / is set at 0.1 and the change in specified angle for turns in both the x-y

plane and z direction is set at 45 degrees. The initial [begins the first branch. The letter C moves the turtle forward one step. The symbols ^^ rotate the turtle upward 90 degrees. The letter A moves the turtle forward one step. The symbol . rotates the turtle down 45 degrees. The letters BB move the turtle forward two steps. The symbol [begins the second branch in which the turtle is rotated 90 degrees to the right, moved forward one step, rotated 45 degrees to the right, moved forward one step, rotated 135 degrees to the left, and moved forward one step. Once the symbol] is reached the turtle returns to the point where it branched earlier and continues form there. The symbol + rotates the turtle 45 degrees to the right and the symbols ** increase the step length to 0.4. The letter B then moves the turtle forward one step.

The ratio of heat flux over area will be used to determine the fitness of each design. MATLAB's genetice algorithm has been set up to allow the production rules for the L system to evolve and this will allow the algorithm to be used obtain the optimum design.

RESULTS

We have been successful in developing MATAB code that allows us to generate three-dimensional graphs in COMSOL using the L-system. We have connected this code to MATLAB's genetic algorithm and are able to use this feature to evolve production rules for the L-system. We have also been successful in developing a working three-dimensional baseline model in COMSOL. We are currently in the process of transferring the boundary conditions from the baseline model to the graphs generated by the L-system. When this process is complete we will be able to determine the fitness of each graph generated by the L-system. This will allow us to use the genetic algorithm to evolve the optimum fin design. When this process is finished we look forward to interesting results.

DISCUSSION

We expect to see significant improvements over the benchmark as established by Krikkis and Razelos. We also expect to see a fairly high level of complexity and a dendritic structure. In addition to improvements in heat dissipating characteristics this type of structure would also provide increased robustness. It is further expected that the level of complexity is more important than smaller details of the structure and that there is in fact an optimal level of complexity. This can be seen in numerous biological systems such as the vascular system in animals and the differing vein structures in leaves of the same species.

CONCLUSION

At this time we have not been able to complete our project. The progress, however, is promising and we anticipate finishing the project within the next month. We have successfully used the L-system to generate 3-D topologies in COMSOL as well as connected these topologies to MATLAB's genetic algorithm. Once the boundary conditions within the L-system generated graphs are set, we should be able to begin running the genetic algorithm and obtain significant results.

ACKNOWLEDGEMENTS

Professor Marcelo H. Kobayashi, Department of Mechanical Engineering, University of Hawaii at Manoa

REFERENCES

Rizos N. Krikkis and Panagiotis Razelos (October 2002) Optimum Design of Spacecraft Radiators With Longitudinal Rectangular and Triangular Fins, Journal of Heat Transfer, Vol 124

Marcelo H. Kobayashi (2007) On a Bio-inspired Topology Optimization Method

Prusinkiewicz, P. and Lindenmayer, A., Springer Verlag, New York, (2004) The Algorithmic Beauty of Plants

PICOSATELLITE NETWORK DESIGN

Tyler N. Tamashiro
Department of Electrical Engineering
University of Hawai‘i at Mānoa
Honolulu, HI 96822

ABSTRACT

A communication system is described for use in ground-to-satellite communication and inter-satellite networking. The network design is centered around the features provided by the Microhard MHX-2400 Spread Spectrum Transceiver. The research and design process is explained based on the hardware and software constraints of the picosatellite. The network design facilitates both reconfigurability and redundancy for a picosatellite network.

INTRODUCTION

The vast majority of satellites designed by and for NASA require many years of research and development before they are launched and become operational. The costs quickly add up and easily run into the millions for each produced satellite. However, picosatellites have the potential to become a viable and economical alternative to conventional satellites. In order for these picosatellites to work efficiently together, a solid communication network needs to be established between the satellites and the ground station.

The main goal of this research is to produce a fully working network implementation that can easily be applied to any network of satellites. This involves designing, implementing, and testing the hardware and software that will be used by each picosatellite in the network. This report covers the design and testing of the communication subsystem in a picosatellite and a network design that can be used for a constellation of picosatellites.

This research was conducted in collaboration with the University of Hawaii's Small Satellite Program. The Small Satellite Program at the University of Hawaii is currently working on its fourth generation of small satellites and continues to improve and incorporate many new and innovative technologies.

TRANSCEIVER

The primary role of the communication system is to facilitate a reliable wireless link between the satellite's microprocessor to another microprocessor located at a ground station or onboard another satellite. To accomplish this goal, a suitable transceiver was chosen for the picosatellite.

The three transceiver frequency bands considered for use are: 430 MHz (downlink)/144 MHz (uplink), 900 MHz (downlink & uplink), and 2.4 GHz (downlink and uplink). The 430/144 MHz band is the most commonly used communication frequencies in the small-satellite community and has been used in the past two CubeSat projects at the University of Hawaii. However, the limited bandwidth of 9,600 bps (bits per second) greatly restricts the satellite's ability to transmit large payloads such as images down to Earth in a timely fashion. Therefore, the lesser used frequency bands of 900 MHz and 2.4 GHz bands were considered. The 2.4 GHz

Microhard MHX-2400 was chosen because of its feature set and increased bandwidth of 115,200 bps in comparison to radios in the 900 MHz band. One of the great features of this radio is its ability to have each radio assigned its own network address and unit address. This is very similar to IP networks where a network address and unit address are linked to each node. A block diagram of the communication subsystem is shown in Figure 1a and the MHX-2400 transceiver is shown in Figure 1b.

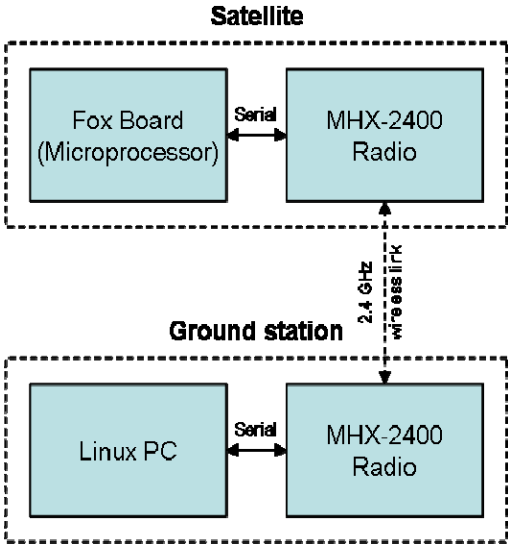

Figure 1a: Block diagram of communication subsystem

Figure 1b: Microhard MHX-2400 Transceiver

SOFTWARE PROTOCOL

The Linux-based Fox Board by ACME is the microprocessor used in the picosatellite. Using Linux made development simpler because the code could first be compiled and tested on a Linux computer before being moved over to the Fox board. However, there were several problems encountered during the software development.

The most significant problem dealt with the serial read and write function being a blocking function. This means that when data was sent to the function to be passed on to the radio, the function would not return until it was done sending. Therefore, should the communication link break (communication window passes), the satellite would essentially be stuck in communication mode. It would not be able to "timeout" because the function would not allow anything else to be done while it was waiting for all data to be sent.

To fix this problem, the serial port needed to be opened with the O_NONBLOCK flag to make all read and write functions immediately return after passing or retrieving the data from the serial port. The problem with this method is that the microprocessor would have no idea if the data was successfully sent after being passed to the radio. This can lead to a buffer overflow if the radio's buffer of four kilobytes gets filled faster than it can output it wirelessly. Therefore, a software flow control protocol needed to be implemented to ensure the reliability of the communication link.

To provide this flow control was a simple acknowledgement to every chunk of data sent. This was needed because after the serial write function sends the data to the radio it immediately

returns without waiting for the data to drain from the radio buffer. Since there was no way of being able to tell if the radio buffer was empty or not, the acknowledgement packet from the other radio was used to indicate when to send the next packet. Although this method does incur extra overhead costs due to the constant sending and acknowledgement packets, it is an acceptable cost for reliability.

GROUND STATION INTERFACE

The ground station program is usually the first to run and will wait until the beacon packet is received from the picosatellite. When the picosatellite turns on and checks for a communication link it is given the beacon packet to send down. If the two radios make contact with each other, the beacon packet which is in the satellite radio's buffer is sent down. The ground station replies with a confirmation packet which can also be used as a method of authentication for security purposes. After the satellite verifies the confirmation packet it then retrieves the directory contents of the satellite and prints it out to the user. Finally, it will go into interactive mode by requesting input from the user. The satellite will go into a command processing mode where it listens for commands from the ground station and processes them sequentially. Figure 2a shows the communication session events and Figure 2b shows the output at the ground station side.

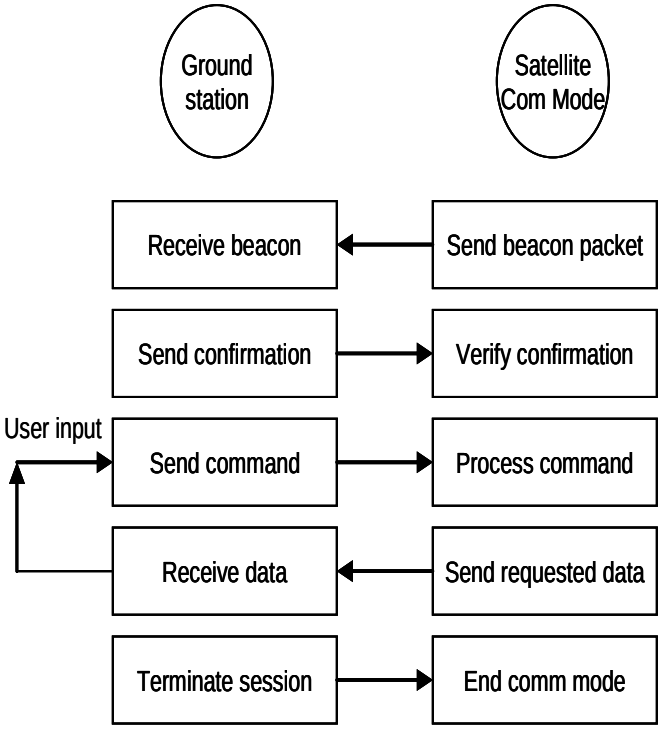

Figure 2a: Communication session diagram

```
Entering Ground Station Communication Mode
Listening for satellite beacon packet

Beacon received
Sending Confirmation packet

Sending Request for diagnostic log
Request sent.  Waiting for diagnostic log.
Diagnostic log received and timestamped.

Removing old dir.fifo
Sending Request for directory
Request sent.  Waiting for directory.

Directory received
1.  imu.fifo
2.  20060419_04_20_58_121.tar
3.  batt.fifo
4.  gps.fifo
5.  diagnostics.txt

List of Commands:
1. Request Directory
2. Request Diagnostic Data

3. *Request Image*
4. *Request GPS data*
5. Request nIMU data
6. Request battery data

7. Restart a subsystem
8. Shutdown a subsystem

9. *Delete all images*
10. Delete GPS data log
11. Delete nIMU data log
12. *Delete diagnostic log*

13. *Terminate Communication mode*

Enter your choice:
```

Figure 2b: Actual ground station interface during communication mode

NETWORK DESIGN

Picosatellites provide an ideal platform for distributed network applications. These applications require the ability to establish clusters or task groups based on the mission. Since clusters of identical satellites nodes serve to increase network redundancy and single-point failure tolerance, the ability to establish a dynamically reconfigurable network is vital.

The implementation of this network design requires that each node initially begin as the master of its own network. Each node will have a list of preferred networks that can be updated by other nodes or ground station control based on the desired network topology. Initially as master of its own network, each node will wait a preset amount of time for slaves to connect to its network before attempting to connect as a slave to another network. This preset amount of time can vary depending on how important it is to establish that particular network. For example, the first network on the preferred networks list should have the highest waiting period as master before attempting to join another network. This will give other nodes a longer period of time to connect to the first preferred network.

If no slaves connect to a master's network during the initial wait period then the master turns into a slave and attempts to join the first network from the list of preferred networks. It continues through the list at preset intervals until it successfully connects to a network. After connecting to a network, the slave will send the master its GPS and unit parameters. The master will add this information to its active table of slaves. The active table of slaves held in the master node will be continuously updated through regular network status updates every few minutes. The updated table will be copied to each slave in the network so that any of the slaves will be able to assume master control should the master fail.

The master will use the GPS information gathered from the slaves to determine the relative distance between the slave and itself. These relative distances will be used to assign secondary hopping patterns to extend the network. Each slave in the network connects to the master either directly using the master's primary hopping pattern or indirectly through a slave/repeater broadcasting the network on its secondary hopping pattern. The slave/repeater connects to the network using its primary hopping pattern while using the secondary hopping pattern as a network extender. Therefore, the nodes closest to the master will connect to the master using the network's primary hopping pattern and that tier of nodes will broadcast a secondary hopping pattern that will allow the next tier of nodes that are outside of the range of the master to connect to the master via the secondary hopping patterns provided by the slave/repeaters closest to the master. This process will continue in set distance increments to allow overlapping and redundancies in the network.

Each slave in the network will use a feature called "roaming" that allows only the network address and encryption key to be specified and the closest working hopping pattern for that network will be automatically discovered. This makes the network very flexible because it allows the slaves in the network to automatically acquire a new path to the master. If a node broadcasting a secondary hopping pattern goes offline, the nodes using that node to connect will automatically search for another valid hopping pattern that is in range for that network. This cuts down convergence time when a node fails to several seconds. This is considerably better than the few minutes required for network status updates in the first design. This allows the network to branch out and extend past the range of the master.

To address master redundancy, all slaves in the network will keep a copy of the active slave table updated by the master. During network updates, the master will assign priority

rankings to each of the slaves in the network. Should the master node fail, the priority rankings will determine who is next in line to become the master. The first in line will have a set countdown time after it loses connection with the master before changing itself to become the master. Should the first in line also go down, the next in line will have a countdown timer that is set to double the countdown interval of the first one. This will allow each node in the priority rankings to have a set time to assume command as master before relinquishing the opportunity to the next in line. This method ensures that a new master will be appointed for the network if the primary master fails. Since each slave has a copy of the active slave table, the new master will be able to use that table to pickup where the master left off.

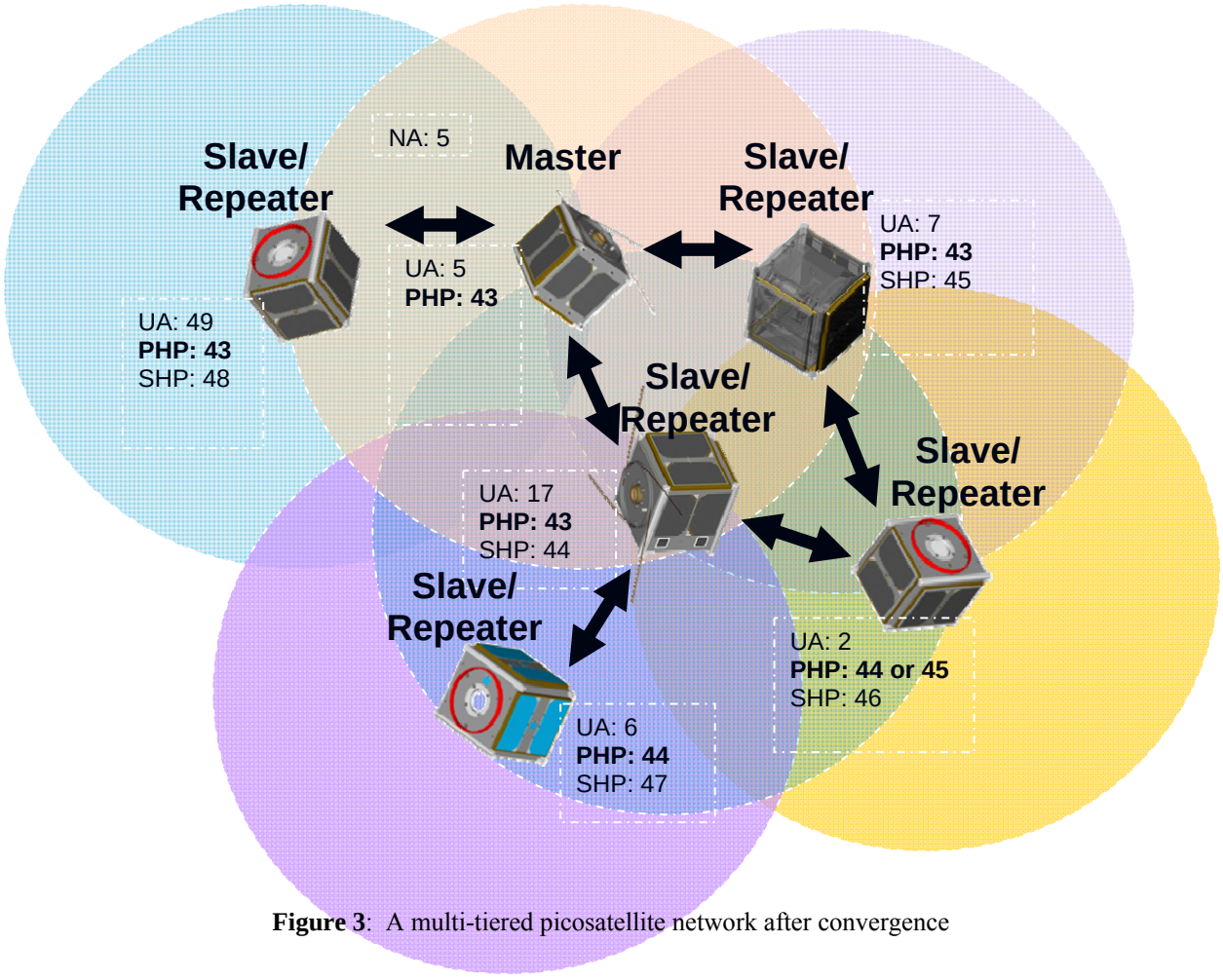

Figure 3: A multi-tiered picosatellite network after convergence

Figure 3 shows an example of a network established through the method described above. The primary master in this network has the unit address 5 and primary hopping pattern of 43. The slaves closest to the master (units 49, 17, and 7) all connect to the master directly using the primary hopping pattern of 43. However, each is assigned a different secondary hopping pattern to extend the network (48, 44, and 45). The last tier of slaves (units 6 and 2) are not in range of the master to connect with hopping pattern 43, but they are in range of the secondary hopping patterns broadcasted by units 17 and 7. Therefore, they will connect to the master via units 17 or 7 which will act transparently as repeaters. These last two nodes will also be given unique secondary hopping patterns of 47 and 46 to further extend the range of the network.

CONCLUSION

The communication protocol created for ground station to satellite transmissions was successfully implemented and tested using a third generation picosatellite built by the University of Hawaii's Small Satellite Team. The successful communication test consisted of taking the picosatellite to the top of Diamond Head crater and setting up a ground station at the University of Hawaii's Holmes Hall (Engineering Building). This test involved having the picosatellite autonomously take pictures and wirelessly transmit the pictures (Figure 4) along with diagnostic data to the ground station approximately 4 miles away.

The network design is based around the features and constraints of the MHX-2400 transceiver and provides a method of using the transceiver's features to setup a virtual picosatellite network. The method presented can be used to create a reconfigurable and redundant picosatellite network with task group clustering abilities.

Figure 4: Image of Waikiki from Diamond Head lookout taken by a picosatellite and transmitted four miles to a ground station at Holmes Hall

ACKNOWLEDGEMENTS

I've been involved with the Small Satellite Program at the University of Hawaii since I was a junior in high school. This program has provided me with valuable hands-on experience that would not be possible without a dedicated mentor/advisor and team. I would like to express my sincere appreciation to Dr. Wayne Shiroma for his dedication and commitment to the Small Satellite Program and its students. I would also like to thank the Hawaii Space Grant Consortium for their continuing support of our program. Finally, I would like to thank the Small Satellite Team for their hard work and devotion to making our projects a success.

TEMPORAL CHANGES IN MARTIAN SLOPE STREAKS

Lisa Tatsumi
Department of Geology and Geophysics
University of Hawai‘i at Mānoa
Honolulu, HI 96822

ABSTRACT

Slope streaks are fan shaped features seen on the surface in dust-covered equatorial region of Mars. Studying slope streaks by comparing overlapping images taken by the Viking Orbiters and the Mars Orbiter Camera allows documentation of changes in slope streaks over 20 to 30 years. The counts of persisting, new, and faded slope streaks in four study localities showed that there were persisting and new slope streaks in all localities whereas fading of streaks took place only in one locality. In addition, the number of new streaks is much larger compared to the number of faded slope streaks. The calculated formation rate was 3% per Mars year. This rate results in doubling the number of slope streaks in 4 decades. The present imbalance between the numbers of new and faded streaks might be temporary. Rather, the span required to have a balance might be longer period than a few decades and sudden large dust storms might be an agent that erases slope streaks. Also, a dust devil's track crossing at the upper tip of a new slope streak was found in a MOC image. It supports the possibility that slope streaks can be caused by dust devils.

INTRODUCTION

Slope streaks are down-slope mass movements on the Martian surface (Sullivan et al., 2001). They were first recognized in the images obtained by the Viking Orbiters in 1977 (Morris 1982; Ferguson and Lucchitta 1984). They consist of dark and rarer bright streaks and have fan shape with several hundred meters to a few kilometers in length and several meters to several hundred meters in width. Places where many of slope streaks are found are the equatorial regions that are characterized by their low thermal inertia and high albedo, where thermal inertia is how easily temperature of a material changes as it gains or loses energy in simple words and albedo is a percentage of reflected solar energy by a surface with respect to the incidence solar energy (Sullivan et al., 2001; Schorghofer et al., 2002). At

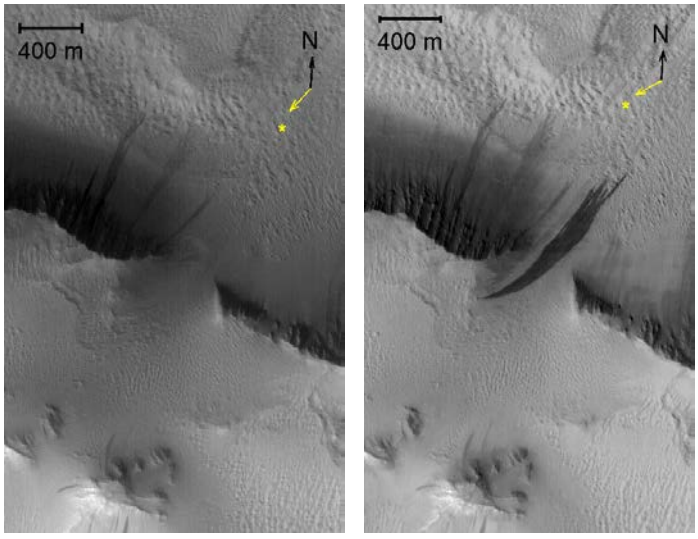

Figure 1: The left image is a part of MOC image M0806884 taken on 1999-10-28. The right image is a part of MOC image E1700689 taken on 2002-06-10. There are some persisting dark slope streaks and a new large dark slope streak formed in the middle of the image. North is up and the incident sunlight is from lower left.

the time slope streaks were found in the Viking images taken in 1977, it was not known that the slope streaks were forming in the present time. However, based on the comparisons between overlapping images from the Viking Orbiters taken in 1970s and the Mars Orbiter Camera (MOC) onboard Mars Global Surveyor taken 2-3 decades later, active formation of slope streaks was discovered (Edgett et al., 2000; Sullivan et al., 2001). Figure 1 is a good example of formation of a slope streak. Both images were taken by MOC, where the left image was taken in 1999 and the right image was taken in 2002. A new dark slope streak formed in the middle of the image over time. The mechanism of formation of slope streaks is still uncertain although several possible triggers such as sublimation of trace amount of water in the ground and aeolian processes are suggested (Sullivan et al., 2001). Fading of slope streaks was also recognized by Gremminger in 2005. Its mechanism also remains uncertain.

METHODS

Temporal changes in slope streaks are recognized and documented by comparing two or more overlapping images taken by the Viking Orbiters in 1977-1978 and MOC in 1999-2005. In addition, morphological characteristics of new slope streaks observed in MOC images are documented. MOC images are obtained by Malin Space Science Systems (MSSS) upon the requests of the area where Viking images are available and slope streaks are likely to form (equatorial dust-covered regions), and are related in their public archive. Map projected images are preferentially used in order to make it easy to compare the overlapping images. If no map projected images are available, non map projected images are rotated based on the given orientation data to give a map projected appearance using the computer software, Matlab. Also, if it is necessary, images are enhanced in contrast and some corrections are performed on, for example, flipping images using Matlab. The numbers of persisting, new and faded slope streaks are counted. Based on the counts, formation rates are calculated for each study locality. The counts are used to calculate formation rates. The formation rate q is defined as the number of new streaks per preexisting streak per Mars year. For an individual pair, **Error! Bookmark not defined.** $q = -\ln(1-\Delta n/n)/\Delta t$, where Δn is the number of new streaks, n is the total number of streaks (persisting + new - faded) and Δt is the time difference between two images. If the number of new slope streaks is small, $\Delta n << n$, and the original equation becomes $q = \Delta n/(n\Delta t)$. Using this notion, the equation for multiple overlap pairs, $\sum_i n_i \Delta t_i = \sum_i \Delta t_i \Delta n_i /(1-\exp(-q\Delta t_i))$ was derived by Aharonson et al. (2003) and is used to calculate the formation rate for each study area (Schorghofer et al., 2007).

RESULTS

In this project, four overlapping regions that involve 14 Viking images and 28 MOC images were surveyed. The coordinates of the study sites were 148°W 28°N, 344°W 2°S, 319°W 8°N, and 320°W 9°N. Spatial resolutions of these images were no more than 23 m/pixel, and the time differences fell in the range of 21.6-27.8 Earth years. The resultant counts of persisting, new, and faded slope streaks and the formation rates calculated for each region are listed in Table 1.

All study localities showed formation of dark slope streaks. Figure 2 shows a representative Viking/MOC pair of a region that shows several new slope streaks in a MOC image that formed since the time when the overlapping Viking image was taken. The

geographical coordinates for the image is 320°W 9°N. Some new slope streaks are circled, and there are some persisting streaks in the same image. On the contrary, only one area showed disappearance of slope streaks. Figure 3 shows the image pairs in which fading of slope streak was observed at 148°W 28°N. The overall formation rate was calculated to be 3% per Mars year, or 1.6% per Earth year. This rate was lower than but comparable to ~7% per Mars year that was the rate obtained from the count on 173 MOC/MOC image comparisons (Schorghofer et al., 2007).

Location	Image ID	Persisting	New	Faded	Time Difference (Earth year)	Formation rate (% per Mars year)
148°W 28°N	441B02, 441B03, 441B04, 441B05, 441B08, 441B09 / E0501067, R1302916, R1801921, R2300240, R2301380, S0200620, S0400171	86	47	5	21.6-27.8	3%
	441B04, 441B05 / M0203210, R1102947, S0200353, S0902427	2	3	0		
344°W 2°S	748A10 / M2100670, E0102238	Yes	Yes	-	22.1-22.7	-
	748A12 / M0401105, M0904689, M2300452	Yes	Yes	-		
319°W 8°N	713A68 / R1001553, R1101493, R1200984	Yes	Yes	-	25.2-26.0	1%
	713A68, 713A70 / R0900862, R1602440, R1701963	11	2	0		
	713A70 / R0802542	10	1	0		
320°W 9°N	713A53 / S1102289	1	2	0	25.4-27.4	3%
	713A57 / R1002664, R1700498	17	7	0		
	713A57 / R1201917, R1601030	13	8	0		

Table 1: The third to fifth columns show approximate number of new, persisting, and faded dark slope streaks. "Yes" indicates the number is not reliable, but there is at least one slope streak. "-" indicates there is no meaningful number obtainable. As for the image ID, IDs before slashes are Viking and after slashes are MOC images (Schorghofer et al., 2007).

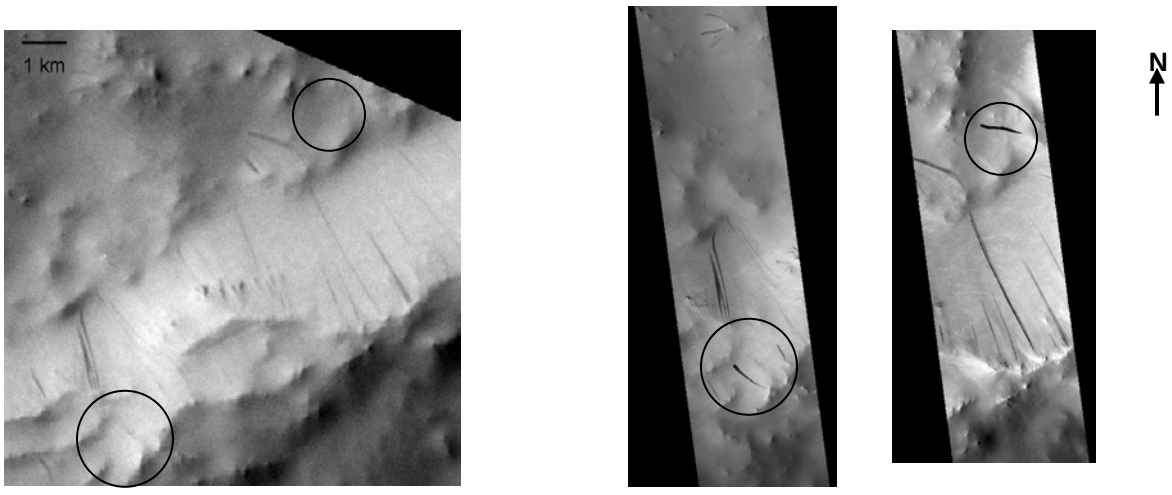

Figure 2: The left image is a part of Viking image 713A57 taken on 1978-06-01. The right images are parts of MOC images R1700498 (2004-05-06) and R1601030 (2004-04-13). There are many persisting dark slope streaks and some new streaks indicated by circles. The contrast of newer streaks is stronger within the same image.

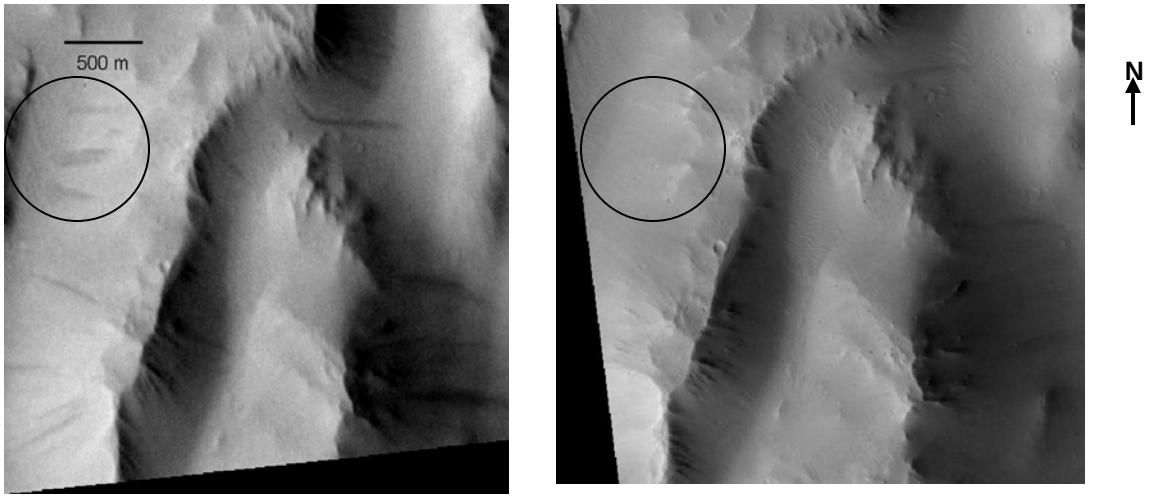

Figure 3: The left image is a part of Viking image 441B03 taken on 1977-11-02. The right image is a part of MOC image S0200620 taken on 2005-01-16. This site is a region of the Olympus Mons aureole (148°W 28°N). The locations where four streaks faded are indicated by circles. There are some persisting streaks in the images.

DISCUSSION

The fact that there are new slope streaks in all image pairs shows slope streaks were active over 2-3 decades. On the other hand, disappeared slope streaks are few. It is inferred that disappearance of slope streaks is a gradual process based on the observation that the contrast of newer dark slope streaks are stronger than that of older slope streaks within the same image. This observation suggests that slope streaks fade due to dust deposition onto the slope streaks in a relatively long period of time. The small number of faded streaks yields an imbalance between the numbers of new slope streaks and faded streaks. Also, the obtained formation rate, 3%, theoretically results in an increase of the number of slope streaks by twice in approximately 40 years, which represents an imbalance. In order to achieve a balance between the two numbers, there are two possible explanations. First, balancing takes place in a span of more than several decades. It is possible that the numbers of new and faded slope streaks in studied image pairs were on the way to be balanced. Therefore, the balance was still unperceivable and new slope streaks appeared to be in excess temporarily. The second possible explanation is that occasional large dust storms erase

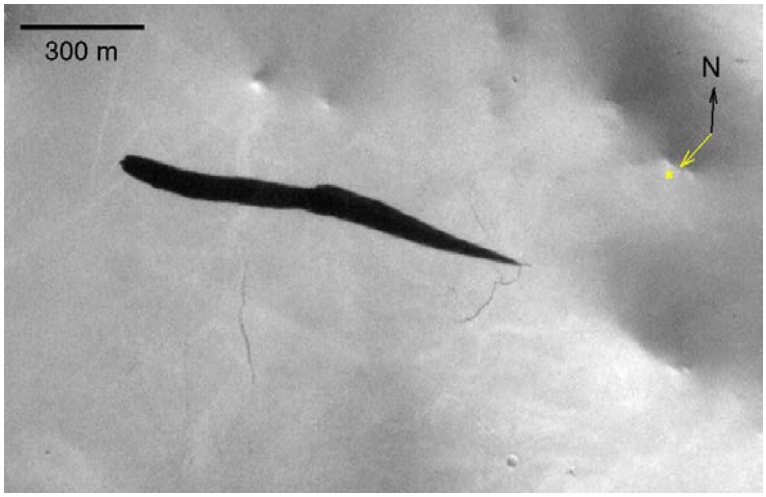

Figure 4: A new dark slope streak in the image has its origination point crossed by a dust devil track. This is a part of MOC image R1201917 taken on 2003-12-17. The streak is formed since Viking image 713A57 taken on 1978-06-01.

slope streaks. Assuming that the slope streaks fade gradually due to dust settling, erasing events by large dust storms contribute to a quick fading and balance the numbers of new and disappeared streaks. However, both hypotheses need evidence to be proven (Schorghofer et al., 2007).

As an interesting feature, there is a new slope streak formed at the location 320°W 9°N in MOC image R1201917 since Viking image 713A57 that has its upper tip, or origination point, intersected by a dust devil track (Figure 3). The track is indicated by an arrow where there are several squiggly lines that are also tracks of dust devils. Judging from the contrast of the image, the direction of the incident sunlight, and a trend of a fan shape of the new slope streak, it is clear that the right side of the slope streak in the image is at a higher elevation than the left side, therefore, the origination point of the streak. This is another example in addition to the one having the same feature reported by Malin and Edgett (2001). This example shows the possibility that dust devils can trigger formation of slope streaks.

CONCLUSION

Persisting and new dark slope streaks are observed in all four study sites in Viking (1977-1978) and MOC (1999-2005) overlapping images. It shows that dark slope streaks were active for the last 2-3 decades. The calculated formation rate is 3% per Mars year. The number of new slope streaks is much larger than the number of faded slope streaks. Based on observations, contrast of the newer dark slope streaks is stronger than the older streaks within the same image. It is deduced that the slope streaks fade gradually from this fact. The imbalance between the numbers of new and faded slope streaks can be solved by hypothesizing that the time span of balancing two numbers is much longer than a few decades or that occasional large dust storms erase slope streaks significantly. From observations of new slope streaks, one new slope streak with its origination point crossed by a dust devil track is seen. It suggests that dust devils can trigger slope streaks although the observation does not prove it.

ACKNOWLEDGEMENTS

I am grateful to NASA and the Hawaii Space Grant Consortium for providing opportunities to undergraduate students to do researches in science. Thank you also to MSSS for monitoring slope streaks in Viking images. I would also like to thank Dr. Norbert Schorghofer as my mentor who supported me throughout this project.

REFERENCES

Aharonson, O., Schorghofer, N., and Gerstell, M. (2003). Slope-streak formation and dust deposition rates on Mars. J. Geophys. Res. **108** (E12), 5138.

Edgett, K. S., Malin, M. C., Sullivan, R. J., Thomas, P., and Veverka, J. (2000). Dynamic Mars: New dark slope streaks observed on annual and decadal time scales. Lunar & Planet. Sci. Conf. XXXI (abstract #1058).

Ferguson, H. M. and Lucchitta, B. K. (1984). Dark streaks on talus slopes, Mars. In: Planetary Geology and Geophysics Program Report, pp. 188-190.

Malin, M. C. and Edgett, K. S. (2001). Mars Global Surveyor Mars Orbiter Camera: Interplanetary cruise through primary mission. J. Geophys. Res. **106** (E10), 23429-23570.

Morris, E. C. (1982). Aerole deposits of the Martian volcano Olympus Mons. J. Geophys. Res. **87**, 1164-1178.

Schorghofer, N., Aharonson, O., Gerstell, M. F., and Tatsumi, L. (2007). Three decades of slope streak activity on Mars. Submitted to J. Geophys. Res. E.

Schorghofer, N., Aharonson, O., and Khatiwala, S. (2002). Slope streaks on Mars: Correlations with surface properties and the potential role of water. Geophys. Res. Lett. **29** (23), 2126.

Sullivan, R., Thomas, P., Veverka, J., Malin, M., and Edgett, K. S. (2001). Mass movement slope streaks imaged by the Mars Orbiter Camera. J. Gophys. Res. **106** (E10), 23607-23633.

PLANAR ANTENNAS FOR SMALL-SATELLITE COMMUNICATIONS

Monte K. Watanabe
Department of Electrical Engineering
University of Hawai‘i at Mānoa
Honolulu, HI 96822

ABSTRACT

A 2.45-GHz microstrip patch antenna was designed for small-satellite communications. Optimization was achieved by trimming the copper patch to minimize the input return loss over the desired 2:1 VSWR bandwidth. Final testing of the antenna included a successful long-range data transmission over which pictures taken by the satellite were sent to the ground station. In addition to the microstrip patch antenna, a 7.3-GHz retrodirective antenna array was fabricated and tested. By combining phase detection with a frequency scanning antenna array, retrodirectivity was achieved at interrogator angles of 0°, -20°, and +15°.

INTRODUCTION – MICROSTRIP PATCH ANTENNA

The University of Hawaii Small Satellite Team completed its third-generation CubeSat in Spring 2006. This satellite named Ho’okele had a geo-referenced imaging payload consisting of a camera, GPS unit, and a nano-IMU. These components would provide a file containing a picture, GPS data, and nano-IMU data which can be used to determine the exact area of earth being imaged. All of the satellite subsystems for this satellite were finalized and a low-profile antenna was needed to complete the satellite.

It was desired to have a low-profile antenna to eliminate the need of a complicated antenna deployment mechanism. In addition there were size and form restrictions due to the physical layout of the satellite exterior. The antenna needed to fit on one end of the satellite structure. The area available for the antenna was 10 cm by 10 cm, minus the area needed for the camera aperture.

MICROSTRIP PATCH ANTENNA DESIGN AND FABRICATION

Microstrip patch antennas are a well-known type of planar antenna. This antenna was chosen for Ho’okele due to its planar structure, and ease of fabrication. Much research has been published about this antenna and numerous programs exist to aide in design.

A MATLAB program developed by Arizona State University [1] was the chosen software for the microstrip patch antenna design. The Microstrip Patch Antenna Designer MATLAB script prompts the user to enter data used to calculate the patch antenna dimensions; patch geometry, substrate thickness and dielectric constant, desired input impedance, feed type, and frequency of operation need to be entered. The code then outputs a file with the required patch dimensions in order to meet the specified requirements. Table 1 shows the parameters specified to the program. The output

	Entered MATLAB & RPDESIGN Input Parameters
Geometry	rectangular
Resonant Frequency	2.45 GHz
Dielectric Constant	2.2
Substrate Thickness	.1575 cm
Input Feed Type	coaxial
Input Impedance	50 Ω

Table 1. Input parameters of patch antenna.

dimensions of the patch antenna are listed in Table 2, and Figure 1 shows how the dimensions relate to patch geometry. The data from the design program indicated that the antenna would be larger than the allocated size on Ho'okele.

	MATLAB Output Dimensions	RPDESIGN Output Dimensions	Final Antenna Dimensions
Width of Patch (W)	4.84 cm	4.83 cm	4.11 cm
Length of Patch (L)	4.05 cm	4.07 cm	3.95 cm
Feed Position (Y_o)	1.42 cm	1.39 cm	2.23 cm
Feed Position (X_o)	2.42 cm	2.415 cm	1.45 cm

Table 2. Dimensions of antenna calculated by design programs and final antenna dimensions.

To verify the results of the MATLAB code, the same parameters were entered into RPDESIGN, another antenna design program. RPDESIGN also produced the same results, leading to the conclusion that the MATLAB dimensions were correct.

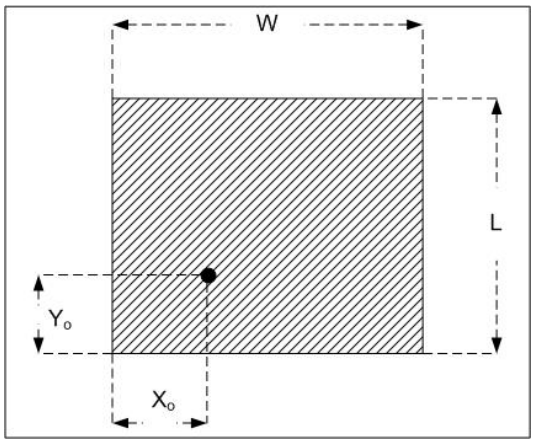

Figure 1. Layout showing the dimensions of a microstrip patch antenna.

The next step in the design process was to fabricate the antenna and optimize the design. A prototype was fabricated using copper tape and 62-mil RT/Duroid substrate with a dielectric constant (ε_r) of 2.2. The copper-tape patch cut to the specified MATLAB dimensions was affixed to the side of the substrate with the ground plane removed. An SMA connector was attached to the specified feed point location. It was then tested on the network analyzer to ensure sufficient 2:1 VSWR (-10 dB) bandwidth needed by the transceiver was available. The 2:1 VSWR bandwidth is a measure of how much power is being reflected by the antenna. In antenna design, bandwidth is commonly determined by the frequency range where S11 (input return loss) is less than or equal to -10 dB.

Optimization was necessary to decrease the footprint of the antenna, so it could fit on Ho'okele. Copper tape was cut away in slices to shrink the size of the antenna. This caused the center frequency and bandwidth to change depending on which side of the antenna was cut. For the most part, cutting pieces of copper tape from the radiating edge decreased the bandwidth while cutting pieces from the non-radiating edge increased the center frequency. Although the other parameter (bandwidth or center frequency) changed somewhat, these relationships were the dominant relationships observed.

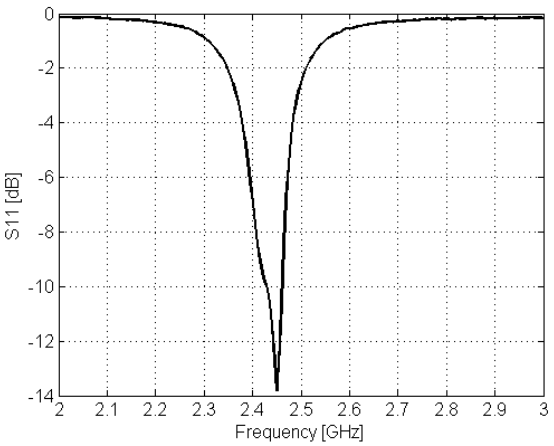

Figure 2. Input return loss versus frequency for final microstrip patch antenna.

It was noticed that when the patch became nearly square and the feed point was close to the diagonal, the 2:1 VSWR bandwidth would increase dramatically. This was an important discovery because decreasing the patch antenna size would decrease the bandwidth. To ensure that the antenna would work with the transceiver, there had to be enough bandwidth, and all previous an-

tenna optimizations did not meet the required bandwidth. When the patch was nearly square, there was enough bandwidth to assure compatibility with the transceiver.

The design was tuned a little further and then final fabrication took place. Figure 2 shows the final bandwidth of the antenna. The copper tape antenna prototype was measured and an exact permanent replica was created through photolithography and etching.

MICROSTRIP PATCH ANTENNA ANALYSIS

After final fabrication, numerous tests were performed to verify proper operation. The bandwidth and center frequency were verified through network analyzer measurements. A polarization measurement was taken to determine the antenna's polarization. The cross-polarization ratio was about 7 dB, indicating that the antenna is elliptically polarized rather than linearly polarized like it normally should be. The MATLAB and RPDESIGN specifications should produce a linearly polarized antenna. In this case, the trimming of the antenna caused the polarization to change.

According to [1], a nearly square microstrip patch antenna with feed point on the diagonal produces a circularly-polarized antenna. This is because a square's sides are equal length and this means that all edges start to radiate creating circular polarization. The diagonal feed position determines the input impedance of the antenna for matching purposes. The final antenna exhibited some elliptical polarization, but not circular polarization because the antenna was not exactly square and fed on the diagonal. This explains why the optimized antenna exhibited strange characteristics.

The final antenna was then mounted onto Ho'okele and field tests were performed. Long-range image transmission tests from Tantalus to UH and Diamond Head to UH were successful. Comparisons between the supplied ground station antenna the extra copper tape antenna showed the microstrip patch antenna improved the signal strength.

INTRODUCTION – RETRODIRECTIVE ANTENNA

A retrodirective antenna is a self-steering antenna system. Retrodirective antennas redirect their transmitting main beam to point in the direction of the target interrogator. This means that the outgoing transmission departs in the same direction as the received interrogator signal. No previous knowledge of interrogator position is needed to achieve self-steering. The benefits of retrodirective antennas over conventional antennas include security and efficiency.

Retrodirective antennas provide secure crosslinks by using a directional beam which points at the target of interest. Retrodirective antennas are efficient because unlike omnidirectional antennas which waste power by radiating in all directions, power is only radiated in the target direction. This is why retrodirective antennas are so attractive; numerous applications such as small satellites require security and efficiency.

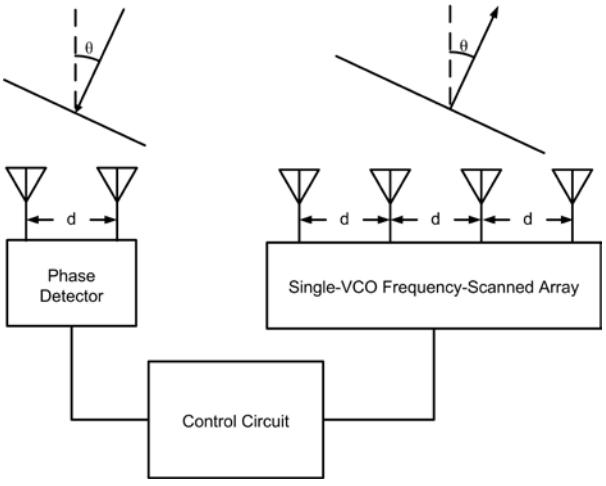

Figure 3. Block diagram of the entire retrodirective system.

The work presented in this paper is a new development from a combination of techniques previously presented in [2], which employs the technique of phase detection to control phase shifters which steer the antenna beam, and [3], which describes a novel frequency-scanned antenna array using a single voltage-controlled oscillator (VCO). The new system presented here combines phase detection of [2], the frequency-scanned antenna array of [3], and a custom control circuit to achieve retrodirectivity. Figure 3 shows a block diagram of the entire system.

RETRODIRECTIVE ANTENNA DESIGN AND FABRICATION

The entire retrodirective system consists of a phase detector, control circuit, and single-VCO frequency-scanned array. Figure 4 is a photo of the phase detector and frequency-scanned array. Phase detection and the single-VCO frequency-scanned array are explained in [2] and [3] respectively. The custom control circuit serves as the interface between the phase detector and frequency-scanned array.

The phase detector array outputs an error voltage corresponding to the angle of incidence by the interrogating signal. This error voltage is put into a control circuit that converts this error voltage into the VCO tuning voltage. The VCO tuning voltage varies the output frequency of the VCO which changes the phase delay between antenna elements and steers the beam.

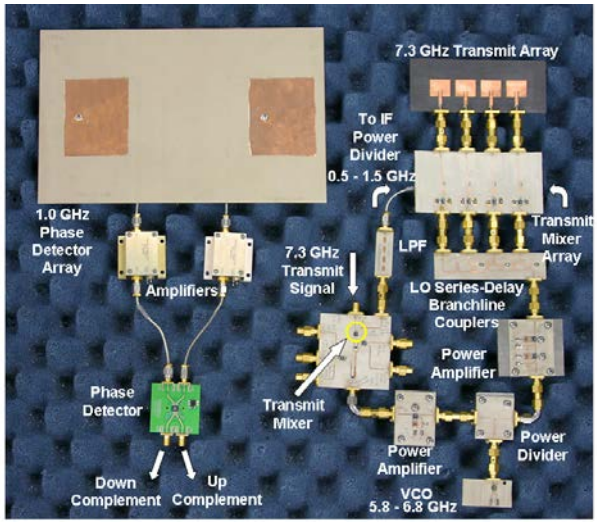

Figure 4. Phase detector array and single-VCO frequency-scanned array.

To find the transfer function of the control circuit, a relationship between phase detector error voltage and VCO tuning voltage is needed. With a direct mathematical relationship between error voltage and tuning voltage, a circuit can be fabricated to transform the phase detector error voltage into the correct VCO tuning voltage. This relation can be found by characterizing the phase detector and VCO, and doing a bit of manipulation.

The characterization of the phase detector consists of placing an interrogator at various angles and recording the error voltage. The angle of incidence can be converted to phase difference between the two elements of the phase detector array using simple trigonometry. The phase difference between elements and error voltage then needs to be plotted. A linear curve-fit is applied to the plot. The equation from the curve-fit describes the error voltage in terms of phase difference.

The VCO is characterized by connecting it to a variable voltage source and recording its output frequency with various input voltages. The frequency is then used to determine the phase difference between elements through simple algebra using the length of delay lines.

Once the phase difference corresponding to the VCO tuning voltage is found, these values of phase difference from the VCO can be put into the curve-fit equation from the phase detector characterization. Then the VCO tuning voltage can be plotted directly against error voltage calculated through the curve-fit equation. A third-order polynomial curve-fit is applied to the plot. The resultant equation is a direct relationship between phase detector error voltage and VCO tuning voltage.

The phase detector array and frequency-scanned array were already fabricated by previous graduate students. The control circuit was fabricated on a breadboard using basic operational amplifiers and voltage multipliers. The control circuit transfer function is the equation from the third-order curve-fit. These three components were integrated together to form the complete retrodirective system.

RETRODIRECTIVE ANTENNA RESULTS

Retrodirectivity of this system was confirmed through bistatic radiation pattern measurements. In the bistatic measurement, the interrogator's position is fixed, with a receiving horn mounted on a rotational arm measuring the retrodirected signal from $-60° \leq \theta \leq +60°$. Figure 5 illustrates the bistatic measurement setup. Figure 6 shows the theoretical and measured radiation patterns. Excellent correlation between theoretical and measured radiation patterns demonstrates the accuracy of the retrodirective system.

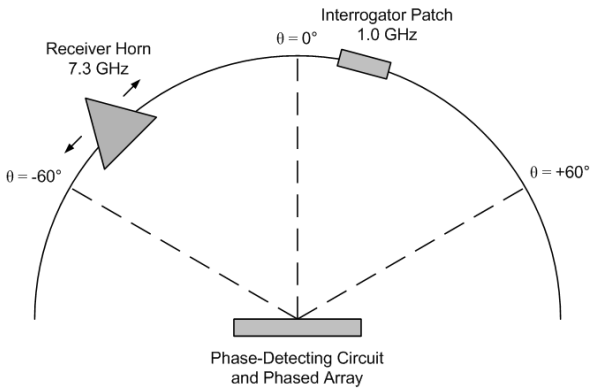

Figure 5. Measurement setup for the bistatic radiation pattern measurement

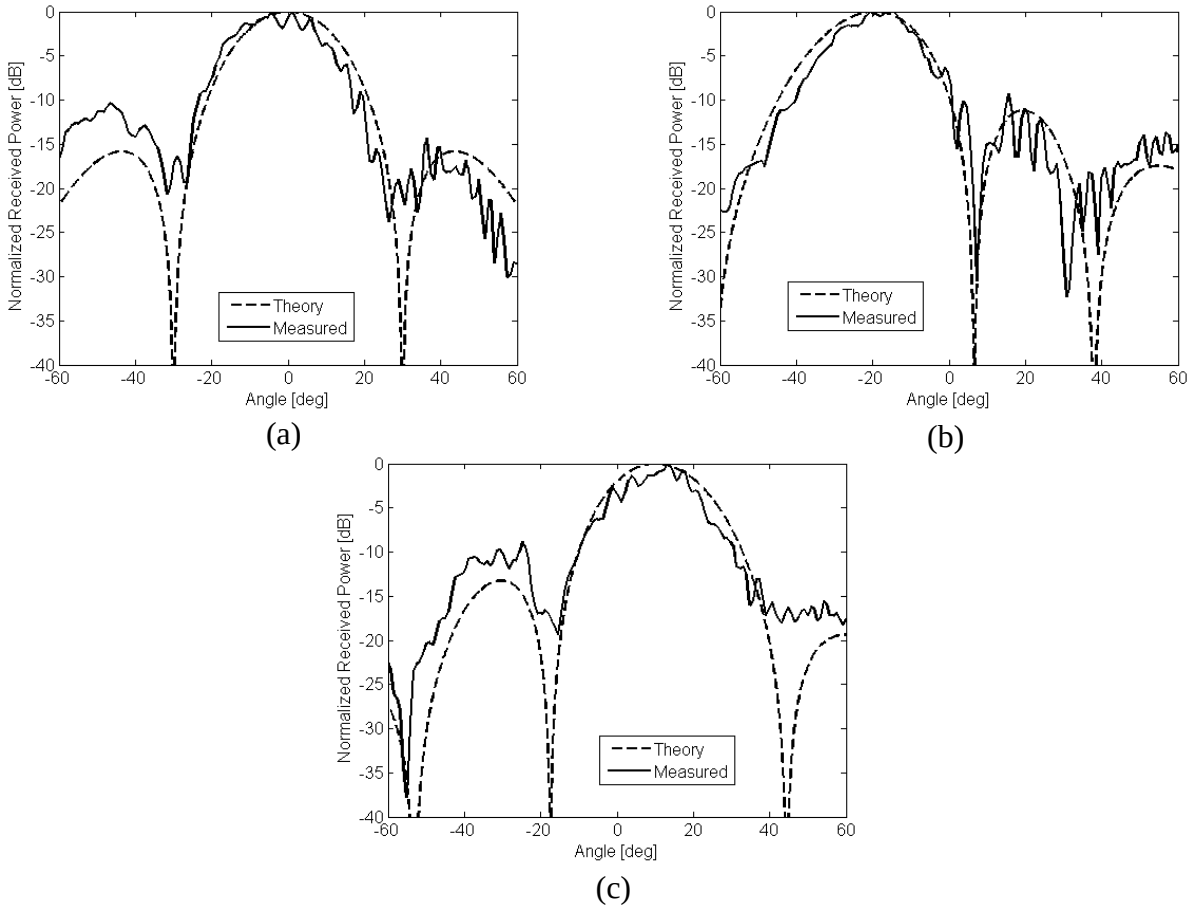

Figure 6. Bistatic radiation pattern with interrogator at: (a) 0°, (b) -20°, (c) +15°.

CONCLUSION

A 2.45-GHz microstrip patch antenna was fabricated and optimized to meet specifications set forth by the University of Hawaii Small Satellite Team. Optimization was done through the fabrication process and results were explained by microstrip patch antenna theory. This patch antenna was used in several successful data transmissions from satellite to ground station.

A 7.3-GHz retrodirective antenna array using phase detection and frequency scanning has been presented. Retrodirectivity has been proven through bistatic radiation pattern measurements with the interrogator at 0°, -20°, and +15°.

Future work will consist of decreasing the size of the array so that it can fit on small satellites. Also, a two-dimensional version of this retrodirective array will be explored.

ACKNOWLEDGEMENTS

The author would like to thank NASA and the Hawaii Space Grant Consortium for their continued support of undergraduate research and for the opportunity to further his knowledge during the conferences at Cal Poly San Luis Obispo and University of Colorado Boulder. He would also like to thank Dr. Wayne A. Shiroma his professor, mentor, advisor, and friend, for his generous help and support. The author sends his appreciation to the past and present members of the University of Hawaii Small Satellite Team and the occupants of Holmes 489 for their help and advice along the way. A final thank you goes out to Marissa and my family for always putting up with me.

REFERENCES

[1] C. A. Balanis, *Antenna Theory: Analysis and Design*, 3rd ed. Indianapolis: Wiley-Interscience, 2005

[2] G. S. Shiroma, R. Y. Miyamoto, and W. A. Shiroma, "A full duplex dual-frequency self-steering array using phase detection and phase shifting," *IEEE Trans. on Microwave Theory Tech.*, vol. 54, pp. 128-134, Jan. 2006.

[3] J. D. Roque, G. S. Shiroma, and W. A. Shiroma, "A full duplex, single-frequency-controlled phased array," in *2006 IEEE MTT-S Int. Microwave Symp. Dig.*, San Francisco, CA, pp. 453-456, June 2006.

FABRICATION OF A WIRELESS SENSOR NETWORK FOR EXTREME ENVIRONMENTS

Faye S.Y. Yuen
Department of Electrical Engineering
University of Hawai‘i at Mānoa
Honolulu, HI 96822

ABSTRACT

The ability to detect and measure water is crucial to identifying possible sites for human colonies/inhabitance in environments beyond Earth. A network of autonomous motes has the potential to augment current missions that have already found water on Mars by covering a greater area to determine how much water is present, over what area, and if it is enough to sustain life. Environmental factors – temperature, humidity, and light – will provide complementary data.

INTRODUCTION

An upcoming Mars Mission Simulation at the Flashline Mars Arctic Research Station (FMARS) at Devon Island will serve as the analog Mars environment in which the sensor network will be tested and for which the component specifications are based. The similar geology and permafrost in the rocky dry deserts of the Arctic make it ideal for testing how permafrost changes as temperature changes and how life responds to those changes. Dr. Kim Binsted, project mentor, will be participating with Dr. Chris McKay and his team in the 2007 Arctic mission.

Note that this project is a continuation of last semester's "Intelligent Sensor Network for Extreme Environments" which sought to find life by detecting bio-signs such as DNA, proteins, and macromolecules. This project, however, has been modified to meet the new goals of the upcoming Mars Mission Simulation. The revised block diagram of each mote is given in Figure 1 and each subsection subsequently discussed.

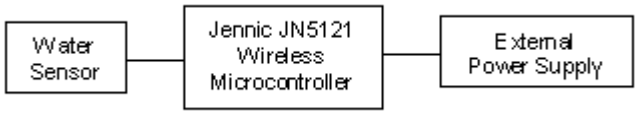

Figure 1: Revised block diagram of a mote.

NETWORK

Jennic's IEEE802.15.4 evaluation kit has been used to implement the wireless sensor network. Data is sent and received via 2.4GHz IEEE802.15.4 compliant radio waves. The star networking topology is currently being used such that each mote is wirelessly connected to a central mote that will send the desired data to the main computer for data collection and analysis. An alternative to the star topology is having the motes communicate between each other, "hopping" information between outlaying motes until it reaches the central mote where it is sent to the computer.

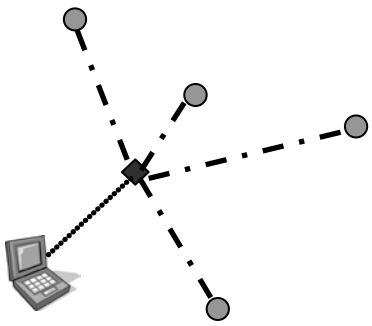

Figure 2: Star networking topology currently configured on the motes.

Figure 2 shows graphically how the motes are connected. The black diamond represents the central mote, while the gray circles represent the outlaying motes. Dashed lines represent the [wireless] communication between motes and the main mote, and between the main mote and the computer.

Data is sent at certain intervals throughout the day, rather than continuously. Data packets can be tracked using the Daintree Sensor Network Analyzer. By monitoring data packets, it can be determined which motes continue to send useable data, and which are no longer functionally working in the network. By collecting data at discrete times, each mote saves power by reducing power consumption during times of inactivity, thus extending the life of the system. To extend the life of the system further, an external power supply has been designed to recharge the rechargeable batteries that are supplying the power to the mote.

The current sensor network will be upgraded to use the Zigbee software so that it will be compatible with the kit purchased by Dr. Chris McKay.

POWER SUPPLY

Since the Arctic will now be the test location, the solar cell's energy conversion efficiency has been recalculated (i.e. from last semester):

Let η = Energy conversion efficiency
Let P_M = Maximum power point
Let E = Input light irradiance
Let A_C = Surface area of solar cell
Let $\eta = P_M/(E \times A_C)$
Substituting values into the equations for P_M, A_C, and η,
$P_M = (6\ V)(0.1\ A) = 0.6\ W$
$E = 5.8\ kWh\ m^{-2}\ day^{-1} = 5800\ Wh\ m^{-2}\ day^{-1}\ (1\ day / 24hours) = 241.667\ W/m^2$
$A_C = (4.5\ inches)(5.9\ inches) = (0.1143\ m)(0.16968\ m) = 0.017129\ m^2$
$\eta = 0.6 / ((241.667\ W/m^2)(0.017129\ m^2)) = 0.14535 \approx 14.535\%$

The input light irradiance was calculated by averaging the input light irradiance for the months May through August (since the 2007 Mars Simulation in the Arctic will span those four months). Monthly values were found on the International Solar Irradiation Database from the University of Massachusetts Lowell Photovoltaic Program. Therefore, on average, the solar modules will convert approximately 14.535% of the absorbed sunlight into usable energy.

For the solar modules to charge the battery, its voltage must be higher than that of the battery. Each solar module consists of 10 cells arranged in two series strings of five cells. One solar module will be used with one battery to ensure that the current from the solar module does not exceed 10% of the battery's operating current (a general rule so as not to damage the components). Justification for the chosen power supply parts are provided in last semester's fellowship report.

The battery will be the source of power for both the mote and the water sensor. Both, however, require different operating voltages, which created the need to incorporate such a constraint into the design.

WATER SENSOR

A Honeywell LLE series sensor was chosen and purchased commercially. The water sensor operates based on the principle of total internal reflection, or the amount of incident light that is reflected at the boundary between two mediums. A LED and phototransistor are housed in a plastic dome. Changes in the internal reflection of light from the LED to the phototransistor at the dome-liquid boundary provide the appropriate output. If water is present, the refractive index at the boundary changes such that light from the LED escapes; otherwise, the light is reflected back to the phototransistor giving a high output, indicating no water. The output from the water sensor, labeled ADC1 in Figure 3, is connected to the microcontroller on the mote via the mote's expansion connector.

FABRICATION AND ASSEMBLY

The circuit below was fabricated in the lab. This prototype circuit recharges the battery pack, and powers the water sensor and mote. From left to right are the solar module, Schottky diode, rechargeable battery, water sensor, and voltage regulator.

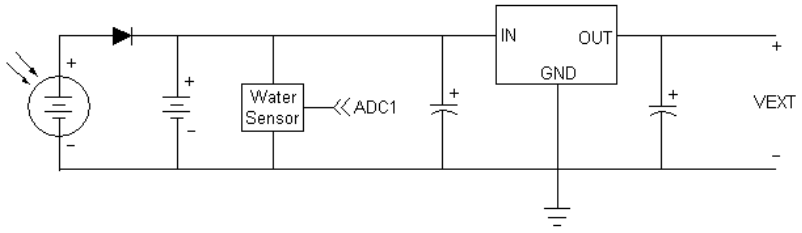

Figure 3: Circuit diagram for prototype

The plastic coating from each of the leads of the solar module was removed using needle nose pliers, being careful not to damage the metal contacts underneath. A digital multimeter was used to test each side for polarity and a sharpie pen was used to mark polarity (+ or –) on the backside of the solar module. As recommended by the solar module data sheet, 24 AWG wire was used. Wires were connected to the exposed metal solar module contacts using a solder "dot." Referencing data sheets for the remaining parts ensured the correct polarity such that all components share a common ground.

The outputs ADC1 and VEXT are inputs into the mote. ADC1 is the output from the water sensor whose voltage is low (i.e. 0 V) when water is present, and high otherwise. Since the water sensor requires 5 to 12 V of power, compared to the 2.7 – 3.6 V required by the mote, it is placed in parallel with the 6 V rechargeable battery. A voltage regulator was used to reduce and maintain the supplied 6 V from the battery to a constant output voltage of 3.3 V, VEXT, which is the supply voltage to the mote. VEXT is connected to a 2.5 mm jack socket that can be plugged directly into the main mote.

EXPERIMENTAL RESULTS

With the star topology, outlaying motes can communicate within a radius of approximately 50 feet from the main mote. The temperature, humidity, and light sensors were tested by comparing measurements from a mote placed in the freezer and a mote placed in the refrigerator. The main mote was kept outside, at room temperature, as a control. Room temperature conditions indoors were measured at 29° C, 75% humidity, with no light. The measurements from the freezer mote decreased steadily to 5° C with 20% humidity; thereafter, decreases were slower, but eventually went to 0° C. In the refrigerator, the temperature steadily decreased to 10° C with 51% humidity; similar to the mote in the freezer, decreases were slower thereafter, eventually reaching approximately 4° C. When the refrigerator and freezer lights turned on, both motes indicated light, however, there was a slight delay in sending that data to the main mote by 1 – 2 seconds.

Alarms on the mote can be specified at a desired value to alert the user when that value is reached. The temperature alarm can be set to go off between 0° C (low) and 100° C (high), the humidity alarm for 0% (low) to 100% (high), and the light alarm for complete illumination (high) to mostly dark (low). A display flashes on the main mote when the desired value is reached.

A partnership was established with Dr. Eric Miller from the Hawaii Natural Energy Institute and his graduate students – Noah Hafner, Blaine Hironaga, and Dennis How – to test the behavior of the solar modules in the lab under ideal conditions. AM1.5 solar simulated light was used to measure the overall cell efficiency, determine the voltage/current characteristics, and obtain the current/voltage response curves. Measuring the quantum efficiency at different cell biases determined the solar module's sensitivity and how it responds to differing sunlight (for example, if there is cloud coverage). The collected data has been plotted by Noah Hafner, Blaine Hironaga, and Dennis How and is given in Figure 4 and Figure 5.

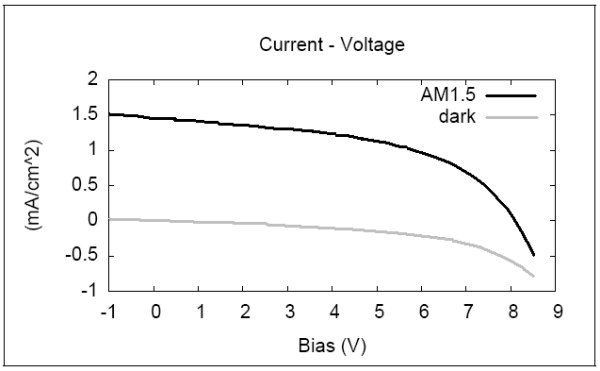

Figure 4: Current-Voltage plot of simulated AM1.5 light and dark JV

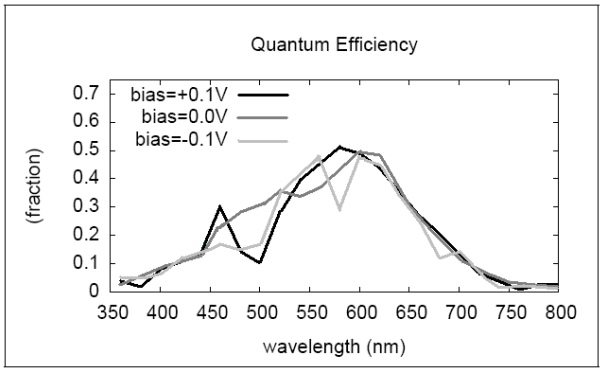

Figure 5: Plot of Quantum Efficiency for different valued biases.

The water sensor output is low when water is present, and high otherwise. In water, the sensor output yields 0 V. With no water, the sensor output voltage starts at the input voltage and decreases continually to about 2 V. Placed against an ice cube and submerged in large shards of ice did not give a positive detection of water. A drop of water on the sensor also did not yield a positive detection of water. The waterproofing on the water sensor was also tested and survived numerous tests of complete submersion in water.

ANALYSIS AND DISCUSSION

For a more accurate measurement of environmental factors, data should be collected between larger intervals to account for the gradual decreases that occur after reaching an initial steady state, which seem to be approximately 5° C greater than the actual final temperature. To extend the range of the network, the star topology can be reconfigured to use the mesh topology. The mesh topology will allow data hopping between outlaying motes if they are unable to reach the main mote directly.

A projected lifetime for the battery and life of the mote can be predicted based on the amount of light measured by the light sensor and absorbed by the solar module. For example, on days of greater sunlight, it would be expected that the batteries are recharging more often than discharging and will have more stored power to supply in times of no sunlight.

From Figure 4, the current-voltage curves for the solar module under the AM1.5 simulated solar light and that in the dark are similar; both decrease with an increasing bias voltage. The quantum efficiency for cell biases at –0.1 V, 0.0 V, and +0.1 V are also similar, resembling a bell-shaped curve as shown in Figure 5. The axis over which the quantum efficiency is plotted represents a range of wavelengths in sunlight from UVB and UVA (320 – 400 nm), the visible spectrum (400 – 760 nm), and infrared (greater than 760 nm). The wavelength at which the quantum efficiency is greatest is within the visible range.

The water sensor will perform ideally when submerged in water. Therefore, it would be best to incorporate several water sensors on each mote to increase the probability that the mote will detect water should only a small area under the mote will result in the positive detection of liquid water. Temperature is crucial in distinguishing between water and ice should water be detected.

CONCLUSION

In conclusion, a robust network of five motes has been designed and built to achieve the goals of this project: water is detected as an element necessary for life; a rechargeable power source extends the life of the system; most components, whenever possible, are RoHS compliant and thus environmentally friendly; data collected provides reasonably accurate and useful information; and low cost and use of commercially available materials make the sensor network easy to manufacture.

ACKNOWLDGEMENTS

Many thanks to the Hawaii Space Grant Consortium for their continued support of this project; Dr. Kim Binsted for her continued guidance as fellowship mentor; John Hauge for the hard work, manpower and good times; Dr. Tep Dobry for serving as the author's EE advisor; Dr. Eric Miller, Noah Hafner, Blaine Hironaga, and Dennis How for their assistance in testing the solar modules; Niel Smith from Jennic America for the technical support regarding the Jennic IEEE802.15.4 evaluation kit; and all those who contributed last semester! The assistance and support received these past semesters are much appreciated!

REFERENCES

Hafner, Noah; Hironaga, Blaine; How, Dennis. EE 693I students. “Amorphous Silicon Solar Cells” [Presentation] 13 November 2006.

Smith, Niel. Field Application Engineer, Jennic America. [Personal E-mails] September – November 2006.

Texas A&M University. “The wavelengths in sunlight.” [On-line] http://coolshade.tamu.edu/uv_3.html, March 2001.

University of Massachusetts Lowell Photovoltaic Program. “Solar Irradiation Database.” [On-line] http://energy.caeds.eng.uml.edu/fpdb/Irrdata.asp.

SYSTEM ANALYSIS OF THE LEONIDAS MICROSATELLITE BUS

Zachary Lee-Ho
Department of Mechanical Engineering
University of Hawai‘i at Mānoa
Honolulu, HI 96822

ABSTRACT

System engineering in a critical role in ensuring that all subsystems are in compliant with the desired mission objectives. A key tool for system engineers to accomplish this task is requirements. Requirements set the procedure, interfaces and the schedule for how the mission will be carried out. Requirements constantly evolve as the definition of the mission becomes more and more clear. The LEONIDAS microsatellite is driven by the set of requirements established by the LEONIDAS concept team in order to perform the desired mission.

INTRODUCTION

The goal of LEONIDAS program, Low Earth Orbit Network Integrated Distributed Autonomous Systems, is to develop a space program with the capabilities to complete an entire microsatellite mission from design to launch and perform operations while in orbit. If the LEONIDAS goal is accomplished it will be a one of the most unique space programs, with the University of Hawaii the only university in the nation with these capabilities. The LEONIDAS program provides valuable work experience and hands on training to UH students that will be difficult attain otherwise due to our geographic constraints. The LEONIDAS microsatellite bus currently being developed will serve as a testing platform for validating experiments in order to demonstrate their capabilities on future missions. In addition, the bus will house two cameras, one equipped with an optical lens for ultra-violet light and the other for visible light. The team working on the LEONIDAS bus will also work in collaboration with engineers from the Jet Propulsion Laboratory (JPL) to assist on the overall design of the microsatellite bus and facilitate in mission tasks to ensure the success of the project.

SYSTEM ENGINEERING

For a given mission typically there are several solutions to accomplish the desired mission goals. It is the job of the system engineer to achieve an overall optimum solution in which the mission objectives are satisfied efficiently. To achieve system optimization the system engineer must be familiar with elements of design, fabrication, testing, assembly, launch and operations. The system engineer is in charge of several critical tasks that entails the monitoring of the mission’s progress and ensure that it the guidelines set by the mission objectives and established requirements. Other tasks include the management and maintenance of budgets for mass, power, fuel and other key resources. Definition, monitoring and control of interfaces between all system elements and between subsystems will be done by the system engineer. The system engineer should have a good overall perspective of the system to interpret and explain motivations for requirements to his team members and thereby gain their acceptance and commitment to objectives.

MISSION OBJECTIVES

The mission objectives are imposed on the system by the user(s) of the data and are the broad goals that the system must achieve to be productive. For the LEONIDAS satellite the mission objectives were derived based on the five potential payloads that the bus will house, they are:

1. Active Antenna
2. Camera (Ultra-Violet and Visible Light)
3. Sublimation Thrusters
4. Surrey Satellite Technology Limited GPS Module
5. JPL Autonomous Software

Mission objectives are statements of the aims of the mission, are qualitative in nature and should be general enough to remain virtually unchanged during the design process. The final design of the bus must meet these fundamental objectives. The following is a list of the mission objectives:

1. To send microsatellite into low earth orbit at 400 km in altitude
2. Successfully command satellite to perform basic housekeeping test to ensure components are properly functioning.
3. To successful communication with satellite and downlink all mission data
4. To correctly orient the satellite to take a ultra-violet and visible picture of Hawaii
5. To perform scientific test of atmospheric anomalies through the operation and verification of the Surrey Satellite Technology Limited GPS module
6. To test and validate Scientific technologies developed at the University of Hawaii (Sublimation Thrusters & Active Antenna)
7. To test and validate the Jet Propulsion Laboratory Hardware for autonomous capabilities upon completion upon previous experiments
8. To verify the capabilities of the reconfigurable bus to have the ability to accommodate various payloads

As a system engineer the first task that must be accomplished, is to define the mission requirements from the given mission objectives.

MISSION REQUIREMENTS

Mission requirements are quantitative expressions of how well the objectives are met by balancing what is wanted against what the budget will allow. Throughout the mission lifetime it is common practice to trade requirements as the spacecraft bus is more clearly defined. Mission requirements will largely establish the operational concepts that will meet the mission objectives. The system engineer must identify what aspects of the mission and what elements of the design provide the major influences on the type of satellite that will meet the given mission requirements.

#	Title	Functional Requirement	Allocation	Accommodation
1.1	Acquisition	Acquire the sun after separation from the launch vehicle	Mission	ACS
1.2	Pointing Strategy	Satellite will maintain nadir pointing to earth in order to perform payload observation	Mission	ACS
1.3	Launch	Launch vehicle must place satellite into 400 km orbit	Mission	Launch
1.4	Communication	All housekeeping data from subsystems and experimental data from payloads must be downlink to ground station	Mission	COMM
1.4.1		Downlink of data must be accomplish within 6 minute viewing window	Mission	COMM
1.4.2		Receiving and Transmission of data must be accomplished within a maximum of 2 orbits	Mission	COMM
1.5	Payloads	Operation of each experimental payload for validation test	Mission	C&DH
1.5.1		Each payload experiment shall run separately during a designated orbit(s)	Mission	C&DH
1.6	Pointing Performance	Satellite must have the ability to pointing within +/- 1 degree to take pictures	Mission	ACS
1.7	Data Processing	All data processing will be performed on the ground	Mission	COMM

Table 1: List of mission requirement for LEONIDAS microsatellite bus

MISSION SUCCESS

A set of milestones must be attain before progress of the satellite can continue. Success of the mission is determine by the completion of several critical milestones. The keys for mission success have been set based on the milestones that are need to be reach to achieve the mission requirements. These keys for mission success have been divided into three different phases and are listed as follows:

- Phase I: Documentation
  - Successful completion of Mission Concept
  - Successful completion of documentation for Preliminary Design Review
  - Approval of spacecraft design
- Phase II: Assembly & Testing
  - Successful integration and testing of each subsystem
  - Successful integration and testing of the entire spacecraft system
  - Approval for launch
- Phase III: Launch
  - Successful delivery into mission orbit
  - Connection of satellite when initially delivered into orbit

- Satellites completes all housekeeping operations and relays data to ground station
- Payload experiments are tested for validation and results are transmitted to ground station

Completion of each task in a given phase will translate as success for that phase for the team and help in prepertaion for the upcoming phase milestones.

SYSTEM REQUIREMENTS

System requirement duties entail understanding all external interfaces and ensuring the functional architecture correctly captures the mission objectives. The system requirements document should cover every relevant aspect of what the system should do and how well it should do it. In addition, it addresses every aspect of system performance.

#	Title	Functional Requirement	Allocation	Accommodation
4.1	Mass	The mass of the satellite structure and all subsystem components must not exceed 35 kg	System	All
4.2	Durability	Subsystem components must be able to withstand 400 km orbit	System	All
4.2.1		Structure must be able to withstand forces incurred from launch vehicle thrusters	System	Structure
4.2.2		Structure must be able to withstand forces as result of thermal expansion	System	Structure
4.3	Thermal	All subsystem components must be thermally protected to withstand environment at an altitude of 400 km	System	Thermal
4.4	Power	Subsystem components will be provide a maximum of 110 watts to perform required operations	System	Power
4.4.1		Battery power with the capacity to permit the performing of mission operations for a maximum of 12 hours	System	Power
4.5	Data Transfer	Data will be downlink and uplink using S-band or UHF frequency	System	COMM
4.6	Volume	The volume of structure shall be within the linear dimensions 60 cm x 60 cm x 50 cm	System	Structure
4.7	Data Handling	Processing unit capable of orchestrating mission operations and managing subsystems and data flow	System	C&DH
4.7.1		Unit capable of running the operating system and components software	System	C&DH
4.7.2		Unit that can store all necessary software, housekeeping and experimental data	System	C&DH
4.7.3		Computer capable of managing operating modes	System	C&DH
4.8	Optical Viewing	Camera optics capable of taking a picture from an altitude of 400 km	System	Payload

Table 2: A list of LEONIDAS system requirements

CONCLUSION

From the system requirements a number of key elements are derived from or done in conjunction with system requirements which include system plans, test plans, system interfaces, traceability, budgets, risk assessment, mission lifetime and mission operations. System requirements lay the architecture of how each subsystem will be designed. Test plans will reflect validation and verification of these requirements. Interfaces between subsystems

Through the system requirements interfaces are declared in the interface control document, which state how integration and maintenance of relationships between subsystems will be met. Traceability is also down through system requirements, which indexes the methods that permits traceability upwards as well as across all elements. Budgets numerically list components for any overall system parameters. The Mission Operations Plan describes in users and operator terms the operational attributes of the flight and ground based elements and are written in conjunction with system requirements.

ACKNOWLEDGEMENTS

I would like to thank Professor Lloyd French for his guidance, insight and giving me the opportunity to be apart of such a significant project. I will like to thank Dr. Luke Flynn for making it possible for me to be a part of this significant project. Many thanks to Marcia Sistoso for her patience, attentiveness and informative reminders to ensure that the team meets its deadlines and has everything it needs. I will also like to thank to new incoming team members Jennie Castillo, Kaipo Kent, Lynette Shiroma, Mike Menendez and Minh Evans for volunteering their time and helping ensure this project progresses. And to the many others that gave a helping hand and words of encouragement during the development of this report, Thank You.

REFERENCES

Fortescue, Peter; Stark, John; Swinerd, Graham; (2003) Spacecraft Systems Engineering Third Edition, John Wiley & Sons Ltd.

Larson, Wiley J.; Wertz, James R.; (1999) Space Mission Analysis and Design Third Edition, Space Technology Library.

PAYLOAD DESIGN FOR A MICROSATELLITE

Aukai Kent
Department of Mechanical Engineering
University of Hawai‘i at Mānoa
Honolulu, HI 96822

ABSTRACT

Conventional satellites are extremely large, highly expensive, and may take several years to design and build. Microsatellites have the potential to reduce cost and risk when compared to conventional satellites. The main purpose of the LEONIDAS project is to prove that the University of Hawaii has the capabilities to design, build, test, launch, and operate a microsatellite. The payload subsystem is the heart of the microsatellite and consists of all the different hardware and software on the satellite that is used to satisfy the mission objectives. The payload subsystem will consist of four different instruments. An imager system will be used to test the satellites capability to house a camera and will take pictures of Hawaii in the ultraviolet, visible, and infrared spectrum. A retro directive antenna designed by the University of Hawaii and a GPS unit provided by SSTL will test the satellites capability to demonstrate new technologies. The satellite will also house health monitoring software provided by JPL/AMES.

INTRODUCTION

Currently, conventional satellites are extremely large, highly expensive, and may take several years to design and build. Not to mention each satellite is as unique as its mission. These factors are causing NASA to push toward the use of microsatellites. Microsatellites have the potential to reduce cost and risk when compared to conventional satellites.

First of all, a microsatellite can reduce cost by cutting down the design and integration and testing time since the satellite will be less complex. The manufacturing may also be reduced since the satellite will be smaller and therefore require fewer materials. Second, a microsatellite can reduce operations cost, since a smaller, less complex satellite should take less people to manage and operate it. Third, a microsatellite could reduce launch cost by requiring the use of a smaller rocket. Fourth, once a “cookie cutter” microsatellite has been design long-term costs will be reduced.

A microsatellite can also be used to test new technologies and therefore reduce risk. As missions become progressively more daring, and thus more difficult, more advanced capabilities are needed. While an emerging technology may seem promising and likely to provide the technical capabilities NASA requires, it may also present an unacceptable risk to any exploration mission using it for the first time in space. However, before new, untried technologies are used for the first time on complex exploration missions, engineers and scientists want to make sure they will operate well, and safely, in the hazardous environment of space.

The main purpose of the LEONIDAS project is to prove that the University of Hawaii has the capabilities to design, build, test, launch, and operate a microsatellite. Proving these capabilities will lead to many new opportunities within the aerospace industry. The success of the LEONIDAS project could lead to partnerships with NASA and could push the University of Hawaii to start its own aerospace program.

The payload subsystem is the heart of the microsatellite and determines many of the capabilities and limitations of the mission. The payload consists of all the different hardware and software on the satellite that is used to satisfy the mission objectives. The main purpose for the other subsystems of the satellite is to keep the payload subsystem happy and healthy.

DESIGN

In order to determine the design of the payload subsystem mission requirements need to be formulated. To satisfy our mission objectives the satellite will have to function at a 400 km orbit, a 92.6 minute orbital period, and a ground track speed of 7.2 km/s. The payloads must perform with a pointing accuracy of ±0.5°, determined by the capabilities of the Attitude Determination and Control subsystem. The payloads must also have a total mass of less than 2.2 kg and a total power consumption of less than 8 W. The satellite will house four different instruments: an imager system, GPS unit, retro directive antenna, and health monitoring software package.

The objective of the imager system is to test whether the microsatellite has the capabilities to house a camera. The imager system must successfully take a picture of Hawaii in the ultraviolet, visible, and infrared spectrums. The same model camera (Sony XCD) will be used for each spectrum. Using the same model camera will ease the process of testing and integration. At a certain orbital position, the satellite command and data handling system will trigger the imager to take five pictures to insure that a successful image is taken.

Each image will be processed onboard the camera and will be sent to the C&DH system via a firewire interface. The advantage of using a firewire interface is the quick transfer rate and the elimination of a separate power interface. The data volume was calculated by multiplying the pixels and the pixel depth. The specifications for the cameras are given in table 1.

Each image will have a ground resolution of 100x100 km. The field of view for the imager system was calculated using the 400 km orbit and the required ground resolution. The field of view for the imager system is approximately 14.0°. Lenses were chosen to match the field of view and the specifications are also given in table 1.

XCD-X710 / XCD-SX910

	UV	VIS	IR
Manufacturer	Sony via Edmund Optics	Sony via Edmund Optics	Sony via Edmund Optics
Model number	XCD-SX910UV	XCD-SX910CR	XCD-SX910
sensor size	1/2”	1/2”	1/2”
Pixels (H x V)	1392 x 1040	1393 x 1040	1394 x 1040
pixel depth	8	10	8
shutter speed	1/100,000 – 17.5 sec	1/100,000 – 17.5 sec	1/100,000 – 17.5 sec
Interface	firewire	firewire	firewire
Mass	250 g	251 g	252 g
Power	via firewire	via firewire	via firewire
Dimensions	44mm x 33mm x 116mm	44mm x 33mm x 116mm	44mm x 33mm x 116mm
Operating temp.	-5°C to 45°C	-5°C to 45°C	-5°C to 45°C
data volume	11.5 Mbits/image	14.5 Mbits/image	11.5 Mbits/image
Cost	$6,450.00	$2,417.00	$2,417.00

	Lens	Lens	Lens
FOV	14.0°	14.0°	14.0°
Mass	33g	33g	33g
Dimensions	30.0mm D x 58.4mm L	30.0mm D x 58.4mm L	30.0mm D x 58.4mm L
Cost	$900.00	$900.00	$900.00
	total mass	849 g	

Table 1: Imager Specifications

The GPS unit will test the satellites capabilities to perform technology demonstrations and will be provided by the Surrey Satellite Technology Ltd. (SSTL). The GPS unit is a spacecraft orbit determination sub-system designed specifically for small low earth orbiting satellites. This unit provides GPS standard time, position and velocity in a compact unit. The GPS unit also supports multiple antennas to improve visibility under changing orientations and attitude determination.

The GPS unit works by receiving and decoding the L-Band signals from four or more GPS satellites and, through ranging techniques, is able to calculate the position of the spacecraft to an accuracy of better than 20 meters and determine accurate velocity and time. The carrier phases measured from multiple antennas can be used interferometrically to determine the attitude of the spacecraft. The GPS unit and its specifications are shown in Table 2.

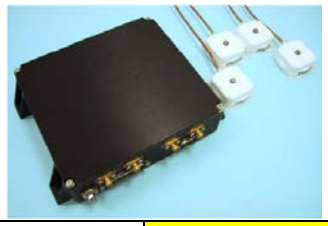

	GPS Receiver
Model Number	SGR-20
Operating Temperature	-20º C to 50º C
Volume	295mm x 160mm x 35mm
Mass (Unit)	950 g
Mass (Antenna)	50 g
Total Mass	1.15 kg
Power	6.3 W
Voltage	18-38 V

Table 2: GPS Specifications

The GPS unit must accurately obtain orbital and altitude information. Measurements will be taken every 18.5 minutes during the test orbit. These measurements will be sent to the C&DH system via an RS-232 interface. The attenuation of the GPS signal may also be used for atmospheric data. In order to perform successfully the GPS must meet the performance requirements that are given in Table 3.

	Typical (95%)	Max (90%)
Orbital Position (3-D)	10 m	20 m
Orbital Velocity (3-D)	0.15 m/s	0.25 m/s
Time	0.5 µs	1 µs
Time to First Fix (cold)	200 s	350 s
Time to First Fix (warm)	50 s	90 s
Attitude Determination	0.5 – 1 °	TBD

Table 3: GPS Performance Requirements

For attitude determination, configuration of antennas is important. Four antennas are required for accurate attitude determination and each antenna will have to be placed two meters apart. Either all four antennas will be positioned on one side pointing spaceward or three antennas will be positioned on one side and one antenna on the opposite side pointing spaceward. The two configurations are shown in figure 1.

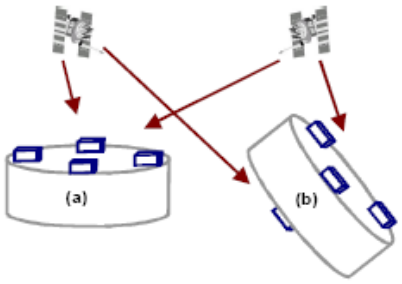

Figure 1: Orientation of GPS Antennas

Originally the satellite was supposed to house an active antenna developed at the University of Hawaii by Dr. Wayne Shiroma's. However, Dr. Shiroma and his students are currently in the process of redesigning the active antenna. The new retro directive antenna will be able to locate and communicate with other satellites. Since the antenna is still being designed no other information is available at this time.

JPL and AMES research center will be providing us with an autonomous spacecraft control and health monitoring software package. This software will be a part of the C&DH system and will demonstrate the following benefits:

- Low cost and flexible modeling, allowing health management algorithms to be tailored to the C&DH as it is developed and refined
- Ability to rapidly and safely update health models, providing the capability to improve health management with learned flight behavior
- On-board detection and isolation of C&DH errors and anomalies, greatly reducing operations overhead and risk to the microsatellite
- A flexible microsatellite operations concept that reduces costs, improves the cost predictability, enhances reliability, and enhances microsatellite capability.

CONCLUSION

There is still a great deal of work that needs next to be done next semester before the design for the payload subsystem is complete. I need to work with Dr. Shiroma's students in order to understand how their new retro directive antenna will work. Then I will need to take the specifications of the antenna and make sure that the fit within requirements of the subsystem and meet the mission objectives of the satellite. I will also need to work with JPL and AMES research center to insure that the health monitoring software can be implemented in our satellite. Once I have the design for the antenna and the software I will need to perform an iterative analysis on the subsystem as a whole. Part of this analysis will be to calculate the data rates of the instruments to make sure that they fit within the specifications of the C&DH system. In order for the analysis to be complete, I will need to make sure that all the instruments meet the payload requirements, can satisfy the mission objectives, and are able to interact with the other subsystems in the satellite. After the analysis is finished, my subsystem will be ready for the critical design review in April.

REFERENCES

Larson, Wiley J., and James R. Wertz. Space Mission Analysis and Design. 3rd ed. El Segundo, CA: Microcosm Press, 1999

TELECOMMUNICATION SUBSYSTEM FOR THE LEONIDAS MICROSATELLITE

Dennis D. Dugay
Department of Electrical Engineering
University of Hawai‘i at Mānoa
Honolulu, HI 96822

ABSTRACT

An S-Band Telecommunication Subsystem of a microsatellite is researched, analyzed, and planned. The Low Earth Orbit Nanosatellite Integrated Distributed Alert System (LEONIDAS) project will need a Telecommunication Subsystem in order to have a communication link between the spacecraft and the ground station. Also, the spacecraft will have an Ultra High Frequency (UHF) secondary Telecommunication Subsystem that will serve as a redundancy and a back up. The University of Hawaii at Manoa (UHM) has an X-Band ground station that will be formatted into S-Band for communicating with the microsatellite in orbit.

INTRODUCTION

The LEONIDAS project will assemble a Low Earth Orbiting (LEO) microsatellite. Currently the LEONIDAS team consists of nine mechanical and electrical engineering students. Each student is a lead in there own specified subsystem such as: systems, payloads, command and data handling (C&DH), telecommunications, attitude and control system (ACS), power, thermal, orbits, and structure. The satellite will be assembled with components off the shelf (COTS). The integration of the subsystems to coincide with one another will be very crucial to our success.

Hawaii has the capabilities and the facilities to manufacture, integrate and test space flight hardware. Also, the cost of a microsatellite is approximately 1% of manufacturing and launching large satellites, which is over $300 M. Since 2002, the LEONIDAS project has been working on building a microsatellite as an engineering demonstration for the University of Hawaii. It will give students a great learning experience on space technology and the process on how to build a spacecraft. Students will gain networking skills, communication skills, and the experience in working in an engineering team effort environment.

BLOCK DIAGRAM

The Telecommunication Subsystem provides a communication link between the spacecraft and the ground station, using S-Band and UHF frequencies. Figure 1 illustrates a block diagram of the Telecommunication Subsystem. It includes an S-band transmitter, S-band receiver, S-band antenna, UHF antenna, UHF transceiver, and a Terminal Node Controller (TNC).

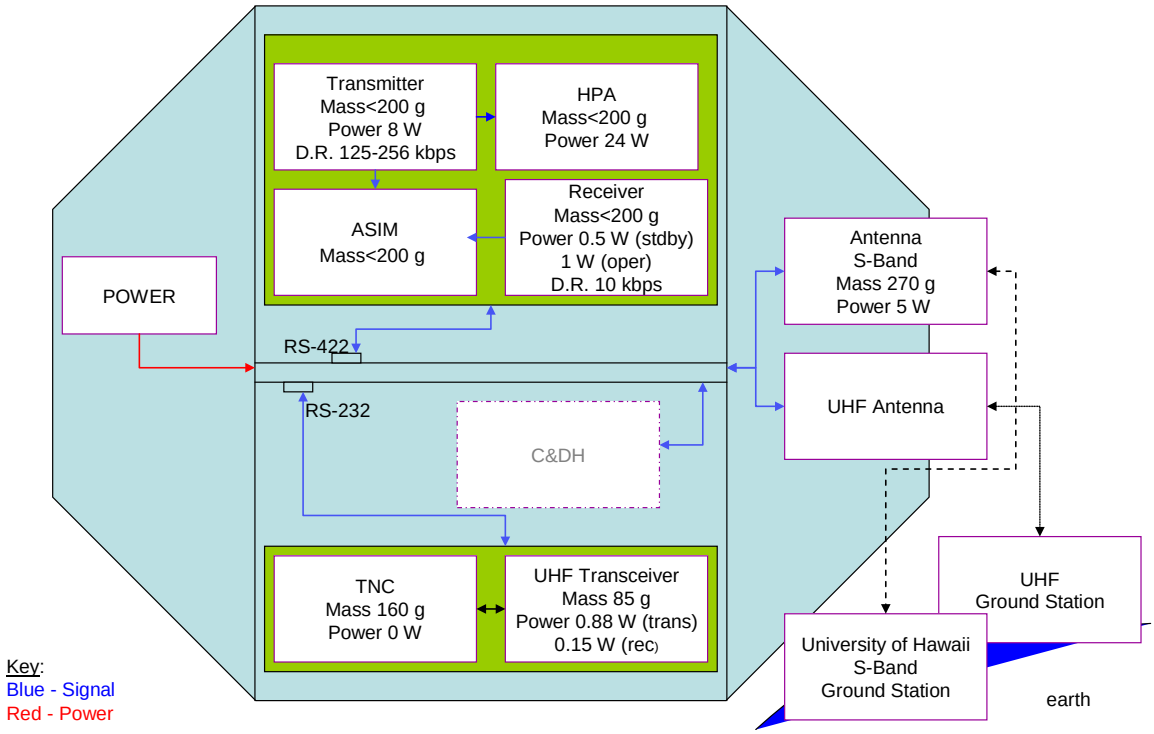

Figure 1: Telecommunication Subsystem Block Diagram

S-BAND

There are four components that make up the S-Band subsystem. It includes an Appliqué Sensor Interface Module (ASIM), a High Power Amplifier (HPA), a transmitter, and a receiver developed by AeroAstro. It is connected with an RS-422 interface to the interface board which then routes to the Command and Data Handling (C&DH) Subsystem. Also, the components are then connected to the S-Band Antenna by Antcom that is placed on the outer surface of the spacecraft. The data that is compiled from the C&DH Subsystem is sent to the transmitter. This is where the data is then modulated onto a carrier. The transmitter has an output data rate of 125-256 kbps that will route the data to the antenna where it will radiate to the ground station. The ground station will be able to receive spacecraft telemetry and send command data to the spacecraft. This frequency signal will enter through the antenna and to the receiver that has an input data rate of 10 kbps. It will demodulate the frequency signal and route the data to the C&DH Subsystem. The reason in having an S-Band rather than an X-Band subsystem is to eliminate interference because there is a heavy exploit of X-Band in Hawaii due to military usage.

UHF

Separately, the Alinco DJ-C5T UHF transceiver built by Yaesu Company is connected to the TNC by PacComm. It is connected with an RS-232 interface to the interface board which then routes to the C&DH Subsystem. Also, the components are then connected to a UHF antenna that is placed on the outer surface of the spacecraft. This is a second Telecommunication Subsystem that will act as a redundancy and a back up in the situation when or if the S-Band subsystem fails.

REQUIREMENTS

The Telecommunication Subsystem has a set of requirements that has to be met in order to function well with the other subsystems in the spacecraft. Table 1 states the Telecommunication Subsystem requirements.

Table 1: Telecommunication Subsystem Requirements

REQUIREMENTS	
Volume	20 cm x 27 cm x 11 cm
Power Budget	40 W + 2 W
Mass Budget	2.5 kg + 0.5 kg
Frequency	S-Band (2.0-4.0 GHz)
Altitude	300-400 km
Lifetime	6 months

SPECIFICATIONS

The S-Band Telecommunication Subsystem has a volume, power consumption, mass, and frequency that accommodate the requirements. The power describes the power assumption during the transmitting operation and the receiving operation phases. Also, with the UHF transceiver, it shows its power assumption during its transmitting and receiving operation.

Table 2: Telecommunication Subsystem Specifications

SPECIFICATIONS	
Volume	8.9 cm x 5.1 cm x 2.5 cm (each module) x3
Power	Transmitting Operation: 37.5 W Receiving Operation: 6 W Transmitting with UHF Transceiver Operation: 1.42 W Receiving with UHF Transceiver Operation: 0.69 W
Mass	Less than 1.341 kg
Frequency	S-Band (2.0-4.0 GHz)

LINK BUDGET

A link budget of the Telecommunication Subsystem is calculated with a radio link budget calculator (Shown in figure 2). The white boxed values are the inputs that were given and researched. The green boxed values are the outputs that were calculated. This is in the case of working at S-Band, specifically at a frequency of 2.4 GHz.

Frequency GHz	2.4
Transmit antenna diameter m	.663
Transmit antenna aperture efficiency e.g. 0.65	.85
Transmit antenna transmit gain dBi	23.72
Transmit antenna, power at the feed W	35
Transmit EIRP dBW	39.16
Range km	400
Path (spreading) loss dB	152.0
Power flux density at receive end dBW/m^2	-83.8
Bandwidth Hz	22000000
Receive antenna diameter m	5
Receive antenna aperture efficiency e.g. 0.65	.65
Receive system noise temperature (antenna+LNA) K	300
Signal power at output of receive antenna dBm	-40.941309
Receiver sensitivity (see manufacturer spec e.g -80 dBm)	-80
Receive margin dB (0-5dB=marginal, 10-15dB=good)	39.058690
Receive antenna gain dBi	40.113323
Receive G/T dB/K	15.342110
Link C/N dB	57.59

Figure 2: Link Budget Calculator

COST ANALYSIS

A cost analysis on the Telecommunication Subsystem components is given in Table 3. This is to accommodate the cost budget that is given for the LEONIDAS project, specifically the Telecommunication Subsystem.

Table 3: Cost of Components

COST ANALYSIS	
S-Band Transceiver	$150,000.00
S-Band Antenna	$540.00
UHF Transceiver	$150.00
TNC	$179.00
Total	**$150,869.00**

GROUND STATION

LEONIDAS has an S-Band (2.0-4.0 GHz) subsystem with an X-Band (7.0-12.5 GHz) ground station associated with Dr. Torben Nielsen. He said the ground station is a 5-m Cassegrain system with a G/T of 32 dB/K in X-Band and that it is also equipped with a parasitic S/L-Band feed. The 5-m Cassegrain system is fitted with an S-Band parasitic feed where the gain is more than enough for this mission.

CONCLUSION

The S-Band Telecommunication Subsystem of the microsatellite is qualified for this mission. The Subsystems volume that occupies the spacecraft will be adequate. The mass and power allocated for the subsystem is accommodated. The cost analysis has a reasonable amount for funding and the link budget associated with the ground station is sufficed. The Telecommunication Subsystem will serve its purpose in having a communication link between the spacecraft and the ground station.

ACKNOWLEDGMENTS

I would like to thank the Hawaii Space Grant Consortium for all the support. Thank you to Dr. Lloyd French for being my teacher, friend, and mentor. I have gained a great deal of knowledge and experience. Thank you to Dr. Luke Flynn for supporting the LEONIDAS project. Also, thank you for allowing and giving me a place to do my research. Thank you to Ms. Marcia Rei Sistoso for being kind and patient. Thank you for all the emails and letters that kept our relationship organize and on task. Thank you to everyone who made this project a success and all who supported me.

REFERENCES

AeroAstro Website: S-Band Transceiver pdf file.
Available [Online]: http://www.aeroastro.com/datasheets/S-Band_Transceiver.pdf

Alinco Website: UHF Transceiver.
Available [Online]: http://www.alinco.com/usa.html

Dr. Torben Nielsen. Ground Station. Interview via e-mail. (January 9, 2007)

PacComm Website: Terminal Node Controller.
Available [Online]: http://www.paccomm.com/pico.html

Radio link budget calculator – line of sight link.
Available [Online]: http://www.satsig.net/link-budget.htm

POWER REGULATION AND DISTRIBUTION SYSTEM

Matthew J. Patterson
Department of Mechanical Engineering
University of Hawai‘i at Mānoa
Honolulu, HI 96822

ABSTRACT

This paper consists of the process and research that has undergone in the Leonidas Nanosatellite project. The team has accomplished many things in the short time we were together and has shown in the increasing help and interest we are getting from outside companies. The team allowed me to handle the power subsystem of the satellite, which has gone under many transformations. At the beginning of the semester I couldn't tell you a thing about a power subsystem and now I have gained much knowledge from my research.

INTRODUCTION

In January 2006 the LEONIDAS Mission Concept Study Team (LMCST) was established by Professor Lloyd French to develop a satellite concept report that demonstrates Hawaii capabilities to produce a low Earth orbit mission. This was completed in the summer of 2006. Starting the fall semester 2006, the LMCST prepared for the mission proposal for the Air Force Office of Scientific Research (AFOSR) University Nanosat Program. Upon the completion of this proposal the LMCST prepared for a Jet Propulsion Laboratory (JPL) presentation. Now that these are completed, the next goal for the LMCST is to prepare for the JPL Preliminary Design Review (PDR) in the spring semester of 2007.

My main priority while working with Professor Lloyd French will be to continue to the work that the LMSCT began in spring of 2006 and to ensure that the LMCST doesn't fall behind because of my lack of work. My next step is to begin preparing for the JPL PDR.

The basis of the JPL PDR will come from the JPL presentation done in the fall of 2006. In the PDR, the LMCST was given the opportunity to present their own subsystem to a group of engineers from JPL. Here the LMCST was shown the true meaning of how to present in the professional carrier. The team was asked questions on the spot and needed to react without looking up the answers in their notes. It is expected that the JPL PDR will be more intense. The engineers from JPL will be less forgiving for some of the mistakes we presented in our first meeting. They will want us to show how we are going to spend their money and if we are capable enough to complete a mission from design to launch. I believe that the LMCST is capable of completing a mission from design to launch and will earn the respect of JPL.

METHODS

My main focus for this semester will consist of the completion of the power subsystem requirements and prepare for the JPL PDR. I will complete the analysis needed to gain a better understanding of the actions of the power subsystem. To do this I will find and answer my most updated list of system requirements:

- Orbital Requirements
- Orientation Stability
- Grounding
- Shunt Requirements
- Charging time
- Operational Requirements
- Battery Life
- Power Quality
- Transient Response
- Temperature Requirements
- Integration and Testing Requirements
- Interface
- Transmission Requirements
- Regulation Requirements
- Photovoltaic Life
- Noise Control

Over the entire time of doing this research, I've learned so much about satellites, the power subsystem, and my peers that work along side of me. The knowledge and experience I'm getting from all this research and teachings from our mentor Lloyd, could never be matched in the classroom. If you asked me two semesters ago, what the power distribution and regulation unit on a satellite looked like, I probably couldn't tell you. Ask me now and I would tell you that the Power Generation and Distribution subsystem will provide the power necessary for the nanosatellite's electronic components. Power regulation is mainly made up of battery charge and discharge converters, a shunt resistor, and a mode controller that talks to the bus voltage error signal.

Power is generated with 28.3% efficiency Ultra Triple Junction (UTJ) Solar Cells, manufactured by Spectrolab, Inc. Seven of the eight sides of the nanosatellite will be mounted with these solar cells measuring 22 cm by 50 cm. This will provide about 100 W of continuous power. From the solar cells the power will pass through the PRU (Power Regulator Unit), provided by Crisa. This PRU could provide for a 40 Volt bus, our bus will be running on 3, 5, +-12, and 28V. A series of controllers will check the system, including the Lithium Ion batteries (100 Wh), to see if it should enter any of four the error modes: shunt mode, charge cut-back mode, discharge mode, and PRU bypass mode. Here is a short list of modes and the power they will require:

- Check - Varies
- Standby - 14.8 W
- Charge - 14.8 W
- Communication - 50.36 W
- Payload - 42.36 W to 47.36 W
- Maneuver - 41.36 W

These modes are ways to control the power input and output in the system. For example, when in shunt mode the solar cells will pass the power they receive through shunt resistors (NHR NHS 2-T220 T221), manufactured by Riedon, and excess power is dissipated out as heat from the satellite. The Power Distribution Unit (PDU) will power the subsystems directly. The PDU will ensure that all loads are powered through switches and fuses. The fuses are to protect the power

system from errors in the user equipment. The PDU will be hooked up to the back of the power subsystem tray (nearest to the interface board), so that the other loads can be connected to the power without much wiring.

Later in the semester I went into greater depth with some of the components. First I started with the solar cells and decided to work UTJ cells. The dimensions of these cells would be 0.5 meters by 0.22 meters and weigh about 76 mg, this is for each cell. The satellite would consist of about 7 cells, working on where we can put more. For our limited surfaces area and mission life, these cells will help the team reach peak output for power. The cells have a beginning of life (BOL) average efficiency of about 28% and end of life (EOL) average efficiency of about 24%. From this I can make some quick calculations:

- BOL power output
  - Power @28.3%x1,367 W/m2(average solar illumination intensity) = 386.86 W/m2
  - Power of Sat : 386 W/m2 x .114 m2 = 44 W per panel
  - Peak Power output of solar panels (ideal 3 panels) = 106.225 W

- EOL (5 year lifetime) power output
  - Power @24.3% = 332.181 W/m2
  - Power of Sat = 37.9 W per panel
  - Peak Power output of solar panels = 91.499 W

This shows us that at the beginning of our mission, the solar panels will be putting out a peak power of 106 Watts to charge the batteries. If our mission was to last 5 years, the solar cells would only put out about 91 Watts of power.

The next component I went and did more research on was the secondary battery for our satellite. Secondary battery just stands for a battery that is able to recharge, while primary batteries cannot be charged. I decided to go with a rechargeable Lithium-ion MP 176065 battery from Saft Batteries. These batteries were perfect because they are fairly small and would fit perfectly anywhere on the satellite. Also they have a good Watt hour per kg ratio and have a long life cycle. They put out a 26 Watt hour and only weigh about 150 grams. The charge rate at which we will be charging will be at four amps. This will take about 3 to 4 hours to charge a battery because of the PRU I chose can only charge at 4 amps. We are not exactly sure how many batteries we will be using yet, but we came up with a number of batteries we would need in a total failure of Solar Cells and be able to stay alive for 12 hours and we would need 16 batteries. So that isn't that bad, and I would still be under my weight budget.

Along with the secondary batteries and the solar cells, I looked into a PRU unit from CRISA. Here, I found something that helps me meet some of my system requirements. CRISA calls it a HESC 104, but that's short for high efficiency and smart charging vehicle power supply. It is very small in size and mass and I might use more than one, so it makes it very volatile. It can have an input voltage of 6 to 40 Volts. The main thing that sold me though was that it was able to support the different voltages I stated in my requirements; 3, 5, +12, and -12. Depending on what voltages the other subsystems need, will determine how many HESC 104 boards I will need.

Problems will come up everyday in the life of research. The biggest problem and the one thing that I've learned over and over, was during my research. Every time I answered one

question, it leads me to at least three new questions. At times this was frustrating, but it leads to a better understanding of my subsystem. Right now I have no real problems with my design of the subsystem, mainly because I have nothing to test right now. The buying and testing of the components comes next semester, which will be exciting. Another problem is just in the communication of the team. We have a hard time of meeting together, to integrate what we have to see if it fits. This happens once a month and this is where a lot of things go wrong or don't seem to fit. Next semester, the team needs to meet TOGETHER more, thus we can move along faster.

CONCLUSION

In all, I've learned so much about satellites and the power subsystem especially, this semester. The experience I have received out of this project is priceless. I have done multiple presentations and a PDR with real companies. I have co-authored a proposal and a concept study which was published (waiting on the results of the proposal to the Air Force). I have received much practice in technical writing and extensive research that will help me in the furthering of my education. This project did take a lot of commitment and time, but I would not have traded that for anything. This project only seems to grow. My research will continue for as long as this project gets funded. Our projected launch date is in 2009. I can't wait to begin again next semester.

By continuing to work with Professor Lloyd French I hope to attain added knowledge of the mission design process, have a great knowledge of the power subsystem to be able to support to our satellite. I hope to also help the team when the help is needed because the work will grow as the mission gets more and more close to the JPL PDR. The team has also grown from 4 undergraduate students to eight undergraduate students and one graduate student. These new team mates will need the help to catch up to the rest of the team and for the team to move forward. I am currently still in the process of completing my system requirements. I hope to reach a point in my research, in which when asked a question by the group of engineers from JPL during the PDR, I will be able to answer with no confusion and no hesitation. I will be ready for this design review.

REFERENCES CITED

1. Patel, Mukund R. Power Systems. New York. CRC Press. 2005.

2. "Space Solar Panels" Spectrolab Photovoltaic Products online datasheet. http://spectrolab.com/DataSheets/Panel/panels.pdf

3. "Battery Regulator Unit", Crisa online datasheet http://www.crisa.es/pdf/bru.pdf#search='Power%20Regulator%20Unit%20for%20Power%20Subsystem'

4. "NPR NPS 2-T220 T221 Power Resistors", Riedon online datasheet http://www.riedon.com/eu/eng/images/stories/pdf/NPRNHRT22x_eu.pdf

MISSION TIMELINE AND MODES OF THE LEONIDAS SATELLITE

Zachary Lee-Ho
Department of Mechanical Engineering
University of Hawai‘i at Mānoa
Honolulu, HI 96822

ABSTRACT

In the previous semester we derived system and subsystem requirements for the LEONIDAS bus which will allow us to accomplish the mission goals for the initial launch. This report focuses on the mission operations of the LEONIDAS bus while in orbit, emphasizing the mission timeline and the various mission modes that compile a mission sequence. Taking the various sequences from pre-launch to end of life we will look at the various actions that takes place during each sequence. In addition, we will look at the various modes that carry out each action of a mission sequence.

INTRODUCTON

The University of Hawaii strives to stand in a class of its own by becoming the only university in the nation to have the capabilities to complete an entire spacecraft mission from conception to end of life. The UH space program will serve as an avenue to test experiments developed by the engineers and scientist at the University of Hawaii. The program will also serve as an educational tool, providing hands on experience to students in the aerospace field. The LEONIDAS, Low Earth Orbit Nanosatellite Integrated Defense Autonomous Systems will focus on completing these goals for its initial launch which subject to take place in the end of 2009. The LEONIDAS bus design is part in house development and part commercial off the shelf (COTS) product which will take advantage of the cost effective COTS software for functions that are generic across spacecraft and all in-house developers to customize software to meet the specific requirements for our mission. With the use of COTS components we hope to encourage the pursuit of appropriate partnerships with the emerging commercial space sector.

The completion of the mission and system requirements for the LEONIDAS bus, the next step is to determine what functions will be done and how they will be performed. Planning and scheduling within mission operations refers to the process of evaluating which future activities should be conducted on a mission over a particular time period. Mission operations are the collection of activities performed by the satellite while in orbit to complete the mission objectives. Activities will include both spacecraft housekeeping functions and instrument payload activities. A good mission operations plan assures that the requirements are met at the lowest cost, and defines the best way to use resources to accomplish the mission goals. Mission planning produces rough activity timelines across mission phases that identify the schedule and resources to complete major activities. Resources that we are concerned with the most will include the trajectory, consumables over the spacecraft's lifetime, and long-range facility support. Mission description tells us the trajectory, launch dates and windows, trajectory profile, maneuver profile needed to meet mission objectives, mission phases and the activities required during each phase. The operating philosophy for the initial mission will be to maximize the

involvement of educational institution and teach students key aspects of issues like operations or space physics.

The mission operations will also serve as a blueprint for developing the testing procedures for the satellite bus. During testing a few commands will be sent to the spacecraft to verify that the commands were formatted, transferred, transmitted, received and executed properly. Mission operations' testing validates the system before launch to ensure its ability to support spacecraft on-orbit operations. Once the planning, control, and assessment functions are integrated together into the system, testing becomes necessary to verify proper operation. Mission operations' testing is done through the use of simulators at various stages in program development. Testing of mission operations is performed at both subsystem level and at a system level. Subsystem testing consists of testing individual components and systems. Component testing involves database validation along with the testing of individual functions and tools within the planning, control, and assessment areas. System level testing typically involves simulating operations for days and weeks at a time. Hardware and software simulators can be used in place of spacecraft components not available for mission operations testing.

These same tests performed on each subsystem in the laboratory will be carried out with each subsystem when the satellite is in orbit. The telemetry from subsystem check -out will then be compared with the results conceive during the test of each subsystem in the laboratory.

Often times, it is not known what is desired until the payloads capability in flight is determined. So what we establish a baseline process prior to launch which may be subject to change and be refine once the spacecraft is in orbit.

MISSION TIMELINE

The mission timeline is a list of events from T-10 till the end of life of the satellite, which can be seen in Figure 1. The mission life is broken up into eight major sequences: pre-launch, launch, post seperation, stabalization, power initialization, connection with ground station, check out, instrument operation, and end of life. Each is sequence comprised of several mission modes to carrys out the task require to full fill each sequence. Mission modes is the various states of the spacecraft that based on the desired action to be completed and the various subsystem that are running.

Mission Sequence

Time	Action	What is happening.
T_{-10}	Pre-launch Sequence	Spacecraft is attached to launch vehicle and is monitored and powered using T_0 connection Pre-launch checkout T_0 connection triggers a physical interlock that prevents the S/C from firing thrusters prior to launch.
T_0	Launch	Three Kick stages -Spacecraft released from final kick stage at approximately 5 rpm -Release Yo-Yo Weights -Spacecraft is slow down to 1 rpm
T_{120}	Post Separation	Separation is detected from launch vehicle through the separation ring, and will be backed up through onboard separation clock Post Separation Check-Out -C&DH -Power -Telecom -ACS -Thermal Turn on Transponder send out beacon Switch main power source to Solar panels -Battery power used A secondary energy source -Shunt excess power production
1st- 2nd orbit	Stabilization Mode	Stop Tumbling -Spacecraft orients itself to mission attitude without ground intervention. -Maneuvering performed using sun sensor, magnetic torquers and reaction wheels
2nd orbit	Power Initialization	Begin recharging of the batteries
3rd orbit	Connection with Ground Station	Attempt to send out transmission
4th orbit	Begin Check-Out	Loose sight of ground station for the day Subsystem Check-Out (1 week) -C&DH (3 weeks) -ACS (1 week) -Power (2 weeks) -Payloads -Thermal (Thermal Check-Out will be performed through out the 7 week Check-Out period) -Telecomm (Telecomm Check-Out will be performed through out the 7 week Check-Out period) Full System Check-Out (2 weeks) -System check-Out will be perform by running through the various mission modes
10th week	Instrument Operation	Operation of the various Payloads Collection of data through Payload operation Transmission of Payload data (4.6 weeks) Camera UV-Visible (4.6 weeks) -Active Antenna (4.6 weeks) -Sublimation Thrusters -JPL Autonomous Software (JPL software will run through out spacecraft mission life)
24th week	End of Mission	End of Mission Operations Operation of Spacecraft is handed over to JPL for further Autonomous Operations

Figure 1: Table of the Mission timeline for the LEONIDAS BUS

The time line begings at T_{-10} of pre-launch sequence 10 sec before launch, during this sequence the final checkout of the spacecraft prior to launch, which is performed while the spacecraft is secure on the launch vehicle. The spacecraft is connected to the T_0 connection cable which will power the satellite, monitoring the satellite consumables and computer activities. During the entire Pre-launch sequence the satellite will be in physical interlock that will prevent the premature firing of the satellites sublimation thrusters prior to release from the launch of vehicle.

Launch sequence begins at T_0 and involves the placement of the satellite into mission orbit. The launch vehicle will go through three different kick stages which will last within a 2-3 minute windo;, the final kick stage will place the satellite 400 km altitude tumbling at 5 rpm. After the final kick is burned and released from the satellite, yo-yo weights are deployed to reduce the momentum of satellite to a manageable 1 rpm. The reduction of the satellite rpm is vital because if not the rpms will be to great for us to gain control of the satellite, therefore if the yo-yo weights are ineffective we will lose the mission.

After the momentum of satellite reduce to managable rpm, the satellite goes through post seperation sequence. The release of the satellite from the launch vehicle through the separtion ring is checked by the onboard seperation clock and the physical interlock triggers. After seperation, a minimal check out is performed to ensure that the satellite is still entact and that and that no major damage was incurred during separtion. During post separtion check-out, the transponder is powered on to send out a beacon in an attempt to make contact with the ground station. Primary power source is switch from battery to solar panels. However, shall the satellite complete seperation while it is eclipsed by the earth the battery power will run until the satellite is able to sufficiental able to power itself through the solar panels and then commence to recharging the batteries in prepartion for the duration of orbit when eclipsed by the Earth again. Extra power produced by solar panels after the batteries are fully charge will be dumped through the shunt resistors where it will be transferred as heat and released by the radiator panels into space.

Upon completing post separtion sequence the satellite will go through stabalization sequence. Stablization sequence consist of orienting the spacecraft into mission attitude without ground intervention. This sequence is vital because if the satellite shall endup oriented so that the instrumentation face is pointed towards the sun it can potentially fry all the computer components and prematurely end the mission. Orientation will be perform through the use of attitude knowledge attain from sun sensors and attitude manuevering through the use of the magnetic torquers and reaction wheels. The stablization sequence will run again later in the mission shall the satellite be subject to unforseen damage or circumstance which forces it to turn off and reboot itself, therefore loosing its orientation.

The next two sequences are dependent on the field of view of the ground station of the satellite. Those subsequent orbits post stabilization will deticated to making initial contact with the ground station or power regenaration. Those orbits that the satellite is out of the view of the ground station it will continue to recharge the batteries and shunt excess power through the shunt resistor.

When the ground station is able to make contact with satellite, the ground station will then initiate satellite check-out. Check-out will begin with the check out with each subsystem, starting with the most vital system of satellite the Command and Data Handling (CDH) system. C&DH check out will run approximately a week then followed by the Attitude and Control System ACS for 3 weeks, Power system for a week, and Payload for 2 weeks. Thermal and Telecommunications check-out will be done sparatically throughout the entire 7 weeks, partially due to the importantance of constant monitoring of the satellites thermal health and the ability to cotact the ground station.

After subsystem check, a check out of the entire system will be performed during the two weeks afterwards. During system check out we run through the various mission modes to ensure desire operations between various subsystes.

Information from each check-out will be telemetry down to the ground station dnring every viable communication orbit.

Performance of the spacecraft while in orbit involves analyzing the housekeeping telemetry from the spacecraft to determine whether it is operating in the desired manner, how well it is working, and what its state of health is. Housekeeping data will be analyzed for long-term trends to detect and account for spacecraft aging characteristics before they become problems, such information will also be extremely valuable when developing the mission operations for the sequential missions.

Times needed to do each set of steps and determine which steps can run in parallel or have to be serial. Most missions are designed around a specific agency's ground system. We will be no different, being that a UHF ground station is already in place through prior work done by Dr. Shiroma's CubeSat program will communicate to the satellite using UHF frequency. However, we have the ability to retrieve data from the satellite in S-band using Dr. Torben Nielson's ground station that will be in place later this year. By utilizing the ground station already in place we will lower the overall mission cost.

On the tenth week mission operations with respect that all subsystem check-out is acceptable and everything is running properly. Instrumentation operation is intiated, which we will operate the various payloads beginning first with the ultra-violet camera then followed by active antenna experiment, and the sublimation thrusters. The sublimations thruster will used solely as a experimental payload and not for attitude control or momentum dumping because the force produce by thruster are not sufficient enough to perform those actions and to prevent contamenation of the camera lense. A After the completion of the instrumentation operation of the six month mission life, the spacecraft will be handed over to Jet Propulsion Laboratory to perform further experimentation using the autonomous software.

MISSION MODES

Mission modes are the actions the spacecraft will carry out in order to complete the Mission operations. By cross referencing the various mission modes with each subsystem component we produce a Power modes chart which can be seen in Figure 2, allows us to see which components are on during each mode. From the information gather from the Power modes chart we can see what mode will be the most power demanding during the mission life and what the minimal power required to sustain the life of the satellite.

During check-out each subsystem will check out individually and then telemetry data collect during check-out and then compared with the test performed during the testing of each subsystem done in the laboratory. The various check-out modes are as followed:

- Check-out 1 C&DH
- Check-out 2 ACS
- Check-out 3 POWER
- Check-out 4 TELECOMM
- Check-out 5 THERMAL
- Check-out 6 PAYLOAD

Taking the power comsumption of every component during each mission mode we can see the total power comsumption for each mode. Those notibly import is peak power

consumption which takes place during Telecommunications check out, consuming roughly 67 watts and the lowest power consumption of 14 watts which takes place during launch and seperation modes.

		MODES																				
Subsystem	Component	Power consumption (W)	Launch	Separation	Stablization	Orientation/ Manuever	Power Intialization	COMM	Backup COMM	Payload 1	Payload 2	Payload 3	Standard Ops (stby)	Recovery (Reboot)	Power Save	Safe	Check out 1	Check out 2	Check out 3	Check out 4	Check out 5	Check out 6
Payload	Imager	-6.00	OFF	OFF	OFF	OFF	OFF	OFF	OFF	ON	OFF	OFF	OFF	OFF	OFF	OFF	OFF	OFF	OFF	OFF	OFF	ON
	Active Antenna	-0.54	OFF	OFF	OFF	OFF	OFF	OFF	OFF	OFF	ON	OFF	OFF	OFF	OFF	OFF	OFF	OFF	OFF	OFF	OFF	ON
	Thrusters	TBD	OFF	OFF	OFF	OFF	OFF	OFF	OFF	OFF	OFF	ON	OFF	OFF	OFF	OFF	OFF	OFF	OFF	OFF	OFF	ON
	JPL Autonomous Software	N/A	ON	ON	ON	ON	ON	ON	ON	ON	ON	ON	ON	ON	ON	ON	ON	ON	ON	ON	ON	ON
C&DH	MIP405T Processor Board	-5.00	ON	ON	ON	ON	ON	ON	ON	ON	ON	ON	ON	ON	ON	ON	ON	ON	ON	ON	ON	ON
	FireSpeed 2000 Interface	-3.00	ON	ON	ON	ON	ON	ON	ON	ON	ON	ON	ON	ON	ON	ON	ON	ON	ON	ON	ON	ON
	USBP4 Interface	-0.50	ON	ON	ON	ON	ON	ON	ON	ON	ON	ON	ON	ON	ON	ON	ON	ON	ON	ON	ON	ON
	Emerald MM Serial Interface	-0.40	ON	ON	ON	ON	ON	ON	ON	ON	ON	ON	ON	ON	ON	ON	ON	ON	ON	ON	ON	ON
	Emerald MM Serial Interface	-0.40	ON	ON	ON	ON	ON	ON	ON	ON	ON	ON	ON	ON	ON	ON	ON	ON	ON	ON	ON	ON
	Onyx MM Control Timer	-0.60	ON	ON	ON	ON	ON	ON	ON	ON	ON	ON	ON	ON	ON	ON	ON	ON	ON	ON	ON	ON
	Diamond MM Analog Interface	-0.90	ON	ON	ON	ON	ON	ON	ON	ON	ON	ON	ON	ON	ON	ON	ON	ON	ON	ON	ON	ON
Power	Batteries Modules (6)	104.00	ON	ON	ON	OFF	OFF	OFF	OFF	OFF	OFF	OFF	ON	ON	ON	ON	OFF	OFF	ON	OFF	OFF	OFF
	Solar Panels (Lithium Ion)	102.00	ON	ON	ON	ON	ON	ON	ON	ON	ON	ON	ON	ON	OFF	ON	ON	ON	ON	ON	ON	ON
	PRU	TBD	ON	ON	ON	ON	ON	ON	ON	ON	ON	ON	ON	ON	ON	ON	ON	ON	ON	ON	ON	ON
	PDU	0.00	ON	ON	ON	ON	ON	ON	ON	ON	ON	ON	ON	ON	ON	ON	ON	ON	ON	ON	ON	ON
	Power Conditioning Unit	TBD	ON	ON	ON	ON	ON	ON	ON	ON	ON	ON	ON	ON	ON	ON	ON	ON	ON	ON	ON	ON
ACS	Reaction Wheels (3)	-18.00	OFF	OFF	ON	ON	ON	ON	ON	ON	ON	ON	ON	ON	ON	ON	ON	ON	ON	ON	ON	ON
	GPS	-3.20	ON	ON	ON	ON	ON	ON	ON	ON	ON	ON	ON	ON	ON	ON	ON	ON	ON	ON	ON	ON
	GPS Antenna	0.00	ON	ON	ON	ON	ON	ON	ON	ON	ON	ON	ON	ON	ON	ON	ON	ON	ON	ON	ON	ON
	Gyroscope	-2.00	OFF	OFF	ON	ON	OFF	OFF	OFF	OFF	OFF	ON	OFF	OFF	OFF	OFF	OFF	ON	OFF	OFF	OFF	OFF
	Star tracker	-2.00	OFF	OFF	OFF	ON	OFF	OFF	OFF	OFF	OFF	ON	OFF	OFF	OFF	OFF	OFF	ON	OFF	OFF	OFF	OFF
	Magnetometer		OFF	OFF	ON	ON	OFF	OFF	OFF	OFF	OFF	OFF	OFF	OFF	OFF	OFF	OFF	ON	OFF	OFF	OFF	OFF
	Magnetic Torquers		OFF	OFF	ON	ON	OFF	OFF	OFF	OFF	OFF	OFF	OFF	OFF	OFF	OFF	OFF	ON	OFF	OFF	OFF	OFF
	Sun Sensor	0.00	OFF	OFF	ON	OFF	OFF	OFF	OFF	OFF	OFF	OFF	OFF	OFF	OFF	OFF	OFF	ON	OFF	OFF	OFF	OFF
Telecomm	S-band Transponder		OFF	ON	ON	ON	ON	ON	OFF	ON	ON	ON	ON	ON	ON	ON	ON	ON	ON	ON	ON	ON
	S-band Transciever (transmitter)	-8.00	OFF	OFF	OFF	OFF	OFF	ON	OFF	OFF	OFF	OFF	OFF	OFF	OFF	OFF	OFF	OFF	OFF	ON	OFF	OFF
	High Power Amplifier	-24.00	OFF	OFF	OFF	OFF	OFF	ON	OFF	OFF	OFF	OFF	OFF	OFF	OFF	OFF	OFF	OFF	OFF	ON	OFF	OFF
	S-Band Antenna (2)	0.00	OFF	OFF	OFF	OFF	OFF	ON	OFF	OFF	OFF	OFF	OFF	OFF	OFF	OFF	OFF	OFF	OFF	ON	OFF	OFF
	UHF Transceiver (Transmit)	-1.74	OFF	OFF	OFF	OFF	OFF	OFF	ON	OFF	ON	OFF	OFF	OFF	OFF	OFF	OFF	OFF	OFF	ON	OFF	OFF
	UHF Transceiver (Receive)	-0.84	OFF	OFF	OFF	OFF	OFF	ON	ON	OFF	ON	OFF	OFF	OFF	OFF	OFF	OFF	OFF	OFF	ON	OFF	OFF
	TNC		OFF	OFF	OFF	OFF	OFF	OFF	ON	OFF	ON	OFF	OFF	OFF	OFF	OFF	OFF	OFF	OFF	ON	OFF	OFF
	UHF-Band Antenna	0.00	OFF	OFF	OFF	OFF	OFF	OFF	ON	OFF	ON	OFF	OFF	OFF	OFF	OFF	OFF	OFF	OFF	ON	OFF	OFF
Structure	Launch vehicleChassis	N/A	N/A	N/A	N/A	N/A	N/A	N/A	N/A	N/A	N/A	N/A	N/A	N/A	N/A	N/A	N/A	N/A	N/A	N/A	N/A	N/A
	Spacecraft Structure	N/A	N/A	N/A	N/A	N/A	N/A	N/A	N/A	N/A	N/A	N/A	N/A	N/A	N/A	N/A	N/A	N/A	N/A	N/A	N/A	N/A
	Lightband interface ring	N/A	OFF	N/A	N/A	N/A	N/A	N/A	N/A	N/A	N/A	N/A	N/A	N/A	N/A	N/A	N/A	N/A	N/A	N/A	N/A	N/A
	Adapter interface	N/A	N/A	N/A	N/A	N/A	N/A	N/A	N/A	N/A	N/A	N/A	N/A	N/A	N/A	N/A	N/A	N/A	N/A	N/A	N/A	N/A
Thermal	film heater	TBD	TBD	TBD	TBD	TBD	TBD	TBD	TBD	TBD	TBD	ON	TBD	TBD	ON	TBD	TBD	TBD	TBD	TBD	ON	TBD
	Temperature Sensors (6)	TBD	ON	ON	ON	ON	ON	ON	ON	ON	ON	ON	ON	ON	ON	ON	ON	ON	ON	ON	ON	ON
	Thermostats (5)	TBD	ON	ON	ON	ON	ON	ON	ON	ON	ON	ON	ON	ON	ON	ON	ON	ON	ON	ON	ON	ON
	Multi Layer Instulation	TBD	ON	ON	ON	ON	ON	ON	ON	ON	ON	ON	ON	ON	ON	ON	ON	ON	ON	ON	ON	ON
	Shunt Resistors (16)	TBD	ON	ON	ON	ON	ON	ON	ON	ON	ON	ON	ON	ON	ON	ON	ON	ON	ON	ON	ON	ON
Subtotal	Consumption of Components w/o power source		-14.00	-14.00	-34.00	-36.00	-32.00	-64.84	-34.58	-38.00	-35.12	-36.00	-32.00	-32.00	-32.00	-32.00	-32.00	-36.00	-32.00	-66.58	-32.00	-38.00
Total	Consumption of Components w/ power source																					

Figure 2: Chart of the Power Modes consist the mission modes and the components of each subsystem.

CONCLUSION

With the development of the mission scenarios, we can assign machines or people to carry out each step. Using the mission operations plan we can gather the people related steps and form an organization around them, assigning the teams to the steps and analyze the organization to establish operational interfaces. For those steps that are machine related we set up a data-flow diagram showing processes, points for data storage, and interrelationships between various subsystems and between the spacecraft and ground station.

The mission operations plan is subject to change as assumptions change and more data becomes available during the mission design process.

ACKNOWLEDGEMENTS

I would like to thank the Hawaii Space Grant Consortium, Dr. Luke Flynn, Dr. Peter Mouginis-Mark, and Lloyd French for allowing me to have the opportunity to be a part of such an awesome program. A great thanks goes to Lloyd French for is extensive insight of not only mission design but life in general. I am extremely grateful for the time I have a part of the LEONIDAS program and knowledge attain while be working on it. I want to thank the LEONIDAS student team for all the work, dedication, and friendship. I wish to also show my gratitude to Marcia Sistoso for her patience and attentiveness to ensure that I meet my deadlines and have everything I need. And to the many others that had an opportunity to work with or just gave words of encouragement during my time working on the LEONIDAS project, Thank you.

REFERENCES

Larson, Wiley J. and Wertz, James R. 2005 "Space Mission Analysis and Design." Space Technology Library: 587-603.

Baer, Glen; Harvey, Raymond; Holdridge, Mark; Huebschman, Richard; and Rodberg, Elliot, "Mission Operations." http://www.jhuapl.edu/techdigest/td2004/baer.pdf

PAYLOAD DESIGN FOR A MICROSATELLITE II

Aukai Kent
Department of Mechanical Engineering
University of Hawai‘i at Mānoa
Honolulu, HI 96822

ABSTRACT

Conventional satellites are extremely large, highly expensive, and may take several years to design and build. Microsatellites have the potential to reduce cost and risk when compared to conventional satellites. The main purpose of the LEONIDAS project is to prove that the University of Hawaii has the capabilities to design, build, test, launch, and operate a microsatellite. The payload subsystem is the heart of the microsatellite and consists of all the different hardware and software on the satellite that is used to satisfy the mission objectives. The payload subsystem will consist of four different instruments. An imager system will be used to test the satellites capability to house an imager and will take pictures of Hawaii in the ultraviolet and visible spectrum. A retro directive antenna and a propulsion unit, both designed by the University of Hawaii, will test the satellites capability to demonstrate new technologies. The satellite will also house health monitoring software provided by JPL/Ames. The following report includes requirements for each payload and an analysis and design of the imager.

INTRODUCTION

The LEONIDAS project is designed to prove the capabilities of the University of Hawaii to design, build, test, launch, and operate a microsatellite. Proving these capabilities will lead to many new opportunities within the aerospace industry. The success of the LEONIDAS project could lead to partnerships with NASA and could push the University of Hawaii to start its own aerospace program. The main objective for the current mission design is to conduct technology demonstrations in the laboratory of space.

The payload subsystem is the heart of the microsatellite and determines many of the capabilities and limitations of the mission. The payload consists of all the different hardware and software on the satellite that is used to satisfy the mission objectives. The main purpose for the other subsystems of the satellite is to keep the payload subsystem happy and healthy.

The payload subsystem will consist of an imager, a retro-directive antenna, a propulsion unit, and health monitoring software. The imager will capture pictures of Hawaii in the ultraviolet and visible spectrums and will test the satellites capability to house a camera. A retro-directive antenna and a propulsion unit, currently being designed by the University of Hawaii, will test the satellites capability to demonstrate new technologies. The retro-directive antenna is a ground breaking technology that uses “self steering” to communicate to the ground or with other satellites. However, since very little information is available on the retro-directive antenna, it has been excluded from this report. The propulsion unit utilizes solid sublimation micro thrusters, which has the capability to advance attitude control of microsatellites. A health monitoring software will also be on board the spacecraft and is being developed by JPL/Ames. This software could help reduce the cost of operations by automatically detecting and repairing anomalies.

In order to successfully complete a design for the payload subsystem, the requirements for each payload needed to be determined. An analysis was accomplished for each payload using the respective requirements. The analysis was used to complete a design of the payload subsystem.

REQUIREMENTS

In order to understand the function, operations, and performance of each payload of the spacecraft, the requirements for need to be determined. The requirements are important because they will become the constraints that will shape and mold the design of each payload. Since the requirements affect my design, any changes will also affect the design of other subsystems. Because each payload is different, each payload will have its own set of requirements, which will be split into three different categories: physical requirements, operational requirements, and performance requirements.

The first set of requirements consisted of constraints on the payload subsystem as a whole, which were determined by the mission objectives. In order to satisfy these requirements the subsystem needed to have a total mass of less than 2.2 kg and consume a total power of less than 8 W. The payloads would also have to function at an altitude of 400 km and with a ground track speed of 7.7 km/s.

In order to fit within the spacecraft, the imager must have a mass of less than half the total payload mass (1.1 kg). The imager must also be situated in the spacecraft where its view will be unobstructed, and on the face of the spacecraft that will be nadir pointing.

The objective of the imager is to take a picture of a desired target. This target will vary due to the customer's interest. For the first mission the desired target is Hawaii, 21°18'n, 157°50'w. In order to get successful picture the imager must take a series of three pictures. The camera must work in the 300 – 700 nm wavelength range (ultraviolet and visible). The imager must also have a pixel resolution of 10 m X 10 m and a resolution around 1.5 mega pixels.

The flight computer will be used to trigger the imager as well as change settings if necessary. The imager will turn on as it approaches the desired latitude and longitude (21°18'n, 157°50'w). Each image will be sent directly to the flight computer, which will be responsible for all the processing.

The propulsion unit, which is currently being designed by the University of Hawaii at Manoa, will consist of no less than eight thrusters. Each thruster will be less than 6 cm in length and less than 2 cm in both the width and height. A cartridge heater will be used to heat each thruster and will require less than 1 W. The total propulsion unit must have a mass of less than .5 kg. Each thruster will be individually controlled by the flight computer. The flight computer will test each thruster in two modes, impulse fire and continuous fire. Each thruster will be tested separately and will fire 10, one second bursts under the impulse fire mode and fire for 10 seconds under the continuous fire mode. Temperature vs. thrust and time response will be recorded for each thruster and each mode.

The Health Monitoring Software (HMS) by JPL/AMES is a software technology that analyzes system data to detect anomalies, classify faults, and track degradation in physical systems. This software will require a certain amount of memory from the flight computer. Since the software is still in development, it is unknown exactly how much memory it will require. In order to detect anomalies the HMS will receive four types of data. The first type of data is discrete status variables changing in time – modes, switch positions, health bits, etc. – from

sensors or software. The second type of data is real-valued sensor data at fixed rates – performance sensors or dedicated diagnostic sensors. The third type of data is command information – typically discrete. The final type of data is fixed parameters – varying only when commanded to change but containing important state information. The HMS will process and compare the data to example data sheets that can constantly be updated. Faults and anomalies will be detected and corrected. The performance of the HMS will be judged by the amount of detections that are monitored and how fast the faults are detected.

ANALYSIS

The requirements were used to conduct a preliminary analysis of each respective payload. An analysis is very important to the design of my subsystem because it will determine whether or not my payloads fit the specifications of the spacecraft. Since the propulsion unit, the retro-directive antenna, and the health monitoring software are still in development, an analysis was only performed for the imager.

According to the requirements the imager needed to have a pixel width of 10 m and a ground resolution around 1.5 mega pixels. The data rate, integration time, and data volume were calculated for the imager. These values will be used to determine whether or not the flight computer has the ability to process the information and to determine the imager that will be used for the mission. The calculations were carried out for an average imager output of 10 bits per pixel.

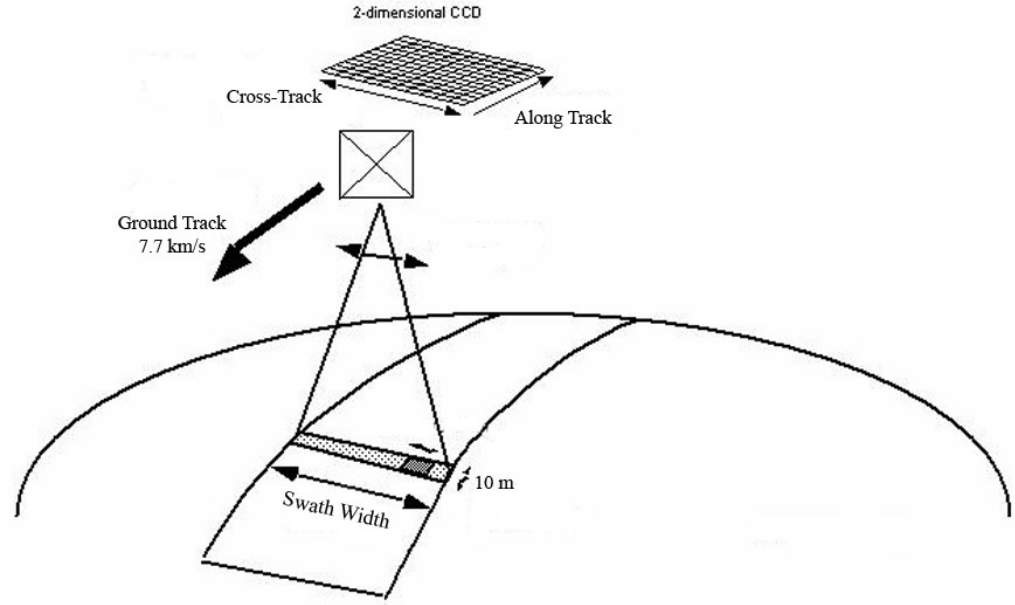

Figure 1: Image parameters of an observation satellite

Figure 1 shows image parameters for an observation satellite. The along-track resolution is the number of pixels along the line of movement of the satellite. The cross-track resolution is the number of pixels perpendicular to the line of movement of the satellite. The swath width is the number of cross-track pixels times the resolution per pixel. These values are used to determine the data rate. This analysis used a cross-track resolution and along-track resolution of 1224 pixels (~1.5 mega pixels).

The data rate required for observation payloads depends on the resolution, coverage, and bit output. The data rate is determined using the number of pixels recorded per second (Z) and the number of bits per pixel (B) with the relationship given in equation (1).

$$DR = Z * B \qquad (1)$$

The number of pixels recorded per second (Z) is determined using the number of cross-track pixels (Z_c) and the number of swaths recorded along-track per second (Z_a) with the relationship given in equation (2).

$$Z = Z_c * Z_a \qquad (2)$$

The number of swaths recorded along-track per second (Z_a) is determined using the ground track speed (V_g) and the pixel width (Y) with the relationship given in equation (3).

$$Z_a = (V_g * 1 \text{ sec})/Y \qquad (3)$$

Using equation (3), V_g = 7.7 km/s, and Y = 10 m, the number of swaths recorded along-track per second was determined to be 770 swaths/s. With equation (2), Z_a = 770 swaths/s, and Z_c = 1224 pixels, the number of pixels per second was determined to be 942,480 pixels/s. Applying equation (1), Z = 942,480 pixels/s, and B = 10 bits, the data rate was determined to be 9.4 Mbps.

The integration time is the time it takes to capture a single image. The integration time was determined using the along-track ground resolution (X) and the ground track speed using the relationship given in equation (4).

$$T_i = X/V_g \qquad (4)$$

Using equation (4), X = 12.24 km, and V_g = 7.7 km/s, the integration time was determined to be 1.6 s.

The data volume is the total amount of data given to the flight computer per observation session. The data volume is determined using the number of pictures (n), the data rate, and the integration time with the relationship given in equation (5).

$$DV = n * DR * T_i \qquad (5)$$

Using equation (5), n = 3, DR = 9.4 Mbps, and Ti = 1.6 s, the data volume was determined to be 44.83 Mbits. The flight computer subsystem will determine if the values for data rate and data volume fit within the specifications of the spacecraft.

DESIGN

An imager was selected that met the requirements and fit within the specifications of the analysis. The imager that will be used for the first mission is a Sony XCD-SX910UV. The imager observes in the 300-700 nm wavelength range, which meets the mission objective requirement. It has a 10 bit output per pixel and a maximum resolution of 1,376 pixels cross-track and 1,024 pixels along track (~1.41 mega pixels). The imager also has a frame rate up to

15 fps and a shutter speed ranging from .1 microseconds to 17.5 seconds. The camera consumes 4 W of power and has a mass of 250 g, which meets their respective requirements of 8W and 1.1 kg. A firewire interface is used to download data from the imager to the flight computer. The firewire is capable of transfer rates up to 200 Mbps, which is far greater than the estimated data rate of 9.4 Mbps, therefore data transfer from the imager to the flight computer should not be a problem. Vibration and Shock loads due to launch should not be a problem due to the imager's capability of withstanding vibration and shock up to 10 G and 70 G respectively.

The data rate, integration time, and data volume were determined for the selected imager. Using equations (1), (2), and (3), with V_g = 7.7 km/s, Z_c = 1024, and Y = 10 m, the data rate was determined. The imager acquires one image at a rate of 7.8 Mbps. Using equation (4), with V_g = 7.7 km/s and X = 10.240 km, the integration time was determined. The image captures a single image in 1.8 s. Using equation (6), with n = 3 images, and DR and T_i for the imager, the data volume was determined. The total amount of data being transferred to the flight computer is 42.12 Mbits.

The calculated integration time for the imager was 1.8 seconds. In order to reduce the "smear" affect of an image, the shutter speed should equal the integration time. Since a shutter speed of 1.8 seconds falls within the possible shutter speed of the imager, the imager is justified. The data rate and data volume for the selected imager is less than the respective values for the preliminary analysis, therefore the selected imager fits within the specifications of the spacecraft.

CONCLUSION

There is still some work that needs next to be done before the design of the payload subsystem is complete. In order to complete the design of the imager, the optical specifications need to be studied. The field of view and magnification properties in order to achieve the desired resolution per pixel need to be determined and analyzed to see if they fit the specifications of the mission and spacecraft. Filters also need to be selected for the imager. Once the design of the propulsion unit has been completed its respective researcher, its specifications will need to be studied to determine whether they fit the requirements stated earlier in the report. Work also needs to be done with JPL and the Ames research center to insure that the health monitoring software can be implemented in our satellite. Once the design of the software is complete, an iterative analysis on the subsystem as a whole will follow. In order for the final analysis to be complete, I will need to make sure that all the instruments meet the payload requirements, can satisfy the mission objectives, and are able to interact with the other subsystems in the satellite.

REFERENCES

Larson, Wiley J., and James R. Wertz. Space Mission Analysis and Design. 3rd ed. El Segundo, CA: Microcosm Press, 1999

Mackey, Ryan, California Institute of Technology/Jet Propulsion Laboratory. "Generalized Cross-Signal Anomaly Detection."

Mackey, Ryan, California Institute of Technology/Jet Propulsion Laboratory. " BEAM: Technology for Autonomous Self-Analysis "

Mackey, Ryan, California Institute of Technology/Jet Propulsion Laboratory. " Integrated System Health Management (ISHM) Technology Demonstration Project Final Report"

STRUCTURE SUBSYSTEM

Michael Menendez
Department of Mechanical Engineering
University of Hawai‘i at Mānoa
Honolulu, Hawaii 96822

ABSTRACT

Building a full size and traditional satellite is a very expensive and time costly procedure. A single satellite can cost several million dollars, and another several million to launch. Micro satellites are a way to design, build, test, and launch a fully functional satellite at a fraction of the cost. By reducing the cost to build and launch the satellite, less is at risk during launch or orbit. The University of Hawaii Manoa LEONIDAS team has a mission to change the development of a microsat. University of Hawaii will be able to house the entire satellite project from start to launch, and maintain control of the satellite communications while in orbit. This will be the first and only university in the world with these capabilities, and will revolutionize this industry by reducing costs, time and testing new technology.

INTRODUCTION

The LEONIDAS project is designed to prove the capabilities of the University of Hawaii to design, build, test, launch, and operate a microsatellite. Proving these capabilities will lead to many new opportunities within the aerospace industry. The success of the LEONIDAS project could lead to partnerships with NASA and could push the University of Hawaii to start its own aerospace program. The main objective for the current mission design is to conduct technology demonstrations in the laboratory of space.

The Structure subsystem is the backbone of the satellite. It will provide a lightweight, extremely strong chassis to house the physical satellite components. The structure will have to maintain its form during all phases of the mission, primarily the launch. During the launch, the frame will have to withstand over 12G’s of force and vibration to hold the system components in place for proper operation.

The framework will consist of a truss like design, similar to the ones used in bridge building, aluminum plates machined out for mass savings, and aluminum and titanium fasteners for proper thermal transfer. The main pieces will most likely be made from 6061T6 aluminum. This material was chosen for its little mass and high performance. When designing a microsat, the mass is crucial to keep minimal. The framework will also have the capability of mounting the solar panels, imager, telecom, acs, power, and thermal subsystems where it is most ideal for them.

Panels will be made from solid sheets of 7mm thick, 6061T6 aluminum, then fastened together for maximum strength. To reduce thermal transfer of energy between panels of the structure, special G-10 spacers will act as an isolation spacer, allowing for the structure to better assist the thermal subsystem. With details such as these to be analyzed, a detailed set of system requirements for the structure system will have to take place. This is to keep the certainties certain, and the uncertainties solved.

REQUIREMENTS

For a more thorough understanding of the specific needs, conflicts and imposed requirements, a set of system requirements helps to guide the way. The requirements are crucial as they will shape and design the way in which other systems can and will function. The requirements will allow the structure system to take shape, and have maximum functionality. The structure, as simple as it sounds, has many parts to interact with. Since there are so many parts and different requirements to meet, the system requirements can be split into two different main groups: structure requirements, and mechanical requirements.

	Structure Requirements - Michael Menendez	Given By	Given To	Dates Modified
External Dimension Constraints				
5.01-	5.01.01 The structure will be contained within the launch vehicle of (TBD) (cm)	Mission	Structure	3/1/2007
	5.01.02 The structure will determine the surface area of (TBD) area.	Structure	Power	2/18/2007
	5.01.03 The structure will not have any moving parts.	Structure	Structure	2/18/2007
Forces / Stress (Dynamic)				
5.02-	5.02.01 The structure will withstand launch forces of 12G's.	Launch vehicle	Structure	2/18/2007
	5.02.02 The structure will be resilient to vibration of the (TBD) resonant frequency.	Launch vehicle	Structure	2/18/2007
	5.02.03 The structure will not flex or deflect under torsional, compressive, tensile stress. Stiffness	Launch vehicle	Structure	2/18/2007
Thermal Constraints				
5.03-	5.03.01 The structure will control heat using conduction and radiation.	Thermal	Structure	2/18/2007
	5.03.02 The structure will provide strapping to dissipate heat.	Thermal	Structure	2/18/2007
	5.03.02.01 The structure will mount heat dissipation radiator plates (TBD)	Thermal	Structure	2/18/2007
	5.03.03 The structure will control scatter with a (TBD) surface finish.			
	5.03.04 The structure will be (TBD) color to dissipate (TBD) heat.	Structure	Structure	2/18/2007
	5.03.05 The structure will allow for (TBD) amount of thermal expansion.	Structure	Structure	2/18/2007
Mass Constraints				
5.04-	5.04.01 The structure cannot exceed the 12 kg mass budget.	Mission	Structure	2/18/2007
Antenna & camera Placement				
5.05-	5.05.01 The placement of the camera and antenna will allow for maximum visibility towards Earth.	Payloads	Structure	2/18/2007
Configuration				
5.06-	5.06.01 The satellite's center of mass must be placed within(TBD) of the center of the structure.	ACS	Structure	2/18/2007
	5.06.02 The satellite's system components shall not overlap or come within (TBD) of each other.	Structure	Structure	2/18/2007
	5.06.03 The structure's rack space constraints are (TBD cm).	Mission	Structure	2/18/2007

	5.06.04 The structure will be able to mount at least one reaction wheel near the (TBD) center of mass. 5.06.05 The structure will locate the avionics equipment facing Earth. 5.06.06 The structure will divide up the bus into different bays in accordance to the center of mass.	ACS	Structure	2/18/2007 3/1/2007 3/1/2007
Insulation 5.07-	5.07.01 The structure will be insulated to control (TBD) thermal energy.	Thermal	Structure	2/18/2007
Fasteners 5.08-	5.08.01The structure shall be assembled using mechanical fastening. 5.08.01The mechanical fastening will allow for thermal transfer. 5.08.01.1The mechanical fasteners shall be tapped into the frame. 5.08.02 The structure will have a (TBD) surface texture at joints in contact.	Structure Thermal	Structure Structure	2/18/2007 2/18/2007
Interface Board 5.09-	5.09.01 The structure will have a centeral interface boards. 5.09.02 The structure's interface board will have (TBD) space between for cabling and plugs. 5.09.03 The circuit boards will be mounted on a standardized structural member. 5.09.04 All circuit boards will be removable for easy access. 5.09.05 The structural 'rack' will be locked into place. 5.09.06 The connections between system components shall be effective through (TBD) temperature range. 5.09.06.1 The connections shall fall within (+/- TBD %) signal loss. 5.09.06.2 The connections shall lock with a (TBD) mechanical device.	 Structure Mission Structure Thermal	 Structure Structure Structure Structure	3/1/2007 3/1/2007 2/18/2007 2/18/2007 2/18/2007 2/18/2007
Radiation 5.10-	5.10.01 The structure will have shielding for system protection against (TBD) radiation.	Structure	Structure	2/18/2007
Wiring 5.11-	5.10.01 The structure shall determine most efficient paths for cabling. 5.10.02 The structure will fasten cables for minimal movement. 5.The structure will provide a grounding system for system components. The structure shall be conductive.	All Structure All	Structure Structure Structure	2/18/2007 2/18/2007 2/18/2007
Gussets 5.12-	The structure will use gusseting and brackets.	Structure	Structure	2/18/2007
Panel mounting (solar) / camera 5.13-	The structure will provide rigid framework for solar panels. The structure will allow for framework to mount glass on the outsides of the frame. The outer panels of the structure will be machined.	Power Structure	Structure Structure	2/18/2007 2/18/2007

Materials Selection				
5.14-	The structure will be made from a material that can handle (TBD) temp. range.	structure	structure	3/1/2007
	The structure will be made from a material with good thermal conduction properties	structure	structure	3/1/2007
	The structure will be made from a material with (TBD) yield strength.	structure	structure	
Payloads				
5.15-	The structure will have structural brackets to hold the payloads.			3/1/2007
	The structure will use isolators to reduce vibration.			3/1/2007
	The structure will use isolators to have thermal control.			3/1/2007

The mechanical requirements are for parts that move, and require mechanical properties for proper system requirements. The structural requirements are physical system requirements for parts of the structure subsystem that have to be stiff and stationary while fulfilling other subsystem requirements which it has originated from.

ANALYSIS

The specific structure system requirements allow for a more specific goal in mind, and simplified solutions to get there. This is why the analysis is so important. The analysis tells us if the structure system is meeting its listed requirements, and if not how it can be addressed in a specific way. It is important not to overlook the specifics of the system requirements when doing the analysis.

Using SolidWorks 2005, a model was created to exact scale to represent the frame/structural bus mentioned and designed with the listed requirements. This CAD drawing allowed me to stress test basic parts of the satellite to know where the weak points were for further analysis. The model also showed component placement. Within the program SolidWorks 2005, I created a scale part of every subsystem and payload component for optimal placement and center of mass weight distribution.

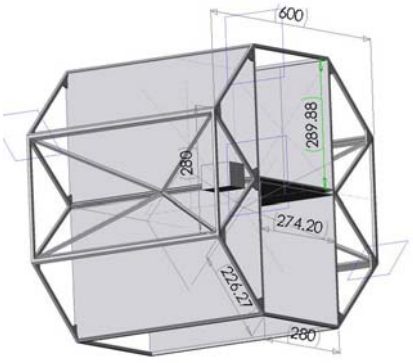

In the picture above, a bare bones non-populated frame designed around the structure system requirements and analysis is shown. This is to show the basic truss framework to support the 12G load. The dimensions are labeled in mm to show exact outer dimensions.

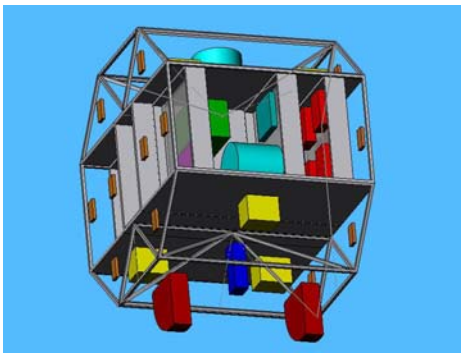

The CAD drawing above shows the populated version of the structure system with its component placement. The solar panels are removed to show the inside with its 'racking' system. This 'racking' system is there to allow for a reconfigurable bus system that will allow us to quickly make changes and additions using off the shelf parts. The components are also placed in a way that is logical for the thermal system, convenient cabling and a good center of mass. With the configuration shown, the center of mass is very near the center. This is necessary for vehicle control and stability while pitching and yawing in space to slew over the islands and take a picture.

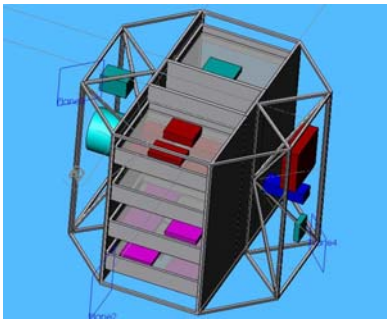

This is another close up of the reconfigurable bus with its 'racking' system. The blue box represents the imager; therefore that side will always be facing earth.

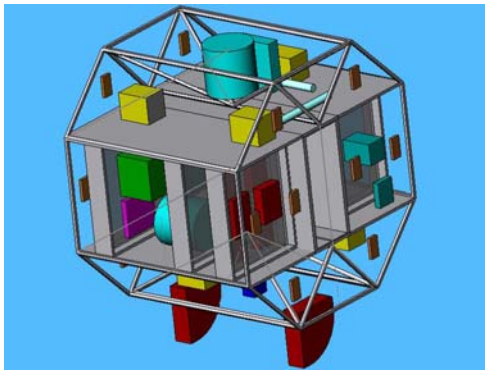

There are a number of thermal shunt resistors that allow heat to be transferred to the radiator plates located on the top and bottom of the satellite. The top and bottom can be defined as the sides in the shape of the octagon. The octagon was chosen as the primary shape due to its

great efficiency of space, strength properties and little mass. In this drawing there are approximately 16 shunt resistors which are the small, dark red boxes floating at the surface.

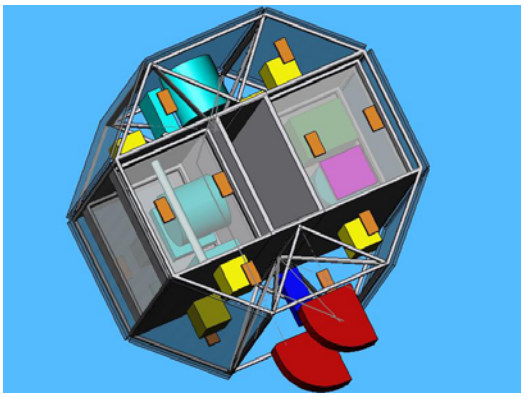

As a requirement placed on the structure subsystem, the s-band antennae are placed on the outside of the satellite, facing earth at all times. since the satellite is going to stay is the same orientation while orbiting earth, the s-band antennae will also face earth along with the imager. In the picture above, the red, fin shaped objects are the two s-band antennae.

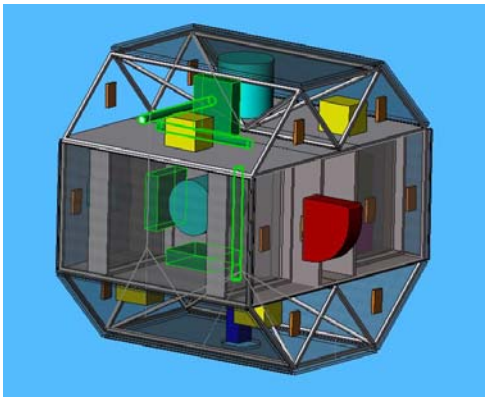

In this picture, the highlighted green tubes are the magnetic torquers. These are another form of propulsion to maneuver the satellite along with the light blue colored reaction wheels. The magnetic torquers have to be strapped to the frame in such a way that the 3 axes of the satellite can be maneuvered accurately and easily. To do so, the magnetic torquers have to be mounted around the center of mass, similar to the reaction wheels. The magnetic torquers are similar to a coil or wire in an elongated cylindrical shape. When current is passed through the coil, it creates an electromagnetic field that can react with the magnetic field of earth.

CONCLUSION

Most of the testing and analysis was done using a CAD program called SolidWorks 2005. This software gives a calculated evaluation on how the frame will react to stresses and loads. It also gives a 3-D physical representation of the placement and center of mass of the satellite. This means the results and analysis are calculated, computer generated results of which changes will be made when fabricating in reality. Testing and assembling in reality will allow for optimal

analysis and component placement. Work still needs to be done to continue the detailed analysis of the LEONIDAS satellite structure system in order to have the most accurate results. More stress analysis and load testing needs to be done to finalize the structural integrity of this satellite. Mass reduction needs to increase to make this frame optimal. And research still needs to be done on further material and thermal development. All of these components need to be done to have a final analysis of the structure system, and for a premium balance of functional requirements.

REFERENCES

Larson, Wiley J., and James R. Wertz. Space Mission Analysis and Design. 3rd ed. El Segundo, CA: Microcosm Press, 1999

DEVELOPMENT OF AN ATTITUDE CONTROL SUBSYSTEM FOR A MICROSATELLITE

Lynette T. Shiroma
Department of Mechanical Engineering
University of Hawai‘i at Mānoa
Honolulu, Hawaii 96822

ABSTRACT

One key to the success of the spacecraft mission is a properly designed attitude control subsystem. The accuracy and precision of the attitude control system can directly affect what kinds of payloads can be carried, how much power it can receive through the solar cells as well as the internal temperature of the spacecraft. A reliable attitude control system can be achieved through developing specific achievable requirements of the subsystem, evaluating the performance of the components selected for the initial design and determining if they will integrate with each other, and defining the environment adequately such that the attitude control system may be able to cancel out all expected and unexpected disturbances and maintain desired orientations.

INTRODUCTION

The application of technologies developed for the space program to everyday life has yielded breakthroughs in all walks of life, whether we are talking about moon boot running shoes or even as complex as variable-polarity plasma arc welding. However, many satellites missions suffer from not being able to also benefit from the latest breakthrough technologies, due to the risk in using untested technologies, the time it takes to develop missions and the money invested developing a mission.

The *Low-Earth Orbit Nanosatellite Integrated Defense Autonomous System* (LEONIDAS) envisions a modified “plug-and-play” capability in satellites, where certain subsystems such as payloads are easily exchanged from mission to mission, allowing for subsequent satellites to be developed more economically in less time with reduced risk. This satellite would then serve as the ideal testbed for experiments and science technology developments. This correlates directly with the National Aeronautics and Space Administration (NASA) need to take advantage of the private space sector’s rapid development and create a greater and more competitive market for higher-risk missions. To help aid with the reliability and the robustness of spacecraft operations, *commercial, off-the-shelf* (COTS) components that have been flight tested will be used whenever available.

This project focused on developing the *attitude and control subsystem* (ACS) for LEONIDAS. ACS determines the position and orientation of the craft, then based on this knowledge, orients the craft in desired directions during its orbit, and maintains desired pointing despite external and internal disturbances. An ACS system is needed to perform many different operations on the spacecraft: taking pictures, telecommunications, power acquisition, and passive heat dumping.

During the semester, the goal was to help prepare for the ACS part of the *preliminary design review* (PDR). The PDR is a rigorous evaluation of the whole spacecraft. It determines if

the proposed design of the spacecraft will work before any parts are received and also includes a detailed plan for assembly and testing.

REQUIREMENTS

The most helpful way to creating useful requirements is to go through the sequence of a spacecraft's life. Requirements are specific needs in order to meet mission goals, without divulging too much into how these requirements would be met. This allows the engineer to narrow down from a multitude of solutions to the requirement to several that satisfy our needs without being excessive. Excessive solutions usually result in such things as higher costs and bigger mass which is the very thing that we try to reduce in a spacecraft. For example, "The spacecraft shall have a total pointing error of ±1°" is a good requirement as opposed to "The spacecraft shall be stabilized by reaction wheels." The former is a good requirement because it is specific and objective, while not showing how this requirement could be solved. The latter is a bad requirement because it specifically tells us what design to use (reaction wheels) and there is not a clear differentiation as to whether this requirement is needed for a unidirectional antenna or for very precise and clear spy pictures. "Design-driven" requirements also greatly constrain the engineer's creativity and flexibility in solving a problem. Requirements will let us converge to several possible solutions out of many because it will allow us to choose a design that is "just right" for its purpose.

While the above approach is simple and straightforward, requirements are not always so clear cut. Some shades of grey lie between design and requirements. For example, our subsystem design may drive other subsystem requirements: operating temperatures of the ACS system determine what requirement must be met for the thermal subsystem. However, operating temperatures are usually dependent on what types of components are picked. Therefore, in such a scenario, we are forced to make an educated ballpark estimate of what our requirements will be based on from similar past spacecraft systems and prior knowledge. It is not uncommon to revise requirements again after a design has been chosen in a similar case; however the engineer should always keep in mind why you are writing the requirement. We should know where the requirement is coming from, and who has to meet the requirement. Should the requirement change from the mission goal level or from another subsystem, it is more than acceptable for the system that has to meet the requirement to revise their requirements but it should be noted at what point the requirement changed and to keep the old requirement should you need to revert back to it.

Requirements should be numbered, grouped, and dated to allow for easy reference in the future. It is also important to differentiate which requirements are imposed on your subsystem, and which requirements are required of other subsystems. Some important ACS requirements are listed below:

- 7.1.3 ACS shall hold commanded attitude without ground intervention
- 7.2.1 The spacecraft shall have a total pointing error of ±1°
- 7.2.2 The max slew rate of the spacecraft shall be 0.6°/s
- 7.2.3 The min slew rate of the spacecraft shall be 0.2°/s
- 7.9.1 ACS shall have each of the interfaces in the given quantities: PC104- 1; USB- 1; RS232- 6

Requirement 7.1.3 is important because it is able to tell us that ACS will keep doing what we want it to do, even if no one is there to give it instructions. Requirement 7.2.1 is especially important because it tells us what kind of equipment we can have on the spacecraft such as a camera with a fast enough shutter speed so smearing does not occur. Requirement 7.2.2 tells us how fast ACS can respond to go to specified positions, and Requirement 7.2.3 gives an indication of what the deadband is. Deadband is the error at which we stop correcting to prevent overcorrection and jitter. Requirement 7.9.1 is the most important to the overall spacecraft's mission because constraining the amount of interfaces in which ACS allows us to communicate from demonstrates the feasibility of having a plug-and-play architecture similar to a desktop computer: Plugging in a USB cord from an optical mouse will tell the computer what sort of device it is, and if necessary, lets the flight computer know what additional drivers are needed to run this software. Figure 1 contains the complete set of attitude control requirements.

DESIGN

After the requirements are completed, it is necessary to find components that meet such requirements. As mentioned in the introduction, preference will be given to components that have been flight validated to reduce risk in this mission, however, in subsequent missions it is to be expected that the spacecraft shall fly more components that are not flight validated to correlate with the spacecraft's final goal of making flight-validation more accessible to all space equipment with reduced cost.

The proposed attitude control subsystem is three axes stabilized, allowing for the spacecraft to point and correct in all directions. Other methods of stabilization have been proposed, such as two axis stabilization, because normal operations would really only require control on two axes, but because of requirement 7.4.1 states that "the spacecraft shall be able to point anywhere in 3-D space" during safehold and acquisition, three axes stabilization is required. It would also be advantageous in some cases, because we can get a good power transmission from the solar cells, as well as taking a picture, or dissipating heat in the best way possible at the same time.

Design of the ACS subsystem has not significantly changed over the course of the semester but with two new additions: Medium sun sensors from Aeroastro and magnetic torquers produced by ZARM.

Sun sensors work by reading the signals coming from a set of photovoltaics. From a calibration file, it uses an interpolation subroutine to find at what angle and at what intensity the sun is shining from (that discerns how far away it is). By using more than one sun sensor, we are able to find which direction we are facing in at all times and whether we need to reorient ourselves such that the light-sensitive equipment is protected. We also need to ensure from this data that the solar cells are also getting enough sunlight so that we can meet power requirements.

The medium sun sensors are especially necessary to perform position acquisition at the final stage of orbital insertion where the slew rate may be too high in order for star tracker data to be accurate (as the start tracker is essentially a camera). With sun sensors, we may always be able to tell the direction from which the sun is hitting our spacecraft and protect the sun sensitive equipment by maneuvering. Some concern has also been brought up through preliminary orbital analysis that the star tracker could possibly be exposed in full sun while maintaining nadir pointing during the spacecraft's mission life. With this as a concern, it becomes necessary to

have another method of finding orientation information when the star tracker cannot be used in the periods listed above, and should the star tracker malfunction.

Magnetic Torquers would serve as a replacement for reaction wheels on axes that do not require very precise movements or very fast slew rates. Magnetic Torquers take advantage of the magnetic field of the earth to create moments within the spacecraft. Magnetic Torquers are most often used in spacecraft when small less precise movements are needed due to their small size and no moving parts. They are also frequently used for momentum dumping (getting rid of external disturbance torques) where reaction wheels are unsuccessful as they saturate. Saturation is what happens when the reaction wheels are turning at the maximum rotations per minute but are not turning as fast as they need to in order to overcome these forces. Using magnetic torquers in conjunction with reaction wheels proves very successful as the spacecraft is precise, allows for longer spacecraft life (since the reaction wheels are used only to produce internal torques in the spacecraft).

As it stands, the ACS system is over the mass requirement by approximately a kilogram. The implementation of magnetic torquers and sun sensors along non-major axes would allow for the significant reduction of mass by taking away some reaction wheels and gyroscopes on axes that do not have major slew or accuracy requirements. Additional magnetic torquers could alternately be used to desaturate the reaction wheels, resulting in longer life for the spacecraft, as reaction wheels are usually the determining factor in the life of satellites.

PROPOSED ACS RUN MODES

Right now, there are three proposed run modes for the attitude control subsystem. Before I describe the modes I should mention how these modes were determined. Run modes are basically a program that the subsystem must follow. The easiest way to determine them is not to look at the time in which it happens, but what the system has to do. As with ACS, most often the operations that are performed have an aspect of repeatability so we must find a way to identify and acknowledge this repetition so giving commands to the spacecraft are relatively simple. So far, the run modes that have been identified for ACS are: LAUNCH, SAFETY, and POINT. The description of these modes is given below:

LAUNCH: This mode occurs right after we place the spacecraft into the launch vehicle. After the yo-yo weights are deployed (third stage), a signal will be sent to ACS to find its position and orientation and start slewing, ACS is expected to autonomously orient the spacecraft from launch attitude to mission (orbit) attitude. First, ACS must get rid of any residual spin that the yo-yo weights could not dissipate. The ACS system must then orient itself 90 degrees into launch attitude. During this process, it must ensure that all the light-sensitive equipment is not exposed to the harmful sun rays.

SAFETY: This mode occurs whenever ACS or the spacecraft is not properly functioning and it must be started autonomously. The spacecraft may have been hit by a meteorite, or ACS may not be responding appropriately. It is then essential for C&DH to reboot the ACS program and check to make sure that everything is functioning correctly before giving commands. ACS must then attempt to determine its position and orientation, and then slew appropriately to allow for communication with the ground station for further instructions.

POINT: This mode occurs whenever we want ACS to maneuver. This is the mode to use under normal operation if the spacecraft needs to point at something for communications, for testing or experiments, for power regulation, or for temperature regulation. During this process, ACS should ensure that it takes position and orientation data, navigates the shortest and safest path to the "pointing" destination, stops at the "pointing" destination, and then performs minimal corrections.

FUTURE PLANS & CONCLUSION

Some things that could not be finished by the end of the semester was the in depth analysis of the spacecraft, as well as the preliminary test plan for ACS. From a general standpoint, the current ACS design should meet all existing requirements except mass requirements. Dr. Amit Sanyal is currently working on an algorithm to decrease the acquisition rate for the star tracker: the manufacturer has specified 1 Hz, which is too slow to meet our pointing accuracy requirement successfully. ACS has reached a plateau in its development, and needs to work intensely with the systems engineer and other subsystems in order to ensure easy integration into the spacecraft. In order to perform a realistic analysis of the response of the spacecraft and implement a working control algorithm, the spacecraft's structure as well as the placement of all components needs to be set.

ACKNOWLEDGEMENTS

I would like to give a moment to thank all those who helped me with this project, as well as helping make this project possible. I would like to thank NASA and the Hawaii Space Grant Consortium staff for being supportive of this project. Furthermore, I would also like to thank many mentors that helped guide me in some aspects of the spacecraft development process: Steven Stolper and Dr. Amit Sanyal. I would also like to extend a special thank you to Lloyd French for giving me the opportunity to participate in an unforgettable experience and being an invaluable resource when I needed guidance in all the time of my fellowship. Lastly, I would like to thank the other students of the LEONIDAS team as developing a space mission truly takes a group effort.

REFERENCES

Larson, Wiley J.; Wertz, James R.; (1999) Space Mission Analysis and Design Third Edition, Space Technology Library.

7	ACS Requirements		from	to	Date
#	Title	Requirement			
7.1	Control	ACS shall have autonomous control.			
		7.1.1 The control loop shall run at 8 Hz.	ACS	C&DH, SW	19-Feb
		7.1.2 ACS shall be able to accept commands from C&DH	ACS	C&DH	19-Feb
		7.1.3 ACS shall maintain nadir pointing without ground intervention	Sys	ACS	19-Feb
		7.1.4 The spacecraft shall hold commanded attitude without ground intervention			
7.2	Slew	The spacecraft shall be able to slew.			
		7.2.1 The spacecraft shall have a total pointing error of ±1°	Pay, T&T, Pow	St, ACS	19-Feb
		7.2.2 The max slew rate of the spacecraft shall be 0.6°/s			19-Feb
		7.2.3 The min slew rate of the spacecraft shall be 0.2°/s			19-Feb
		7.2.3 ACS shall point a fully covered solar cell faces within x° perpendicular to the sun	Pow	ACS, Th	19-Feb
7.3	Environment	The S/C shall withstand the space environment.			
		7.3.1 All components shall sustain forces up to 12 G (during liftoff)	Sys	ACS	19-Feb
		7.3.2 ACS shall position the S/C to meet thermal dissipation requirements	Th	ACS, Pow	19-Feb
		7.3.3 S/C must not point TBD equipment toward the sun within x°	T&T, Pay, ACS	ACS	19-Feb
7.4	Safehold/Acquisition	The S/C shall be able to recover in safehold and acquisition.			
		7.4.1 The S/C shall be able to point anywhere in 3-D space	Sys	ACS	19-Feb
		7.4.2 The S/C shall attain position, orientation, and point accordingly when commanded by flight computer	Sys, C&DH	ACS	19-Feb
7.5	Mass	The total mass of ACS shall not exceed 7.25 kg	Sys	ACS	19-Feb
7.6	Power	The maximum power needed to operate ACS shall not exceed 30 W	Sys, Pow	ACS	19-Feb
7.7	Temperature	ACS shall be operate within operating temperatures -20°C -> 70°C	ACS	Th	19-Feb
7.8	Error Requirements	The spacecraft shall have a pointing error of ±1°	Sys, T&T, Pay	ACS	19-Feb
7.9	Data Interfaces	The system shall have either USB, RS232, or PC104 architecture	C&DH	ACS	19-Feb
		7.9.1 ACS shall have each of the interfaces in the given quantities: PC104- 1; USB- 1; RS232- 6			19-Feb
7.10	Max Ext. Torque	The maximum external torque exerted on the craft shall not exceed 1.0*10^-4 N*m	sys	ACS	19-Feb

Figure 1.1. Current ACS requirements are grouped into sections and labeled with who the requirement is coming from and where the requirement is going to, as well as the date it was established. The final requirements document will only include the requirements from which the "to" column states ACS.

*note: Some of the requirements listed above have TBD or x. These requirements are imposed on my subsystem from other subsystems, but the accuracy of such requirements has not been specified yet by the other subsystems.

TELECOMMUNICATION SUBSYSTEM REQUIREMENTS, ANALYSIS, AND DESIGN

Dennis D. Dugay
Department of Electrical Engineering
University of Hawai‘i at Mānoa
Honolulu, HI 96822

ABSTRACT

The LEONIDAS microsatellite project has finished the concept phase and is now in its following phase. The requirements, analysis, and design of the telecommunication subsystem are accomplished. The requirements of the subsystem is to state the constraints and performance that is needed to achieve the telecommunication link between the microsatellite and ground station. Then, the analysis is done with a link budget to understand the performance of the link. Finally, the design of the subsystem defines the components chosen specifically to accommodate the requirements and analysis.

INTRODUCTION

A telecommunication subsystem for a microsatellite will be engineered. The purpose of a telecommunication subsystem for a microsatellite is to serve as a communication link between the microsatellite and the ground station. Research will be conducted to understand telecommunication concepts. Also, design on the subsystem components interaction will be done to analyze the performance of the product. In addition, documentation of the critical design, preliminary design, design and analysis, testing and integration plan, and final product will be filed. Finally, a telecommunication subsystem engineering model will be assembled. The project consists of main key concepts of being a successful electrical engineer. The projects end will be justified by its mean.

TELECOMMUNICATION CONCEPT

The concept of the telecommunication subsystem is to allow a communication link between the microsatellite and the ground station. The subsystem will be placed inside the spacecraft. The mission is to launch a microsatellite into a sun synchronous circular orbit at an altitude approximately 400 km. Also, a ground station complementary to the spacecraft will be located at the University of Hawaii at Manoa. As the spacecraft orbits earth it will have a certain time frame where the spacecraft and the ground station will be in field of view of each other allowing a communication link. This then states the importance of the telecommunication subsystem where it will conduct telemetry and command. It is important because it will allow sending commands to the spacecraft for payload experiments, controlling, and maneuvering. Also, it allows sending telemetry where the ground station can receive data that will be beneficial to the scientist.

REQUIREMENTS

The telecommunication requirements of the microsatellite are essential in the progress of the spacecraft design. The requirements define the key points of the telecommunication subsystem to accomplish the mission goals. Furthermore, it has to complement all the other subsystems such as the payloads, command & data handling, attitude control system, thermal, power, structure, and systems. In table 1, the level 1 and 2 telecommunication requirements are documented. Level 1 requirement defines the area that accounts for the subsystem and level 2 requirements define the level 1 requirement in depth.

The requirements consist of the data flow & processing, interfaces, operating temperature, power, field of view, structure, ground station, cabling, mass, operation mode, and fault. The power subsystem can allocate the telecommunication subsystem a maximum power budget f 40 W. The requirement on the telecommunication subsystem is that it needs a maximum power of 37.5 W. Thus, this condition is settled and at the end, both subsystems are satisfied. Another good example is that the antenna needs to be in view of a two pi steradian pointing field of view of the ground station during downlink and uplink. The telecommunication subsystem must have this requirement to be capable of having a telecommunication link. Now, the Attitude Control System subsystem will create a requirement on itself to accommodate this constraint. (Refer to Table 1)

Table 1: Telecommunication Requirements

	Level 1		Level 2
8	**TELECOMMUNICATION REQUIREMENTS**		
8.1	Data Flow & Processing		
		8.1.1	The communication subsystem will be capable to downlink 819.2 kb during overhead per day.
		8.1.2	The communication subsystem will be capable to support uplink of 819.2 kb during overhead per day.
8.2	Interfaces		
		8.2.1	The S-Band Transceiver needs three RS-422 interfaces to connect with the interface board.
		8.2.2	The UHF Transceiver needs an RS-232 interface to connect with the interface board.
8.3	Operating Temperature		
		8.3.1	Telecom Subsystem Operation needs to be between -20 to +60 degrees Celsius.
8.4	Power		
		8.4.1	Telecom Subsystem must not exceed 37.5 W.
		8.4.2	Need to have the UHF Receiver on 100% of the time.
8.5	Field of View		
		8.5.1	Antenna needs to be in view of a 2*pi steradian pointing field of view of ground station during downlink and uplink.
8.6	Structure		
		8.6.1	Tray needs to able to accommodate components.
		8.6.2	Antenna needs to have a 2*pi steradian view.
		8.6.3	Distance from subsystem to antenna needs to be 0.2 meters apart.
		8.6.4	Telecom Subsystem needs 20-24 bolts to mount components to tray.

8.7	Ground Station		
		8.7.1	Has to work at S-Band and UHF frequency in order to communicate with spacecraft.
8.8	Cabling		
		8.8.1	Cable or waveguide from antenna to UHF receiver needs to be less than 0.3 meters long to account line loss.
		8.8.2	Cable or waveguide from antenna to S-Band transmitter and transponder needs to be less than 0.3 meters long to account line loss.
8.9	Mass		
		8.9.1	The Telecom Subsystem of the spacecraft needs to be less than 1.5 kg.
8.10.	Operational Mode		
		8.10.1	It must take less than 2 minutes lock up the spacecraft receiver.
		8.10.2	It must take less than 2 minutes to lock up the ground station receiver.
8.11	Fault		
		8.11.1	The data would be encoded so the spacecraft will not accept incomplete/distorted commands.
		8.11.2	The data would be encoded so the ground station will not accept incomplete/distorted telemetry.

ANALYSIS

The spacecraft will be in an earth orbit and a telecommunication link will be created when it is in field of view of the ground station. The microsatellite will have a certain amount of time to admit a hand shake with the ground station to lock up. After locking up, it will be able to downlink data during telemetry and uplink data during command. Then, after a few minutes of telemetry and command, the spacecraft will unlock and continue its orbit. The analysis is about the performance of the telecommunication link between the spacecraft and the ground station.

Satellite Tool Kit software and Jan King Link Budget excel spreadsheet was used to create a link budget for the mission. In order to create a link budget the following parameters are required: orbit parameters, downlink frequency, uplink frequency, cable lengths, antenna gain, antenna pointing losses, and modulation/demodulation methods. Then, the uplink and downlink budget would be computed.

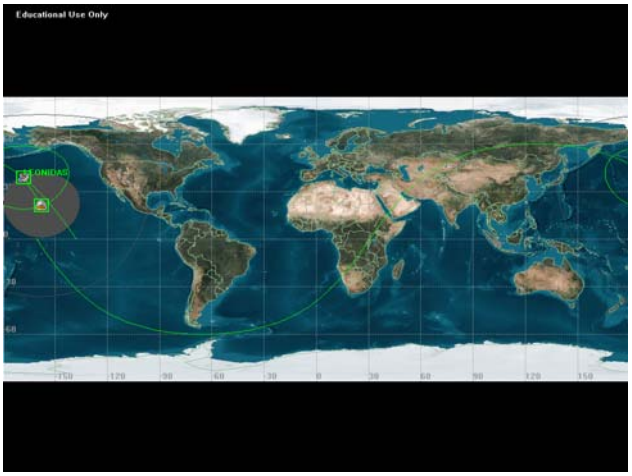

Figure 1: Telecommunication Link in 2-D

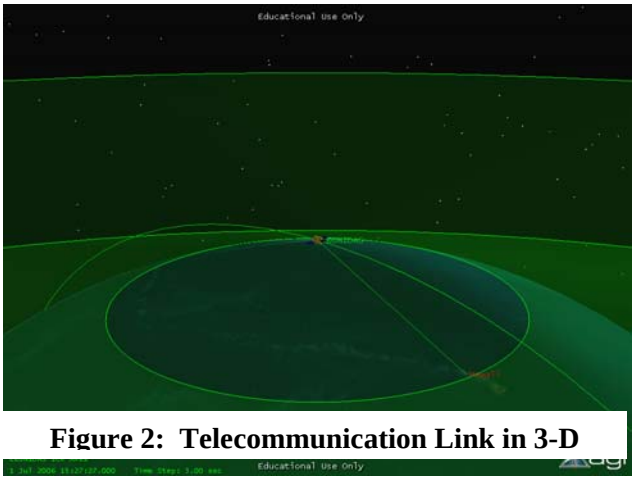

Figure 2: Telecommunication Link in 3-D

The Satellite Tool Kit on the other hand is sophisticated software and it computed the link budget for the entire six month mission. The results of the telecommunication link are still being analyzed. Figure 1 and 2 are snap shot photos taken from the Satellite Tool Kit Software. They show that the microsatellite is orbiting earth and has a telecommunication link with the ground station in Hawaii.

DESIGN

The design phase is the construction of the telecommunication subsystem. The hardware components are chosen specifically for this mission because of its specification and performance. It meets the volume, mass, power budget and it will perform the stated requirements. This will model the exact subsystem and also act as a manual in relation to the components and its block diagram. When the design phase is critiqued and finalized, that will initialize the purchasing of components.

Table 2: Concept Hardware

Component	Company	Linear Dimensions	Mass	Power
S-Band Transmitter	AeroAstro	3.5" x 2" x 1" [89mm x 51mm x 25mm]	<200g	8Wdc
S-Band Receiver	AeroAstro	3.5" x 2" x 1" [89mm x 51mm x 25mm]	<200g	0.5Wdc (standby), 1.5W (operational)
S-Band HPA	AeroAstro	3.5" x 2" x 1" [89mm x 51mm x 25mm]	<200g	24Wdc
S-Band Interface Module	AeroAstro	3.5" x 2" x 1" [89mm x 51mm x 25mm]	<200g	1.1W Transmit: 7.3W
S-Band Antenna	Antcom	1.75" x 5.25" x 4.77" [44.45mm x 133.35mm x 121.16mm]	9.6 oz. (0.27 kg)	0
UHF Transceiver	Yaesu	8.1 cm x 4.7 cm x 2.5 cm	46.5 g	Transmit: 1.740W, Receive: 0.840W, Standby: 0.510W
Terminal Node Controller	PacComm	8.3 cm x 6.3 cm x 2.5 cm	56.9 g	

CONCLUSION

The telecommunication subsystem of the LEONIDAS project has completed the requirements, analysis, and design phases of the mission. The requirement document concludes the constraints of the subsystem and its importance to perform a link for the entire mission. The analysis gives more understanding to the performance of the telecommunication link. Finally, the components are specifically chosen to accommodate the requirements and analysis to fit the mission's needs. The design phase of the telecommunication subsystem will allow continuing the project in to the integrating and testing phase.

ACKNOWLEDGMENTS

I would like to thank Dr. Lloyd French for guiding and being my mentor/advisor. Thank you for allowing me to be a part of your team and your dream of launching a microsatellite from Hawaii. Also, thank you Dr. Luke Flynn and Ms. Marcia Rei Sistoso for giving me a place to study and all the support throughout the year. Thank you to Steven Stolper for helping the team and me with the requirements. Thank you to the LEONIDAS team for all the endless meetings and research we did together. It was great working with all of you. Thank you to everyone who helped and supported the LEONIDAS project.

REFERENCE

AeroAstro Website: S-Band Transceiver PDF file.
Available [Online]: http://www.aeroastro.com/datasheets/S-Band_Transceiver.pdf

Alinco Website: UHF Transceiver.
Available [Online]: http://www.alinco.com/usa.html

AMSAT/IARU Annotated Link Model System. Version: 2.3. March 2007.

Larson, Wiley J. and James R. Wertz. Space Mission Analysis and Design. Third Edition. El Segundo, CA: Microcosm Press, 1999.

Maral, Gerard and Michel Bousquet. Satellite Communications Systems. Fourth Edition. West Sussex, England: John Wiley & Sons Ltd.

PacComm Website: Terminal Node Controller.
Available [Online]: http://www.paccomm.com/pico.html

Satellite Tool Kit (STK). Version: 7.0. April 2007.

POWER DISTRIBUTION AND REGULATION SUBSYSTEM REQUIREMENTS, ANALYSIS, AND DESIGN

Matthew Patterson
Department of Mechanical Engineering
University of Hawai‘i at Mānoa
Honolulu, HI 96822

ABSTRACT

The Low Earth Orbit Nanosatellite Integrated Distribute Autonomous System (LEONIDAS) program consists of a microsatellite design project. The LEONIDAS team consists of nine mechanical and electrical engineering students. Each student is a lead in there own specified subsystem such as: systems, payloads, command and data handling (C&DH), telecommunications, attitude and control system (ACS), power, thermal, orbits, and structure. The integration of the subsystems to coincide with one another will be very crucial to the projects success. The satellite will be assembled with components off the shelf (COTS).

The purpose of a power distribution and regulation subsystem for a microsatellite is to take in raw power and convert it so the microsatellite is able to run and maintain itself during the mission. First, requirements are established to the power subsystem which will define the limitations, constraints, and interactions with other subsystems in the spacecraft. Then, analysis will be prepared to demonstrate and predict the performance. Finally, a design of the subsystem will be edited to fit the requirements and the performance predicted.

REQUIREMENTS

Level 1 and 2 requirements are documented. Level 1 requirement defines the area that accounts for the subsystem and level 2 requirements define the level 1 requirements in depth. This will state what the subsystem needs to accomplish in relation to all other subsystems. It also states the allocation, and accommodation of each requirement to verify who it is coming from, and which is it going to.

	Level 1		Level 2	Allocation	Accommodation
7	7. Power Regulation and Distribution				
7.1	System		The system shall provide enough power throughout the life of the mission.	Power	Systems
		7.1.1	The system shall provide enough power to carry out each mode or state.	Power	ACS, C&DH, Comm, Thermal, Payloads
		7.1.2	The system shall support 3.3, 5, -12, +12, and 28V needed by each individual subsystem and their components.	Power	
		7.1.3	The following must always be powered: ACS, C&DH, receiver, and worst case draw for the Thermal subsystem.	Power	ACS, C&DH, Comm, Thermal
		7.1.4	Be able to support peak power draw from transceiver and receiver together for 20 minutes.	Power	Comm

		7.1.5	Spacecraft must provide telemetry containing: battery charge voltage, battery charge current, solar array output voltage, solar array output current	Power	C&DH, Comm
		7.1.6	Spacecraft must provide telemetry for state of charge of the battery.	Power	
		7.1.7	Carry enough power, in case of total failure of solar cells, to last 12 hours. (52 Wh)	Power	Systems
7.2	Solar Cells		Solar Cells shall create enough raw power to operate and maintain the spacecraft for a minimum of 6 months.	Power	
		7.2.1	Cover seven of the smaller faces of the spacecraft and partially cover the eighth side, taking up as much surface area as allowed.	Power	Structure and C&DH
		7.2.2	Shall begin its life at 28.3% efficiency and not degrade beyond 24.3% at the end of five years.	Power	C&DH
7.3	Converting		The system will convert raw solar energy, convert it to be used by the spacecraft, and charge the secondary batteries.	Power	Power
7.4	Secondary Battery		The system will carry Lithium Ion batteries which will help sustain the life of the spacecraft when the solar cells can not provide adequate power throughout the bus.	Power	Systems
		7.41	Each battery will carry four MP 176065 cells holding ~104 Wh. The spacecraft will carry six batteries.	Power	
		7.4.2	Battery should be able to sustain 5x the expected charge/discharge cycle.	Power	
		7.4.3	Each battery will not be able to discharge 20% full capacity and not over charge at 90% full capacity to help maintain life.	Power	
		7.4.4	By having six batteries, the system provides redundancy, in case the failure of a single battery, the spacecraft will still be operational.	Power	
		7.4.5	Be able to isolate the battery from the Spacecraft bus by ground command.????	Power	C&DH, Comm, Ground
7.5	Shunt		Power not being used by the spacecraft will be shunted out the radiator plate consistently.	Power	Thermal
7.6	Temperature		The system must maintain a constant temperature between 0-75 degrees Celsius.	Power	Thermal
		7.6.1	Solar Cells must maintain a temperature between 0-75 degrees Celsius.	Power	Thermal
		7.6.2	Lithium ion batteries must maintain a temperature between -20-75 degrees Celsius.	Power	Thermal

		7.6.3	HESC 104 must maintain a temperature between -40-85 degrees Celsius.	Power	Thermal
7.7	Distribution		Power subsystem will provide power to all needed systems and payloads.	Power	Systems
		7.7.1	Power supplied to any system must not exceed 6A.	Power	
		7.7.2	Ability to switch power on/off for each circuit	Power	C&DH
		7.7.3	Power distribution must be controllable from flight computer.	Power	
		7.7.4	Relays must be able to maintain TBD cycles.	Power	Systems
		7.7.5	PDU will be able to connect to: C&DH, COMM, ACS, Thermal, and Payloads.	Power	C&DH, Comm, ACS, Thermal, Payloads
7.8	Conditioning		Voltage/Current spikes will not exceed TBD.	Power	Systems
		7.8.1	Be able to supply 3.3, 5, 12, -12, 28 V and fall within a band of 5%.	Power	
		7.8.2	Between the batteries and solar cells, the system must be able to not drop below TBD V and above TBD V.	Power	
		7.8.3	As supplying these voltages, make sure current does not drop.	Power	
7.9	Fault		System will be able to handle and protect against any fault (surge, open/short circuit, overload).	Power	Systems
7.10	Cost		Total cost of subsystem not to exceed $150,000	Power	Budget
		7.10.1	Solar Cells (UTJ) ~ $100,000	Power	
		7.10.2	Secondary Batteries (Lithium Ion) ~ $1260.78	Power	
		7.10.3	PRU (HESC 104) ~ TBD	Power	
		7.10.4	Distribution unit (custom) ~ TBD	Power	

ANALYSIS

The newest analysis that I have been working on is the time that the satellite will be in the sun. This will give a better idea on how much power we will be getting out of an orbit, and how long it will take to charge the secondary battery. The STK software has the ability to measure and orbit and the time that it sees the sun. A single day will look like this:

Sunlight Times

Start Time (UTCG)	Stop Time (UTCG)	Duration (sec)
1 Jan 2006 12:00:00.000	1 Jan 2006 12:49:06.749	2946.749
1 Jan 2006 13:22:52.306	1 Jan 2006 14:21:43.799	3531.492

1 Jan 2006 14:55:28.949	**1 Jan 2006 15:54:20.852**	**3531.904**
1 Jan 2006 16:28:05.599	**1 Jan 2006 17:26:57.908**	**3532.309**
1 Jan 2006 18:00:42.254	**1 Jan 2006 18:59:34.967**	**3532.713**
1 Jan 2006 19:33:18.917	**1 Jan 2006 20:32:12.028**	**3533.111**
1 Jan 2006 21:05:55.591	**1 Jan 2006 22:04:49.091**	**3533.500**
1 Jan 2006 22:38:32.263	**1 Jan 2006 23:37:26.157**	**3533.894**

Average Duration (6 months): 3950s = 65.8 min = 1.1 hrs of sunlight per orbit
Charge rate = 4 A @ 4 hrs. (Longest time expectancy)
= 4 V +/- 0.05
DOD = 90%
Battery Capacity = 104 Wh
Discharge = >10%
Charge up to 90%

80% x 4 hrs = 3.2 hrs

(3.2 hrs) x ((1 orbit) / (1.1 hrs)) = 2.9 orbits
This is to charge a single battery.

This next analysis requires some understanding before reading. The spacecraft spins at .0625 degrees per second, but if you look at my tables, my stages go in one minute intervals. The red boxes are getting seen by the sun and the blue boxes are seen by the albedo from the earth. Figuring the power output of the sun (P(output) = 0.283 * 1367 W/m^2 = 386.861 W/m^2) and the albedo ((output) = 0.283 * 341.75 W/m^2 = 96.7153 W/m^2) and multiplying it by the inherent degradation of 0.77, all was left was to multiply that number times the surface area of the panel and times the cosine of the angle. The spacecraft is rotating in a clockwise direction, and panel 2 starts by being perpendicular to the sun and panel 6 starts perpendicular to the earth. The even panels have a bigger surface are of 0.14 m^2, while the odd panels are only at 0.11314 m^2 (the side with the camera hole will have a surface area of 0.1364 m^2.

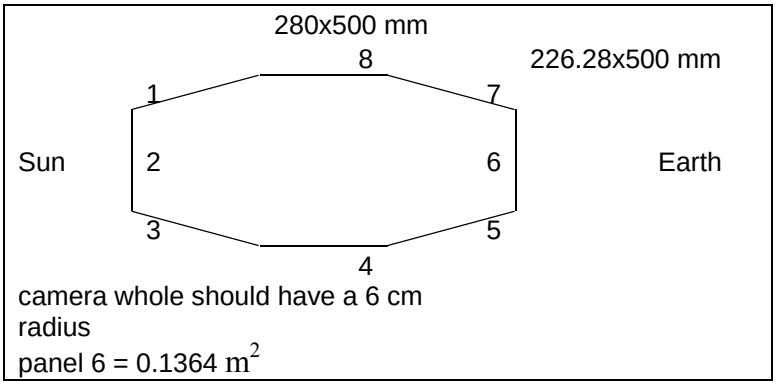

Rotation 0	Stage 1	Stage 2	Stage 3	Stage 4	Stage 5	Stage 6	Stage 7	Stage 8	Stage 9	Stage 10	Stage 11	Stage 12
Panel 1	23.831	22.222	20.517	18.724	16.851	14.906	12.897	10.833	8.7228	6.57503	4.39906	2.20425
Panel 2	41.704	41.614	41.347	40.902	40.283	39.49	38.529	37.403	36.116	34.6753	33.0857	31.3544

Panel 3	23.831	25.339	26.738	28.023	29.187	30.227	31.137	31.914	32.554	33.0549	33.4141	33.6303
Panel 4	0	2.7276	5.4434	8.136	10.794	13.405	15.959	18.445	20.852	23.1693	25.3876	27.4971
Panel 5	5.9578	5.9578	5.9578	5.9578	5.9578	5.9578	5.9578	5.9578	5.9578	5.95782	5.95782	5.95782
Panel 6	10.158	10.158	10.158	10.158	10.158	10.158	10.158	10.158	10.158	10.1578	10.1578	10.1578
Panel 7	5.9578	5.9578	5.9578	5.9578	5.9578	5.9578	5.9578	5.9578	5.9578	5.95782	5.95782	5.95782
Panel 8	0	0	0	0	0	0	0	0	0	0	0	0
Pout(tot)	111.44	113.98	116.12	117.86	119.19	120.1	120.6	120.67	120.32	119.548	118.36	116.759

Rotation 1	Stage 1	Stage 2	Stage 3	Stage 4	Stage 5	Stage 6	Stage 7	Stage 8	Stage 9	Stage 10	Stage 11	Stage 12
Panel 2	29.489	27.497	25.388	23.169	20.852	18.445	15.959	13.405	10.794	8.13597	5.44341	2.72755
Panel 3	33.703	33.63	33.414	33.055	32.554	31.914	31.137	30.227	29.187	28.0226	26.738	25.3389
Panel 4	29.489	31.354	33.086	34.675	36.116	37.403	38.529	39.49	40.283	40.9023	41.3468	41.6143
Panel 5	5.9578	5.9578	5.9578	5.9578	5.9578	5.9578	5.9578	5.9578	5.9578	5.95782	5.95782	5.95782
Panel 6	10.158	10.158	10.158	10.158	10.158	10.158	10.158	10.158	10.158	10.1578	10.1578	10.1578
Panel 7	5.9578	5.9578	5.9578	5.9578	5.9578	5.9578	5.9578	5.9578	5.9578	5.95782	5.95782	5.95782
Panel 5	0			28.023	29.187	30.227	31.137	31.914	32.554	33.0549	33.4141	33.6303
Panel 1/8	0	0	0	0	0	0	0	0	0	0	0	0
Pout(tot)	114.75	114.56	113.96	112.97	111.6	109.84	107.7	105.2	102.34	99.1343	95.6017	91.7542

Rotation 2	Stage 1	Stage 2	Stage 3	Stage 4	Stage 5	Stage 6	Stage 7	Stage 8	Stage 9	Stage 10	Stage 11	Stage 12
Panel 3	23.831	22.222	20.517	18.724	16.851	14.906	12.897	10.833	8.7228	6.57503	4.39906	2.20425
Panel 4	41.704	41.614	41.347	40.902	40.283	39.49	38.529	37.403	36.116	34.6753	33.0857	31.3544
Panel 5	0	2.2043	26.738	28.023	29.187	30.227	31.137	31.914	32.554	33.0549	33.4141	33.6303
Panel 5	5.9578	5.9578	5.9578	5.9578	5.9578	5.9578	5.9578	5.9578	5.9578	5.95782	5.95782	5.95782
Panel 6	10.158	10.158	10.158	10.158	10.158	10.158	10.158	10.158	10.158	10.1578	10.1578	10.1578
Panel 8	0	0	0	0	0	0	0	0	0	0	0	0
Panel 1/7	0	0	0	0	0	0	0	0	0	0	0	0
Panel 2	0	0	0	0	0	0	0	0	0	0	0	0
Pout(tot)	81.651	82.156	104.72	103.76	102.44	100.74	98.679	96.266	93.509	90.4209	87.0145	83.3046

This ends up being for 36 minutes. Within the next 12 minutes the spacecraft will be totally eclipsed and the cycle will most likely repeat itself. It was discovered that the orbit will eventually fluctuate, making the analysis even harder to calculate.

From here I will take the time it takes to charge a single battery and compare it to the orbital analysis I just calculated from above. This analysis will give me a better understanding of how many orbits it will take to charge the secondary battery and then see if the power output will match the need of the spacecraft. The software has some other valuable applications for the power subsystem, but still not sure on how to work it. More analysis must also be done on the placement of my components and how the power will be distributed or allocated to the other subsystems.

DESIGN

The design phase has been started with a concept hardware document which specifies the components, linear dimensions, mass, and power. The design will consist of all its components and a block diagram. This will model the exact subsystem and also act as a manual to help future technicians. When the design phase is critiqued and finalized, then the purchasing of components will come in.

Power Source			
UTJ **ITJ**		**28.3% Efficiency** **15 to +75°C operation** **26.8% Efficiency** **10 to +80°C operation**	**102 W @ ideal 3 panels** **84 mg/cm2** **17 to 19 A** **97.3 W @ ideal 3 panels**
Regulator			
PRU (HESC 104)		**.186 kg** **PC-104 compatibility** **-40 to +85°C operation**	**0 to 4 A Charge Current** **Input Voltage of 6 to 40 V** **Provides 3, 5, +12, -12**
Rechargeable Batteries			
Secondary Batteries Lithium Ion	**MP 176065**	**26 Wh** **.153 kg** **500 cycle life time**	**4 A Charge rate** **-20 to +60°C operation** **3 to 4 h charge time**
	MP 174865	**20 Wh** **.124 kg** **500 cycle life time**	**5 A Charge rate** **-20 to +60°C operation** **2 to 3 h charge time**

FUTURE PLANS

Analysis on the power distribution and regulation subsystem is still be being continued by understanding the different types of parameters and building on them. With each new piece of data collected a new requirement usually pops up. This keeps the requirement list up to date. There are plans to find a distributor off the shelf, but I really think that it will have to be done custom or "in house" do to the fact of our unique plug and play structure. Analysis is always being done, especially now that our orbits leader is learning to use the STK software. In time, I hope to gather much more data from the software, including the light intensity on our orbit. This will give me a much better picture of how much power we will be generating from the sun.

REFERENCE

1. Patel, Mukund R. Power Systems. New York. CRC Press. 2005.
2. "Space Solar Panels" Spectrolab Photovoltaic Products online datasheet. http://spectrolab.com/DataSheets/Panel/panels.pdf
3. "Battery Regulator Unit", Crisa online datasheet http://www.crisa.es/pdf/bru.pdf#search='Power%20Regulator%20Unit%20for%20Power%20Subsystem'
4. "NPR NPS 2-T220 T221 Power Resistors", Riedon online datasheet http://www.riedon.com/eu/eng/images/stories/pdf/NPRNHRT22x_eu.pdf

THERMAL CONTROL DESIGN FOR A MICROSATELLITE

Kaipo Kent
Department of Electrical Engineering
University of Hawai‘i at Mānoa
Honolulu, HI 96822

ABSTRACT

Conventional satellites are extremely large, highly expensive, and may take several years to design and build. Microsatellites have the potential to reduce cost and risk when compared to conventional satellites. The main purpose of the LEONIDAS project is to prove that the University of Hawaii has the capabilities to design, build, test, launch, and operate a microsatellite. The thermal control subsystem monitors and controls the internal temperatures of the satellite and its components. Thermal sensors will monitor temperatures of the satellite components. Thermofoil patch heaters will be attached to components to apply heat when needed. Thermostats will control the activity of the thermofoil heaters, turning the heaters on and off automatically when needed. The following report includes requirements for operational limits for each satellite component and an analysis of the thermal stability of the satellite.

INTRODUCTION

The LEONIDAS project is designed to prove the capabilities of the University of Hawaii to design, build, test, launch, and operate a microsatellite. Proving these capabilities will lead to many new opportunities within the aerospace industry. The success of the LEONIDAS project could lead to partnerships with NASA and could push the University of Hawaii to start its own aerospace program. The main objective for the current mission design is to conduct technology demonstrations in the laboratory of space.

The thermal control subsystem monitors and controls the internal temperatures of the satellite and its components. The main purpose of the thermal control subsystem is to keep the satellite and it’s components within operational limits. In order to make this satellite as simple and self-maintainable as possible, all thermal activity will be controlled passively.

The thermal control subsystem will consist of two radiator plates, thermofoil patch heaters, multi-layer insulator (MLI), several thermal sensors, and several thermostat controllers. Two of the sides of the spacecraft will act as radiator plates to passively dump excess heat while in direct sunlight. Thermal sensors will monitor temperatures of the satellite components. Thermofoil patch heaters will be attached to components to apply heat when needed. Thermostats will control the activity of the thermofoil heaters, turning the heaters on and off automatically when needed. Layers of MLI will be placed between the solar panels of the satellite and the satellites structure itself. This ensures that the satellite will not absorb all of the heat acquired while collecting energy with the solar cells. MLI will also be placed around heat sensitive components so that components that produce high amounts of heat will not transfer its heat to nearby components.

In order to successfully complete a design for the thermal subsystem, the requirements for thermal operational limits needed to be determined. An analysis was accomplished to calculate the overall average internal temperature of the satellite at two different extremes: once

at the highest power consumption rating and highest temperature absorbed from the environment and again at the lowest power consumption rating and lowest temperature absorption from the environment. The analysis was used to start the design process of the thermal control subsystem.

REQUIREMENTS

The thermal control subsystem differs from the other subsystems in one major way: the requirements for the TCS are almost purely performance based. While other subsystems have physical restraints placed on them by the structure of the satellite, the components of the TCS are relatively small, from millimeters to a few centimeters which means that components can be placed in smaller areas or in-between other components, except for the MLI which surrounds the entire structure but does not get in the way of any other components. The components also have a relatively low mass, except for the MLI which may have a final mass of nearly 2kg. This made my job a little easier because all I had to deal with were performance requirements of components.

Each component of our satellite functions at its own temperature, depending on what it does. For example, the C&DH controls the operations of the satellite and can operate at temperatures from 0° - 60° C. The batteries on the other hand only operate at temperatures from 0° - 15° C. What may seem like just a small difference in maximum temperature ranges is very important and, thus, places a requirement on the thermal control subsystem to ensure that each individual component stays within their own temperature limits.

Each component consumes a certain amount of power which creates a certain amount of heat energy. Also, as our satellite orbits the Earth it will absorb radiation from the sun and the Earth. Our satellite uses two radiator plates to passively dissipate all excess heat out into space. That means that the radiator plates must be able to dissipate enough heat to keep the components inside reaching of exceeding its specified operational temperature limit.

The function of a thermal sensor is to read temperatures components, therefore there are no specific requirements for thermal sensors. Thermostats, on the other hand, control the thermofoil heaters. The way thermostats work is that they are directly connected to a component. Each thermostat has a set temperature rating which is the ideal temperature of a specific component and a specific “deadband” value. A deadband tells the thermostat how much the actual temperature of the component it is attached to can differ from the thermostat’s set temperature value before turning off or on. That’s kind of hard to understand so let’s say for example a thermostat is attached to a battery with operational limits from 0° - 15° C. Let's give our thermostat a set temperature rating of 10° C and a deadband value of 5° C. Our battery has a current temperature of 10° C and our thermostat starts in the *off* position, but when the temperature of the battery reaches 5° C (thermostat set rating - deadband value) the thermostat will flip to the *on* position which will then turn on our thermofoil film heaters. Then when the temperature of the battery reads 15° C (thermostat set rating + deadband value) the thermostat will switch back to the *off* position, thus turning off the thermofoil heaters.

Thermofoil heaters, *see figure 1*, do one thing: produce heat when given an electric current. Therefore, all thermofoil heaters will be the same. Thermofoil heaters will be placed near components and attached to thermostats. The thermostats will control when the thermofoil heaters will turn on and off.

Multi-layer insulation is like wearing layers of clothes. They are usually made of aluminum and layered to both repel heat away from the satellite as well as keep heat in the satellite so that the components do not freeze.

The only mode of heat dissipation in our satellite is passive dissipation through two radiator plates. Satellites constantly absorb heat from the environment as well as produce heat from components through power consumption. Our radiator plates must be able to dissipate a specific amount of heat or risk overheating which could result in the malfunction of the out satellite.

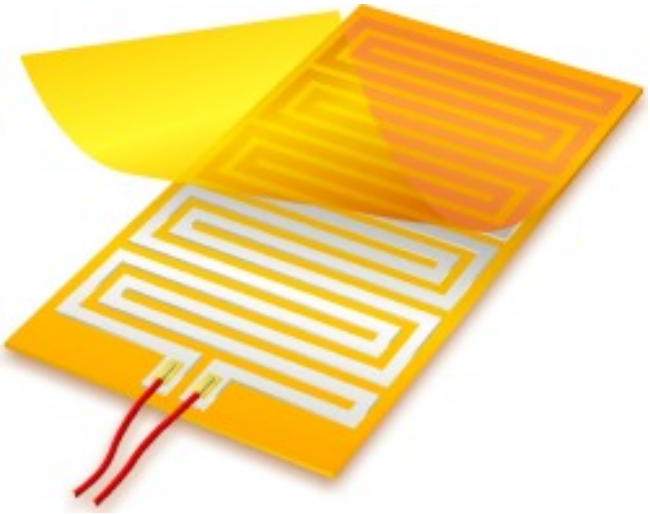

Figure 1- Thermofoil heater:
When an electric current runs through the wires heat is produced

ANALYSIS

Each component has is own operational temperature requirement shown in *table 1* below. With these requirements I was able to conduct a preliminary analysis of the thermal performance of the satellite as a whole. The analysis is the most important part of the design of the thermal control subsystem because the results of the analysis will tell me hot or cold the satellite will get. This will tell me how much thermofoil I will need and where they have to be placed, how much MLI will be needed, and the most important part, if the two radiator plates be able to dissipate enough heat to keep the satellite operational.

Component	Typical Temperature Ranges (°C)	
	Operational	Survival
Batteries	0 to 15	-10 to 25
Reaction Wheels	-20 to 40	-20 to 60
Gyros/IMUs	0 to 40	-10 to 50
C&DH	-20 to 60	-40 to 75

Antennas	-100 to 100	-120 to 120
Solar Panels	-150 to 110	-200 to 130

Table 1 – List of component operational temperature ranges

According to the requirements the TCS needs to keep the satellite within a specific temperature range. In order to simplify my analysis, I chose a realistic low and high temperature for the satellite as a whole. For those temperatures I chose a low of 0° C and a high of 60° C. Given values of power consumption for each component, given to me by the other subsystems, I was able to perform two worse case scenario analyses. First scenario was determining the highest temperature of the satellite while absorbing the maximum amount of heat from the environment while all components are functioning. As a side note, MLI was not accounted for in any analysis due to the uncertainty of the number of layers and other unknown factors. To determine the highest temperature rating I used constants for:

- Solar Radiation (Solar) = 1300 W/m^2
- Earth Radiation (Earth) = 230 W/m^2
- Albedo Radiation (Albedo) ~ 350 W/m^2
- Surface Finish : white chemglaze A276
    - Emittance (ε) = 0.88
- Projection Area for Solar, Earth, and Albedo radiation (Ap) ~ 0.3 m^2
- Surface area of radiator plates (A) ~ 0.66 m^2
- Absorptivity of Solar Cells (α) = 0.805
- Boltzmann's constant (σ) = 5.67051 x 10^{-8} W/m^2K^4

I found the maximum power usage to be 403 W. Then I had to find the temperature of the satellite from its environment using equation (1).

$$\sigma T^4 = (\alpha/\varepsilon) * (\text{Solar} + \text{Albedo} + \text{Earth}) * (Ap/A) \qquad (1)$$

Solving for T and then adding the temperature from the components I get a temperature value of 71° C, which is 11° C higher than the temperature that I chose as an upper limit. That means I might need to use copper strapping to transport heat from warmer components to the radiator plates to dissipate more heat.

For the second scenario I used the same constants and equation. I found to minimum power consumption to be 140 W when only the essential components are functioning, which considerably less than the maximum. In the end, I found the satellite's temperature to be about -13° C, which is 13° less than the value I chose for my lower limit. In this analysis I did not take thermofoil into account because of the complications it would produce for me. Also, the MLI was not accounted for either. I believe that with MLI and thermofoil the satellite will have no problem surviving when temperatures decrease.

CONCLUSION

The actual physical design of the thermal control system depends mostly on the placement of the components in the structure, which is not a sure thing yet. But as of this moment the TCS will consist of approximately 7-10 thermal sensors and thermostats, estimated

10-15 layers of MLI surrounding the structure of the satellite, and an undetermined amount of thermofoil heaters.

The reason the values stated in the previous paragraph are estimated is because depending on the placement of the components I may be able to set up thermal "zones" which may simplify my design. Basically a thermal zone is an area, instead of separate components, that is monitored and controlled.

The thermal control subsystem is not confined to one physical area like most of the other subsystems. The reason being that most of the components will be attached or near every other components on the satellite. But once again, I can not have a definite design until the placements of the components are set.

REFERENCES

Larson, Wiley J., and James R. Wertz. Space Mission Analysis and Design. 3rd ed. El Segundo, CA: Microcosm Press, 1999